UNIVERSIDADE ESTADUAL DE CAMPINAS
Instituto de Geociências

TITO AURELIANO NETO

PALEOHISTOLOGIA DE TITANOSSAUROS (SAUROPODA, DINOSAURIA) DA BACIA BAURU (CRETÁCEO SUPERIOR), SUDESTE DO BRASIL, COM COMENTÁRIOS EM TAFONOMIA

PALEOHISTOLOGY OF TITANOSAURS (SAUROPODA, DINOSAURIA) OF THE BAURU BASIN (UPPER CRETACEOUS), SOUTHEAST BRAZIL, WITH COMMENTS ON TAPHONOMY

CAMPINAS
2020

TITO AURELIANO NETO

PALEOHISTOLOGY OF TITANOSAURS (SAUROPODA, DINOSAURIA) OF THE BAURU BASIN (UPPER CRETACEOUS), SOUTHEAST BRAZIL, WITH COMMENTS ON TAPHONOMY

PALEOHISTOLOGIA DE TITANOSSAUROS (SAUROPODA, DINOSAURIA) DA BACIA BAURU (CRETÁCEO SUPERIOR), SUDESTE DO BRASIL, COM COMENTÁRIOS EM TAFONOMIA

DISSERTAÇÃO APRESENTADA AO INSTITUTO DE GEOCIÊNCIAS DA UNIVERSIDADE ESTADUAL DE CAMPINAS PARA OBTENÇÃO DO TÍTULO DE MESTRE EM GEOCIÊNCIAS NA ÁREA DE GEOLOGIA E RECURSOS NATURAIS

DISSERTATION PRESENTED TO THE INSTITUTE OF GEOSCIENCES OF THE UNIVERSITY OF CAMPINAS TO OBTAIN THE DEGREE OF MASTER IN GEOSCIENCES IN AREA OF GEOLOGY AND NATURAL RESOURCES

ORIENTADORA: PROFA. DRA. FRESIA SOLEDAD RICARDI BRANCO

COORIENTADOR: PROF. DR. MARCELO ADORNA FERNANDES

ESTE EXEMPLAR CORRESPONDE À VERSÃO FINAL DA DISSERTAÇÃO DEFENDIDA PELO ALUNO TITO AURELIANO NETO E ORIENTADA PELA PROFA. DRA. FRESIA SOLEDAD RICARDI BRANCO E COORIENTADA PELO PROF. DR. MARCELO ADORNA FERNANDES

CAMPINAS
2020

Ficha catalográfica
Universidade Estadual de Campinas
Biblioteca do Instituto de Geociências
Marta dos Santos - CRB 8/5892

Aureliano Neto, Tito, 1989-
Au64p Paleohistology of titanosaurs (Sauropoda, Dinosauria) of the Bauru Basin (Upper Cretaceous), Southeast Brazil, with comments on taphonomy / Tito Aureliano Neto. – Campinas, SP : [s.n.], 2020.

Orientador: Fresia Soledad Ricardi Branco.
Coorientador: Marcelo Adorna Fernandes.
Dissertação (mestrado) – Universidade Estadual de Campinas, Instituto de Geociências.

1. Histologia. 2. Tafonomia. 3. Paleopatologia. 4. Paleoparasitologia. 5. Aparelho respiratório. I. Ricardi-Branco, Fresia, 1963-. II. Fernandes, Marcelo Adorna. III. Universidade Estadual de Campinas. Instituto de Geociências. IV. Título.

Informações para Biblioteca Digital

Título em outro idioma: Paleohistologia de titanossauros (Sauropoda, Dinosauria) da Bacia Bauru (Cretáceo Superior), Sudeste do Brasil, com comentários em tafonomia
Palavras-chave em inglês:
Histology
Taphonomy
Paleopathology
Paleoparasitology
Respiratory System
Área de concentração: Geologia e Recursos Naturais
Titulação: Mestre em Geociências
Banca examinadora:
Fresia Soledad Ricardi Branco [Orientador]
Rafael Delcourt de Seixas Ferreira
Sandra Aparecida Simionato Tavares
Data de defesa: 27-04-2020
Programa de Pós-Graduação: Geociências

Identificação e informações acadêmicas do(a) aluno(a)
- ORCID do autor: https://orcid.org/0000-0002-6918-0519
- Currículo Lattes do autor: http://lattes.cnpq.br/3666297020355529

UNICAMP

UNIVERSIDADE ESTADUAL DE CAMPINAS

INSTITUTO DE GEOCIÊNCIAS

AUTOR: Tito Aureliano Neto

PALEOHISTOLOGY OF TITANOSAURS (SAUROPODA, DINOSAURIA) OF THE BAURU BASIN (UPPER CRETACEOUS), SOUTHEAST BRAZIL, WITH COMMENTS ON TAPHONOMY

PALEOHISTOLOGIA DE TITANOSSAUROS (SAUROPODA, DINOSAURIA) DA BACIA BAURU (CRETÁCEO SUPERIOR), SUDESTE DO BRASIL, COM COMENTÁRIOS EM TAFONOMIA

ORIENTADORA: Profa. Dra. Fresia Soledad Ricardi Torres Branco
COORIENTADOR: Prof. Dr. Marcelo Adorna Fernandes

Aprovado em: 27 / 04 / 2020

EXAMINADORES:

Profa. Dra. Fresia Soledad Ricardi Torres Branco - Presidente

Dr. Rafael Delcourt de Seixas Ferreira

Dra. Sandra Aparecida Simionato Tavares

A Ata de Defesa assinada pelos membros da Comissão Examinadora consta no processo de vida acadêmica do aluno.

Campinas, 27 de abril de 2020.

SÚMULA/BIOGRAFIA

Tito Aureliano é graduado em Geologia pela UFPE e está concluindo o Mestrado em Geociências pela Unicamp. Além do mais, também é pesquisador associado do *Laboratório de Paleoecologia e Paleoicnologia*, LPP, UFSCar, e no *Dinosaur Ichnology and Osteohistology Laboratory,* DINOlab, UFRN, e da *Sociedade de História Natural*, SHN, de Portugal. O foco de sua pesquisa é em petrografia, paleohistologia, e morfometria, de fósseis de dinossauros e outros tetrápodes.

DEDICATÓRIA

Para Aline M. Ghilardi.

AGRADECIMENTO

O presente trabalho foi realizado com apoio da Conselho Nacional de Desenvolvimento Científico e Tecnológico (CNPq), processo nº 131777/ 2018-1. O trabalho foi parcialmente financiado através do projeto FAPESP 2016/20927-0 'Modern accumulation studies and fossil bioclast studies in continental and coastal environments'. Eu gostaria de agradecer Oswaldo Jorge e o resto da equipe do Hospital Universitário da UFSCar por conduzirem parte das tomografias. Ao Paulo Saldiva, Milena Picka Santos, Ellison Cardoso, e o resto da equipe da Faculdade de Medicina da USP também por conduzir parte da tomografia computadorizada e comentários sobre um dos espécimes. Para Renata Monteiro, pelos insights sobre osteomielite. Para Fernanda Aníbal e David Soeiro, por suas observações a respeito dos parasitas. Para Erica Tonetto, por conduzir análises de microscopia eletrônica. Ao Kai Casper, por esclarecer a metodologia de medir o calibre de canais vasculares. Ao Martin Sander, pelo curso de preparação em paleohistologia óssea e pelo financiamento parcial dos meus estudos. Ao Hugo Cafasso, pela reconstrução paleoartística. A Rafael Delcourt, Sandra Tavares, Ariel Martine e Carolina Zabini por todos os comentários pertinentes que contribuíram para o enriquecimento desta dissertação. A Luciana B. Fernandes, pela licença do Corel Draw. Ao Paulo Morgato, José e o restante da equipe de laminação, por preparar as seções delgadas. Ao departamento de Pós-Graduação do Instituto de Geociências, Unicamp, e aos *Colecionadores de Ossos*™, ao Marcelo Adorna Fernandes, e à Universidade da Cidade do Cabo, África do Sul, pelo financiamento das lâminas histopetrográficas, do transporte de materiais do estudo, e do financiamento de minha participação no simpósio de paleohistologia. A Aline Ghilardi e aos meus dois orientadores, pelos ensinamentos, paciência e atenção.

RESUMO

Neste estudo, propôs-se preencher lacunas no conhecimento sobre a evolução dos sistemas respiratório e imunológico em dinossauros, com observações a respeito de como a tafonomia impacta na preservação de tecidos em fósseis. Os resultados do presente estudo corrobora a hipótese de que as macroestruturas do esqueleto axial de saurópodes possuem fossas relacionadas à interação de sacos aéreos, semelhante ao observado nas aves atuais. Concomitantemente, pesquisou-se a preservação dos traços produzidos pelos tecidos moles nos organismos estudados (e.g. tendões e pneumósteo) com o objeto de compreender a evolução da pneumaticidade em ossos do pós-crânio, e a preservação destes tecidos fossilizados. Para atender à pesquisa, foram estudadas vértebras de três *taxa* de titanossauros derivados, coletadas em distintos contextos deposicionais do Grupo Bauru. Adicionalmente, descreveu-se uma patologia infecciosa presente em um material associado a um destes *taxa*, em associação a uma nova forma de parasita extinto. De posse destas informações, é desenvolvida uma discussão histológica envolvendo diversos campos, incluindo comentários em paleopatologia, tafonomia e paleoparasitologia. Os resultados contribuem para compreensão dos sistemas respiratório e imunológico em dinossauros, da evolução das doenças tropicais. Por fim, este estudo fornece uma melhor compreensão de como distintos sistemas deposicionais afetaram a qualidade de preservação da microanatomia dos fósseis deste grupo.

Palavras-chave: Histologia, Tafonomia, Paleopatologia, Paleoparasitologia, Sistema Respiratório

ABSTRACT

This study aimed to fill in gaps in knowledge on the evolution of the respiratory and immune systems in dinosaurs, providing observations concerning the impacts of taphonomy on the preservation of fossilized tissues. The results of this dissertation corroborate with the hypothesis that the postcranial pneumatic macrostructures in sauropods are related to the interaction of an avian-like air sacs system. Concomitantly, it was investigated the preservation of soft tissue traces in the studied organisms (e.g. tendons and pneumosteus) in order to understand the evolution of pneumaticity in the postcranial skeleton. Vertebrae of three derived titanosaur taxa supported this study. The fossils were collected in different depositional contexts within the Bauru Group. Additionally, it has been described the development of an infectious pathology in one of these taxa. It has also been described the association of that pathology with a new form of extinct parasite. A histological discussion involving several fields is developed from obtained results, including comments on paleopathology, taphonomy, and paleoparasitology. Therefore, results contribute to the understanding of the respiratory and immune systems in dinosaurs, and to the evolution of tropical diseases. Finally, this study provides a better understanding of how different depositional systems affected the quality of preservation of the microanatomy of dinosaur fossils.

Keywords: Histology, Taphonomy, Paleopathology, Paleoparasitology, Respiratory System

SUMÁRIO

Índice

CORPO DO TRABALHO

1 Introdução

Os dinossauros são um grupo de organismos-modelo para compressão de diversos extremos evolutivos. Desde a sustentação mecânica dos grandes corpos dos saurópodes à leveza e agilidade dos terópodes mais derivados. Seus restos esqueletais evidenciam adaptações das mais diversas, em resposta às mudanças geoambientais (eg. mudanças de distribuição de continentes e oceanos), desde gigantes quadrúpedes com altas taxas de metabolismo, aos grandes predadores semi-aquáticos e pequenos voadores (Aureliano *et al.*, 2018; Dyke *et al.*, 2013; Sander *et al.*, 2011; Wedel, 2003; Xu *et al.*, 2015).

O metabolismo acelerado evidenciado por meio do estudo das taxas de deposição dos tecidos ósseos (Cerda *et al.*, 2017; Mitchell e Sander, 2014), concomitaria, entretanto, no superaquecimento dos organismos. Sobretudo nos saurópodes, afetados pela gigantotermia (Perry *et al.*, 2009; Wedel, 2003). Para reverter esta situação, uma das inovações evolutivas deste grupo foi a sua capacidade respiratória altamente eficiente, através de um sistema de sacos aéreos (projeções de órgãos como o pulmão) que permeiam órgãos, resfriando-os de maneira efetiva semelhante aos mamíferos (Hudgins, Uhen e Hinnov, 2020; Lambertz, Bertozzo e Sander, 2018; O’Connor, 2006; Wedel, 2003). Em Saurischia, foram encontradas diversas macroestruturas em forma de fossas no esqueleto axial, que teoricamente foram apontadas como evidência do contato com sacos aéreos (Wedel, 2003, 2007, 2009; Wilson *et al.*, 2011). Contudo, todos os trabalhos anteriores a 2018 limitam-se a observações em tomografias computadorizadas. Muito pouco se conhece sobre os detalhes dos equivalentes histológicos dos tecidos pneumáticos. Descrevendo-os como pneumósteos, foi publicado pela primeira vez uma evidência concreta para a presença destas estruturas em dois neosaurópodes basais: o *Europasaurus holgeri* e o *Diplodocus sp.* (Lambertz, Bertozzo e Sander, 2018). Sendo muito pouco compreendida, aqueles últimos autores destacam a relevância de se levantar uma amostragem mais compreensiva de *taxa*.

O uso de lâminas petrográficas delgadas para o estudo de ossos fossilizados de dinossauros já é amplamente difundido (Cerda *et al.*, 2017; Francillon-Viellot *et al.*, 1990; Ibrahim *et al.*, 2016; Sander *et al.*, 2011) e constitui uma ferramenta muito útil para obter informações sobre a paleobiologia e paleoecologia destes organismos, além de permitir a análise detalhada de aspectos fossildiagenéticos (Aureliano *et al.*, 2018; Chinsamy-Turan, 2005; Ibrahim *et al.*, 2016; Marchetti *et al.*, 2019; Padian e Lamm, 2013). Existe, contudo, uma amostragem ainda muito reduzida de fósseis do Brasil e há uma forte demanda para compreensão da histologia destas populações nesta área do Hemisfério Sul e nas linhagens gonduânicas.

Também pouco explorados, são os espécimes patológicos no registro fóssil, que fornecem informações extras sobre a fisiologia e o comportamento dos indivíduos, e suas pressões ambientais (Rothschild e Martin, 2006; Surmik *et al.*, 2018; Xing *et al.*, 2018). Vestígios de parasitas são ainda mais antigos no registro fóssil pré-Cenozoico (Dentzien-Dias *et al.*, 2013; Poinar, 2008; Poinar, G. e Poinar, 2004). As evidências anteriores a este projeto foram obtidas a partir de coprólitos ou de vetores preservados em âmbar (Dentzien-Dias *et al.*, 2013; Poinar, 2019; Poinar, G., Jr e Poinar, 2004; Poinar, G. e Poinar, 2004). A associação entre a parasitação quanto da patologia no registro fossilífero, oferece, portanto, uma oportunidade única para observar a interação destes campos.

Os titanossauros do Cretáceo Superior do Grupo Bauru oferecem um bom modelo de investigação, não apenas para o estudo da preservação de restos orgânicos, pois são alguns dos fósseis mais abundantes da bacia (Salgado e Carvalho, 2008; Santucci e Arruda-Campos, 2011; Silva Junior *et al.*, 2019), como para evolução do sistema da pneumaticidade em dinossauros, um carácter adaptativo muito importante do grupo relacionado ao sistema respiratório e ao gigantismo (Lambertz et al., 2018). Ademais, disponibilizam um enorme banco de dados para a busca de paleopatologias (Barbosa *et al.*, 2016, 2018).

A Bacia Bauru representa uma bacia continental do Cretáceo Superior do Brasil (Fernandes e Coimbra, 1996). Esta unidade tectônica ocupa uma área de mais de 350.000 km^2 na porção sudeste do Brasil, englobando partes dos estados do Paraná, São Paulo, Mato Grosso, Mato Grosso do Sul, Goiás e Minas Gerais e parte do Paraguai (Fernandes e Coimbra 1996; Menegazzo *et al.*, 2016). Apresenta uma grande variação litológica e faciológica, compreendendo depósitos eólicos, fluviais, aluviais e lacustres de pouca profundidade (Fernandes e Coimbra, 1996; Dias-brito *et al.*, 2001; Batezelli *et al.*, 2003). Poucos trabalhos foram produzidos sobre fossildiagênese e a histologia de ossos de vertebrados da Bacia Bauru (Andrade, 2018; Marchetti *et al.*, 2019). Portanto, a proposta deste projeto baseou-se no estudo de detalhes histológicos e fossildiagenéticos de três diferentes espécies de titanossauros das Formações Marília e Adamantina, do Grupo Bauru (Cretáceo Superior, Bacia Bauru).

A partir das análises realizadas durante o presente estudo, em três indivíduos já foram encontrados o tecido fossilizado relativo ao sistema de sacos aéreos: no *Uberabatitan ribeiroi* Salgado e Carvalho 2008, o *Aeolosaurus maximus* Santucci e Arruda-Campos 2011, e em um novo táxon de saurópode Saltasauridae (que está sendo descrito paralelamente). Pôde-se comparar três contextos tafonômicos distintos e como estes impactaram na preservação dos pneumósteos. Adicionalmente, pôde ser realizado um aprofundamento na descrição destes tecidos, incorporando conceitos da mineralogia, e que serão muito úteis para pesquisadores que desenvolvam trabalhos neste assunto.

Por fim, descreve-se brevemente um novo morfótipo de titanossauros anões para a Formação Adamantina. Dentre estes, um dos quais apresenta uma patologia na fíbula (LPP-PV-0043). Descreveu-se o crescimento anormal do tecido enfermo e sua respectiva infecção parasítica. Portanto, este estudo também contribuiu para o conhecimento da evolução das doenças tropicais e o sistema imunológico de dinossauros.

CAPÍTULO I - RESUMO PUBLICADO EM ANAIS DE CONGRESSO

AURELIANO, T. GHILARDI, A. A., NAVARRO, B. A., FERNANDES, M. A., RICARDI-BRANCO, F. S.. Growth strategy of nanoid titanosaurs from Southeast Brazil. In: INTERNATIONAL SYMPOSIUM ON PALAEOHISTOLOGY, 4., 2019, Cidade do Cabo: Universidade da Cidade do Cabo, 2019.

Status: Publicado
Evento: International Symposium on Palaeohistology

Growth strategy of nanoid titanosaurs from Southeast Brazil

Tito Aureliano[1,2*], Aline M. Ghilardi[2], Bruno A. Navarro[2,3], Marcelo A. Fernandes[2] and Fresia S. Ricardi-Branco[1]

1 University of Campinas, Institute of Geosciences, Campinas, 13083855, Brazil, **aureliano.tito@gmail.com**; **2** Federal University of São Carlos, Laboratório de Paleoicnologia e Paleoecologia, São Carlos, 13565905, Brazil; **3** Museum of Zoology, University of São Paulo, São Paulo, 04263-000, Brazil.

The Upper Cretaceous Bauru Basin of Brazil is worldwide known to provide abundant crocodilian and titanosaurian remains. Despite the local sauropod diversity, a new morphotype detaches from the rest due its nanoid proportions. These specimens represent a new species, which is being described at this point. Here we characterize the appendicular histology of two nanoid individuals from distinct fossil sites within the Adamantina Formation. Individual A (LPP-PV-201) encompasses a nearly complete ulna (preserved length ~ 45 cm). Individual B (LPP-PV-0043) comprises a fragmentary fibula (diaphysis; preserved volume = 16 x 22 cm). In both individuals, the extent and type of vascularization maintains its pattern across thin sections. The entire cortex has been secondarily remodeled by osteons of multiple generations, and lacks an interstitial laminar primary bone. At least three generations of secondary osteons overlap one another. These latter are chaotically arranged and present remarkable varying sizes and shapes. Each secondary osteon contains up to six layers of centripetally deposited lamellar bone. No LAGs (Lines of Arrested Growth) or anulli

have been identified. There is no evidence of an EFS (External Fundamental System), which is a common feature marked in the growth strategy of mature late titanosaurians. Extreme remodeling activity completely obliterating the primary bone tissue suggest these individuals had long ceased their growth at the moment of death (Type G bone tissue and HOS stage 13 from Klein and Sander (2008). Furthermore, by applying the three-front model of (Mitchell and Sander, 2014) to the anteromedial areas of shafts, the 'senescent' status is reinforced. It is known in literature that titanosaurs present a more secondarily remodeled cortical bone tissue when compared to basal neosauropods. It is no surprise we found this character in specimens A and B. Padian et al. (2016) showed that the cortex in distal appendicular bones are more secondarily remodeled than the humerus or femur within a same individual. Even though considering that effect, a very similar pattern was also observed both in the ulna and the humerus of the nanoid *Lirainosaurus*. Therefore, is expectable that the proximal limb bones of A and B would also present this tissue adaptation. Similarly to what can be observed in *Magyarosaurus*, the strong remodeling in the specimens A and B was caused by the slow down of the resorption front (RF). By reducing the speed of the RF, this dwarf-taxon adapted their long bones with a thick cortex and small medullary volume allowing to support the axial loading regime similarly to *Magyarosaurus* and *Lirainosaurus.* This cannot be observed in the nanoid macronarian *Europasaurus*, which rather presents a predominantly fibrolamellar bone tissue. It is true that titanosaurs such as *Ampelosaurus* and *Alamosaurus* present a greater amount of Haversian bone than other neosauropods, such as *Apatosaurus.* Nonetheless, the extreme abundance of this type of tissue observed in the Brazilian dwarf is more similar to the condition found in *Lirainosaurus* and *Magyarosaurus* than to any other sampled titanosaurs in literature, including the small-bodied *Neuquensaurus*. Therefore, this may correspond an effect of a phylogenetically decreased apposition growth in such clade.

Bibliography:

Klein, N., Sander, M., 2008. Ontogenetic stages in the long bone histology of sauropod dinosaurs. Paleobiology 34, 247–263.

Mitchell, J., Sander, P.M., 2014. The three-front model: a developmental explanation of long bone diaphyseal histology of Sauropoda. Biol. J. Linn. Soc. Lond. 112, 765–781.

Padian, K., Werning, S., Horner, J.R., 2016. A hypothesis of differential secondary bone formation in dinosaurs. C. R. Palevol 15, 40–48.

CAPÍTULO II - RESUMO PUBLICADO EM ANAIS DE CONGRESSO

AURELIANO, T. GHILARDI, A. A., FERNANDES, M. A., RICARDI-BRANCO, F. S.. Detailed histology in a case of appendicular osteomyelitis in a titanosaur. In: INTERNATIONAL SYMPOSIUM ON PALAEOHISTOLOGY, 4., 2019, Cidade do Cabo: Universidade da Cidade do Cabo, 2019.

Status: Publicado
Evento: International Symposium on Palaeohistology

Detailed histology in a case of appendicular osteomyelitis in a titanosaur

Tito Aureliano[1,2*], Aline M. Ghilardi[2], Marcelo A. Fernandes[2] and Fresia S. Ricardi-Branco[1]

1University of Campinas, Institute of Geosciences, Campinas, 13083855 Brazil, **aureliano.tito@gmail.com**; **2**Federal University of Sao Carlos, Laboratório de Paleoicnologia e Paleoecologia, Sao Carlos, 13565905 Brazil

There are few detailed histological studies on non-avian dinosaur pathological specimens. It is here depicted a senile titanosaur from the Upper Cretaceous Adamantina Formation, Bauru Basin of southeast Brazil. Specimen LPP-PV-0043 comprises a fragmentary fibula (diaphysis; preserved volume = 16 x 22 cm). Tomography slices, three-dimensional model, histological thin sections allowed a successful observation of the lesioned bone and its nature. Lesion blend the surrounding bone with a sharply defined transition zone. There are noticeable distinct densities/textures between inflamed and healthy trabeculae. Erosions from the inner cortex and periosteum are united posterolaterally and extend from medulla to the cortical surface. Periosteal reaction is focal posterolateral and anteromedially (but it is much stronger in the former portion). It is dome-shaped, with a geographically eroded surface. Connections between extremities occur two times in tower-like structures. Distinct texture of unhealthy areas follow a filigree pattern ('aero candy-like'). These reactions are elliptical and interrupted on surface. Moreover, periosteum elevates forming Codman's triangles (CdTr) posterolaterally. There is no sign of ruptive tissue obstructions in the surrounding areas of the dome-shaped lesions (eg. those expected in bite marks and other mechanical fractures). The elevated periosteal producing CdTr present reticular primary tissue. In the outer cortex, these structures (lesions) comprise highly vascularized periosteum with radial to reticulated bone, a condition usually observed in fastly growing bone of juvenile amniotes. The frontier between senescent secondary tissue and this newly formed lesioned tissue is well marked and is

unnatural (ontogenetically speaking). Therefore, it could only have been formed from disease. Lesion goes way down to the inner cortex (with noticeably increased local vascularity) and connects to the medulla. Since observed area does not pertain to articulation, spondyloarthropathies (e.g. arthritis) can be discarded. Identification of tuberculosis can be eliminated because tissue anomalies do not comprise solid avascular periosteum. Neoplasm (cancer) can also be discarded because surface eruptions and tissue deformation are not spiculated. Presence of CdTr, periosteal and perimedullary alteration, and dome-like cortical tissue inflammation connecting CdTr to medulla are indicatives of osteomyelitis (Om). In this work, we followed the definition that Om is infection-driven bone lesion not limited to the external surface. Om identification have been historically neglected in dinosaurs due to its rarity in modern-day archosaurs. However, recent findings and reidentification of pathological specimens demonstrated this enfermity also reached sauropodomorphs. Nevertheless, this specimen contributes to enlighten new histopathological information from in this group.

CAPÍTULO III - ARTIGO CIENTÍFICO

AURELIANO, T., GHILARDI, A. M., NASCIMENTO, C. S. I., FERNANDES, M. F., RICARDI-BRANCO, F. S.. Blood Parasites and tissue deformities in a non-avian dinosaur.

Status: Manuscrito submetido considerado para publicação na *Current Biology*

BLOOD PARASITES AND CHRONIC OSTEOMYELITIS IN A NON-AVIAN DINOSAUR

Tito Aureliano*[1,2,3], Carolina S. I. Nascimento[3], Marcelo A. Fernandes[3], Fresia Ricardi-Branco[1], Aline M. Ghilardi*[2,3]

[1]Institute of Geosciences, University of Campinas (Unicamp). Campinas, Brazil.

[2]Dinosaur Ichnology and Osteohistology Laboratory (DINOlab), Department of Geology, Federal University of Rio Grande do Norte (URFN). Natal, Brazil.

[3]Laboratório de Paleoecologia e Paleoicnologia (LPP), Departamento de Ecologia e Biologia Evolutiva (DEBE), Federal University of Sao Carlos (UFSCar). Sao Carlos, Brazil.

*corresponding authors

ABSTRACT

This research documents for the first time the detailed histological description of severe bone inflammation and the exceptional preservation of soft-bodied parasitical microorganisms (*Brontoleishmania rex* gen. et sp. nov.) inside the vascular canals of a non-avian dinosaur. The results bring new insights into the fields of parasitology, pathology, and histology in the fossil record. A senile titanosaur from the Upper Cretaceous of Southeast Brazil presented chronic osteomyelitis, identified by the presence of Codman's triangles, periosteal and perimedullary alteration, and a dome-like cortical tissue inflammation connecting the former to the medulla. Furthermore, tens of large-sized Trypanosomatidae-like forms were identified throughout the specimen's vascular canals. Novel histological insights resulted from the developmental description of chronic osteomyelitis in five stages. Inflammation itself could have been directly caused by the parasitic infestation. This may be the earliest occurrence of leishmaniasis-like disease in the New World, adding new information to the complex biogeographic and evolutionary history of parasitic Trypanosomatidae.

INTRODUCTION

Pathologies preserved in the fossil record can provide valuable information on the physiology and behavior of individuals and their environmental pressures (e.g. [1–3]). Paleoparasitological records, in turn, offer insights not only about the physiology of organisms and the ecology of communities but also about the evolution of parasites, hosts and their relationship over time [4–7]. The association of parasitization and pathology in the fossil record, ultimately, can be considered exceptional. It offers a unique opportunity to access several pieces of information regarding ancient organisms and ecosystems and refine our understanding of the past.

The occurrence of osteomyelitis in dinosaurs has been debated in the past [8], but recent studies have corroborated the occurrence of this form of bone inflammation at least in Sauropodomorpha [3,9,10]. Evidence of fossil endoparasites of vertebrates has already been found in coprolites and invertebrate vectors preserved in amber (eg. [5,6,11–13]). However, fossil parasites preserved directly in vertebrate tissues were unknown until the present date. Herein we describe in detail the developmental histology of a fossil bone disease, responsible for tissue deformities in a long bone of an Upper Cretaceous sauropod dinosaur, and the first record of a trypanosomatid parasite of vertebrates, preserved inside fossilized bone tissue.

MATERIALS AND METHODS

Institutional abbreviations: FM-USP, Faculty of Medicine of the University of São Paulo, São Paulo city, Brazil; **IGe-M**, Laboratory of Electron Microscopy, Institute of Geosciences, Campinas State University, Campinas, Brazil; **Lalgas**, Laboratory of Algae Biotechnology, Federal University of São Carlos (UFSCar), São Carlos, Brazil; **LPP-PV**, Laboratório de Paleoecologia e Paleoicnologia (UFSCar), São Carlos, Brazil.

The studied specimen (LPP-PV-0043; Fig. 1) corresponds to a fragmentary titanosaur fibula. The material is deposited at the Laboratory of Paleoecology and Paleoichnology (LPP) of the Federal University of São Carlos (UFSCar), São Carlos city, São Paulo state, Brazil.

CT-Scan

3D reconstruction of the specimen was attained by using a Philips Diamond Select Brilliance CT 16-slice medical scanner with more than 200 slices and a voxel size of 0.75 mm at the

FM-USP. Software 3D-Slicer v4.6 [14] was used to process images (e.g. density contrast calculation) and generate the model.

Bone histology

For the histological analysis, we followed the general methodology presented by [15]. First, the specimen was saturated with penetrant stabilizer cyanoacrylate glue (PaleoBond®). Then, it was cut and immersed in resin (Araldite® 2020). Finally, samples were polished until section thickness was around 40 µm. Transversal sections were used for skeletochronological analysis and longitudinal sections were used to describe bone lesions. Thin sections were observed and photographed by using a petrographic ZEISS Axioscope microscope with coupled AxioCam MRc 5 camera, and imaging software ZEISS Application Suite v.4.4. Pictures were corrected for brightness and contrast in Adobe Photoshop CC 20.0.1 and composite images were prepared in Corel Draw X6.

Histological nomenclature is in accordance with [16]. Vascular canal caliber measurements followed the procedures of [17,18].

Parasite identification

We used petrographic and non-filtered optical microscopes to observe and track the forms interpreted as parasites. In the first case, the same hardware used for histology was applied. For non-filtered light analysis, thin sections were studied under a Nikon Eclipse optical microscope with attached Nikon DS – Fi2 camera, and imaging software NIS – Elements F v4.0 at the LBA. Electron microscopy was conducted with an Oxford X-act EDS attached to a Zeiss LEO 430i SEM at the IGe-M. Samples were metalized in C (Carbon) before readings. Structures observed were measured using ImageJ v1.4 software [19].

Parasite morphometry

We performed ordinary least-squares (OLS) regression analysis to test the association of individual width and the total length of the parasite population (in µm) in an allometric model. Additionally, it was also related parasite proportion to host area spectrum in order to recover more information regarding their autoecology. All computations were performed using Minitab 17 (https://www.minitab.com).

Data availability

Parasite measurements, further statistical data, EDS readings, and additional images are available as supplemental information. Computed tomography data is available upon request to authors.

Specimen: fragmentary titanosaur fibula LPP-PV-0043.

Locality and horizon: Ibirá municipality, upper Campanian-lower Maastrichtian Adamantina Formation, Bauru Group, São Paulo state, Brazil.

Diagnosis

The shaft is massif and cross-section is 'D shaped' (Fig.1 and Fig 2A.a1-a4). The lateral process is partially preserved and is slightly lateroanteriorly oriented (Fig.1.B-C). Cancellous bone encloses medullary cavity completely, a characteristic typical of sauropods (e.g. [20–23]), absent in theropods (except in Spinosaurinae; see [24]). LPP-PV-0043 is a fibula diaphysis (Fig.1.E) associated with additional elements of a new Saltasauridae titanosaur taxon currently being described separately.

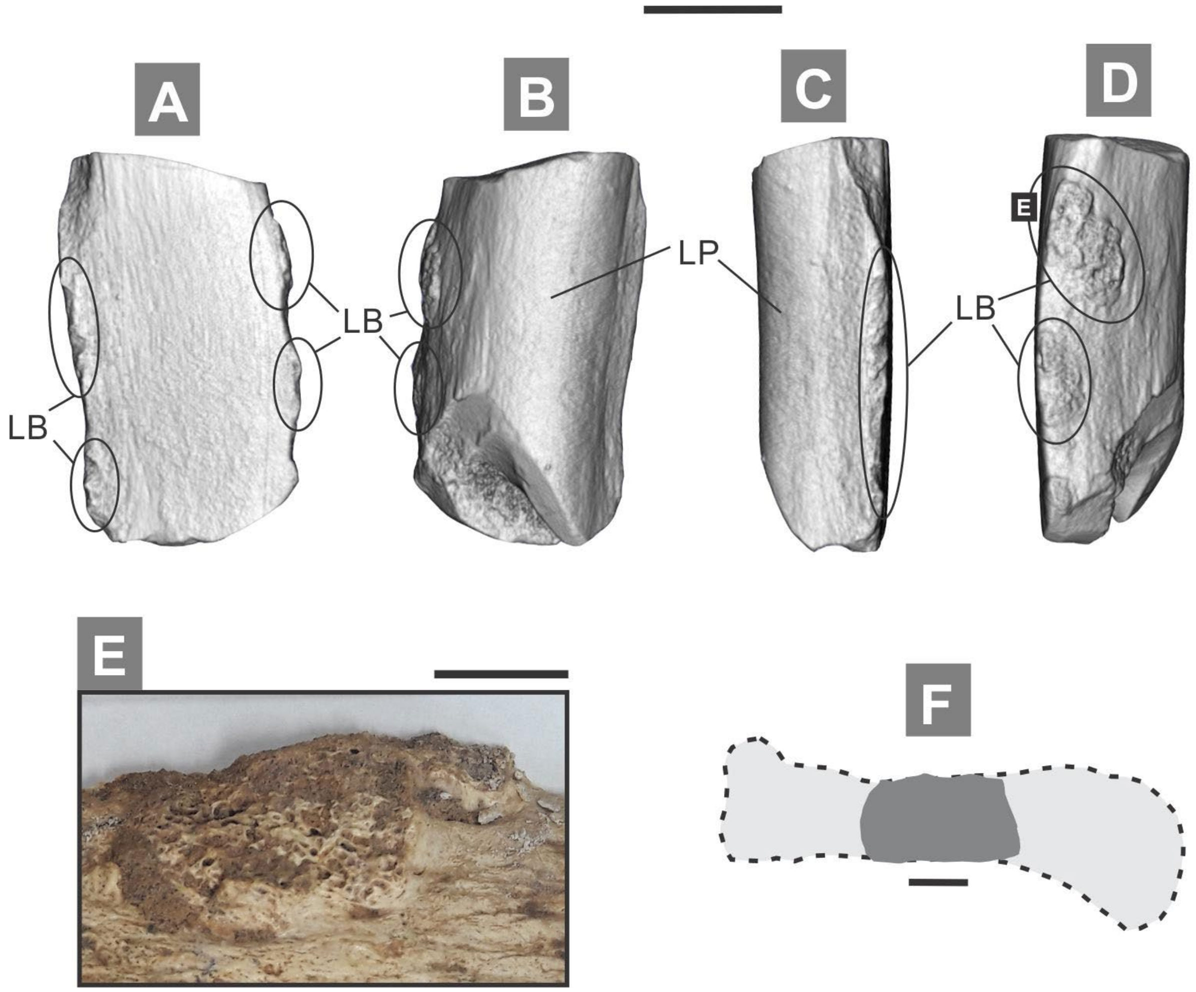

Figure 1. Three-dimensionally reconstructed CT-Scan model of the partial titanosaur fibula LPP-PV-0043, from the Upper Cretaceous Adamantina Formation, Bauru Basin, Southeast Brazil. **A**, medial; **B**, lateral; **C**, anterior; **D**, posterior. ; **E**, detailed photograph of the fossilized lesion showing erupted elliptical shape and ‘aero candy-like’ texture; **F**, reconstructed total size of the fibula. E and F are rotated 90º clockwise. Abbreviations: **LP**, lateral process; **LB**, lesioned bone. Scale bar in A-D, F = 5 cm; in E = 1 cm.

RESULTS

CT-Scan

Tomography slices and three-dimensional model allowed internal observation of the lesioned bone (Figs.1,2). Lesion blend the surrounding bone with a sharply defined transition zone. In Fig.2.B, it is noticeable the distinct densities/textures of inflamed and healthy trabeculae. Erosions from the inner cortex and periosteum are united posterolaterally and extend from medulla to the cortical surface. Periosteal reaction is focal posterolaterally and anteromedially (but it is much stronger in the former portion). It is dome-shaped, with a ‘geographically eroded’ surface (*sensu* [1]). Connections between extremities occur two times in tower-like structures (Fig2.A.a5-7). The distinct texture of pathologically-affected areas follows a filigree pattern (‘aero candy-like’ *sensu* [1]). These reactions are elliptical and interrupted on the surface (Fig1.A-D). Moreover, periosteum elevates forming Codman’s triangles posterolaterally (Fig.2.A.a5,6 and Fig.2.B).

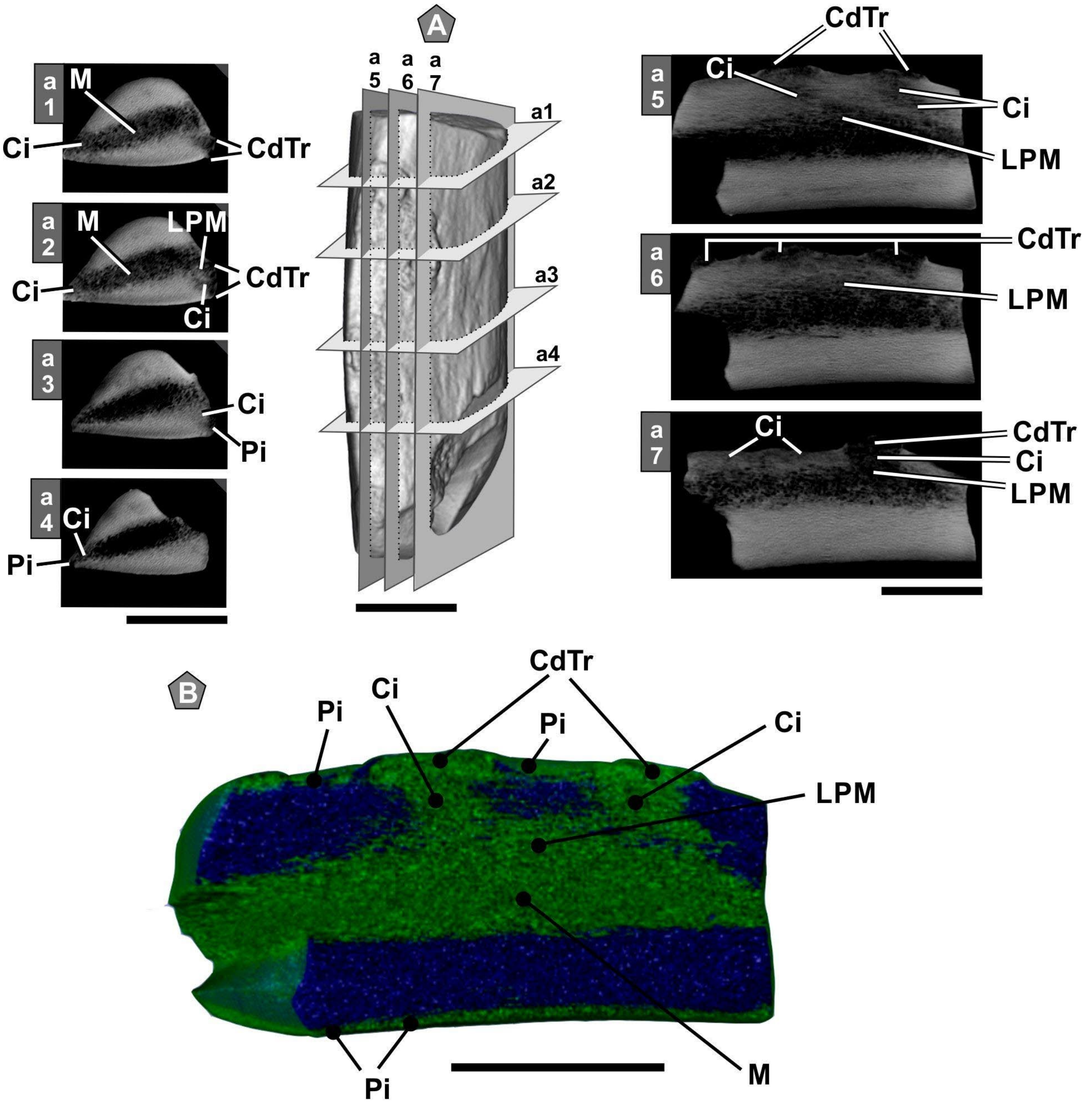

Figure 2. A, reconstructed CT-Scan model of LPP-PV-0043 presenting transverse (a1-4) and

longitudinal (a5-7) x-ray slices. **B**, density contrast applied to CT-Scan model longitudinally sliced. Dark blue represents the denser bone matrix (eg. compacta). Light green comprises lower densities (eg. regular medullary spongiosa - Cb -, and lesioned cortex - CdTr, Pi, Ci, LPM). Note the spread lesion on the surface forming CdTr posterolaterally. Also, observe the connection between these and lesioned medulla throughout tower-like structures (Ci). Abbreviations: **Ci**, compacta inflammation; **CdTr**, Codman's triangles; **LPM**, perimedullary lesion; **M**, medulla; **Pi**, periosteum inflammation. Scale bar = 5 cm.

Paleohistology

Samples were well preserved and histological details could be assessed. Specific topics are subdivided below. Longitudinal and cross sections are present in Fig. S1 (see supplemental information).

Taphonomical remarks

There are no preparation marks on the surface, but isolated spots of truncated osteons populate external bone perimeter anteromedially (Fig.S2.A; see supplemental information). Truncation may have been caused either by pre-burial transport, reworking or by post-exhumation transport. Mineral grains fill cavities in some areas, especially in the medulla (Fig.S2.B). Thin oxide layers invade secondary osteons longitudinally in the medial shaft (Fig.S2.A, C). These are early diagenetic features [25], despite the current absence of sulfur in these samples (see Fig.S3 in Supplemental information). There are a few longitudinal diagenetic cracks (Fig.S2.D). Well-preserved phosphatized microorganisms inside vascular cavities may indicate rapid burial. Nevertheless, thin sections show moderate infilling of mineral grains from earlier burial stages. Despite these subsequent taphonomic features, the microstructure is well preserved. Titanosaur histology and parasite microanatomy could be assessed (Fig.S2 and Figs.5,6).

Skeletochronology

The extent and type of healthy tissue vascularization maintain its pattern across thin sections (Fig.3.A). The entire cortex has been secondarily remodeled and lacks an interstitial laminar primary bone (Fig.3.B). At least three generations of secondary osteons overlap one another (Fig.3.C). These latter are longitudinally arranged and present remarkable varying sizes and shapes. Each secondary osteon contains up to six layers of centripetally deposited lamellar bone. Regarding vascularization (*sensu* [17]), the minimum canal caliber ($\mathrm{Can}_{\mathrm{min}}$) is 26 µm and harmonic mean canal caliber ($\mathrm{Can}_{\mathrm{harmean}}$) is 106 µm. No LAGs (Lines of Arrested Growth) or annuli have been identified. There is no evidence of an EFS (External Fundamental System), which is a common feature marked in the growth strategy of adult-derived titanosaurs [21,22,26].

Extreme remodeling activity completely obliterating primary tissue suggests this individual had long ceased its growth at the moment of its death (Type G bone tissue and HOS stage 13 from [27]). Furthermore, by applying the three-front model of [28] to the anteromedial area of the bone, the ‘senescent’ status is reinforced (Fig.3.D). There is no precise definition of maturity status beyond ‘senescent’ or ‘senile’ in the mentioned literature. However, it is a consensus that with the increasing number of successive overlapping generations of secondary osteons the higher individual ages would have been [21,22,26,28].

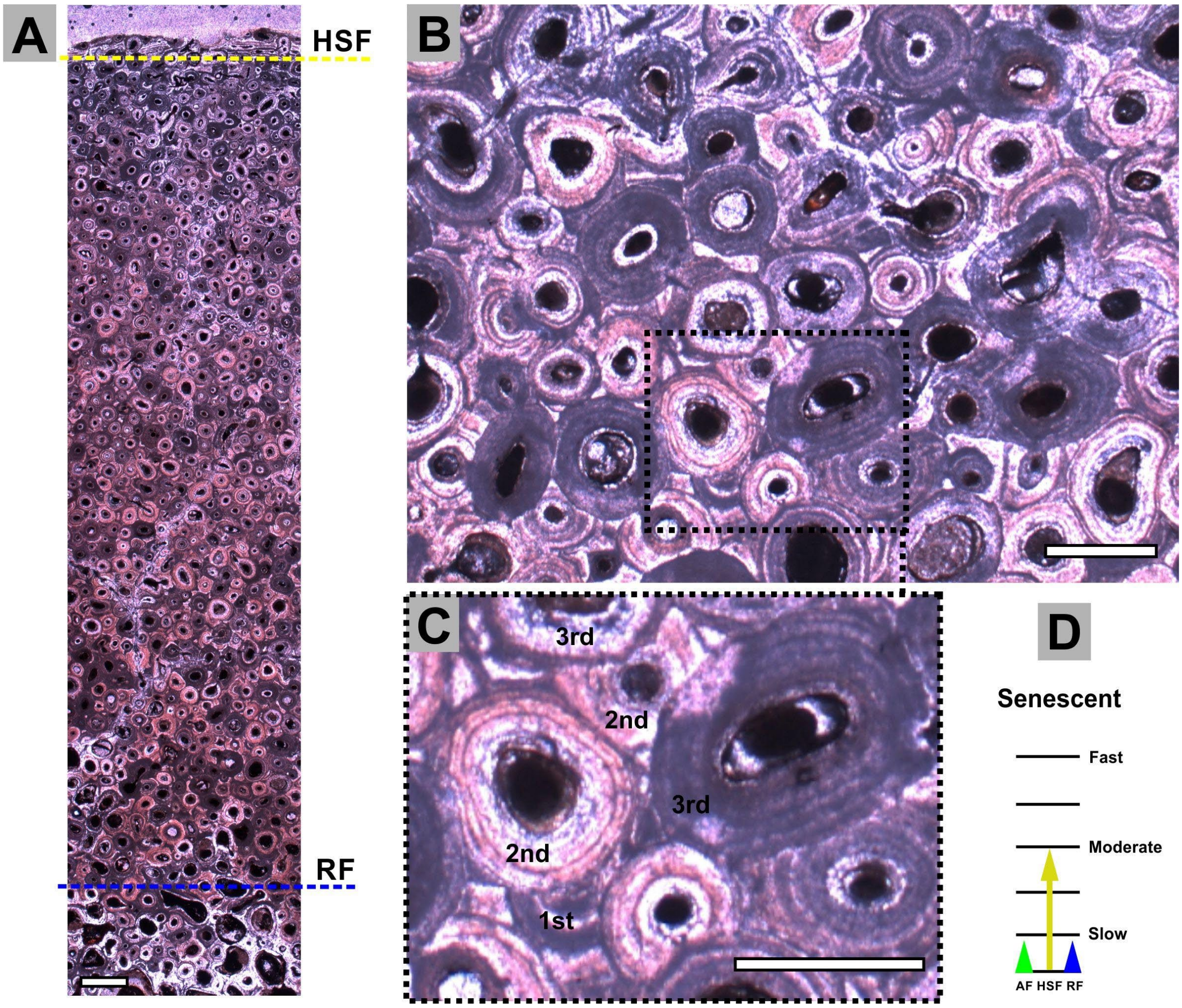

Figure 3. Histology of titanosaur specimen LPP-PV-0043. **A**, profile at the medial portion of the shaft. Marked bone deposition fronts according to [28]. **B**, longitudinally arranged secondary bone in the anteromedial inner cortex. **C**, three generations of secondary osteons overlapping one another. Note there are up to six centripetally deposited Haversian layers around osteons. Images were taken under polarized light (crossed nicols). **D**, Three-front model indicating a senile ontogenetic status according to [28]. Abbreviations: **AF**, apposition front; **HSF**, Haversian substitution front; RF, resorption front. Scale bar in A = 1 mm; in B, C = 500 µm.

Histology of lesion

There is no sign of ruptured tissue obstructions in the surrounding areas of the dome-shaped lesions (e.g. those expected in bite marks and other mechanical fractures) (Fig.4A-E). The elevated periosteal producing Codman's triangles present reticular primary tissue. In the outer cortex, these structures (lesions) comprise highly vascularized periosteum with radial to reticulated bone (Fig.4.D, E), a condition usually observed in the fast-growing bone of juvenile amniotes [29]. The frontier between senile secondary tissue and the newly formed lesioned tissue is well marked (Fig.4.A-C) and is anomalous (ontogenetically speaking). Therefore, it could only have been formed by a disease. Lesion spreads inwards to the inner cortex (with noticeably increase in local vascularity) (as seen in Fig.2.B and Fig.S1.A) and connects to the medulla.

Affected tissues are not uniform across the bone. At the moment of death, the disease was spreading in distinct stages and areas. This enabled the observation of the graded development of this malady. In the early stages of periosteal alteration, there is a localized decomposition of Haversian canals in the outer cortex (Fig.4.A). Moreover, some radial canals appear from the surface (Fig.4.B). The lesion then expands on the surface and penetrates the cortex in a dominant radial pattern (Fig.4.C). Further, injured bone spreads all over the surrounding surface in radial and reticular patterns (Fig.4.D). Finally, the increase both in the reticular vascularization and resorption cavities give rise to the Codman's triangles (Fig.4.D, E).

Diagnosis of lesion

Since the observed area does not pertain to articulation, spondyloarthropathies (e.g. arthritis) can be discarded [1]. Identification of tuberculosis can be eliminated because tissue anomalies do not comprise solid avascular periosteum [2]. Neoplasm (cancer) can also be discarded because surface eruptions and tissue deformation are not spiculated [1]. Presence of Codman's triangles (CdTr), periosteal and perimedullary alteration and dome-like cortical tissue inflammation connecting CdTr to medulla are indicatives of osteomyelitis [1]. In this work, we followed the definition that osteomyelitis is an infection-driven bone lesion not limited to the external surface [30]. In addition, osseous inflammation and the presence of bone sequestrum characterizes a chronic infection [31] (see Fig.4). The occurrence of concentrated horizontally-deposited dark dots localized strictly on top of CdTr indicates bacterial colonization [25] (see Fig.4.F, G). Notwithstanding, this might have been an effect of secondary infection with bacteria after ulceration [32].

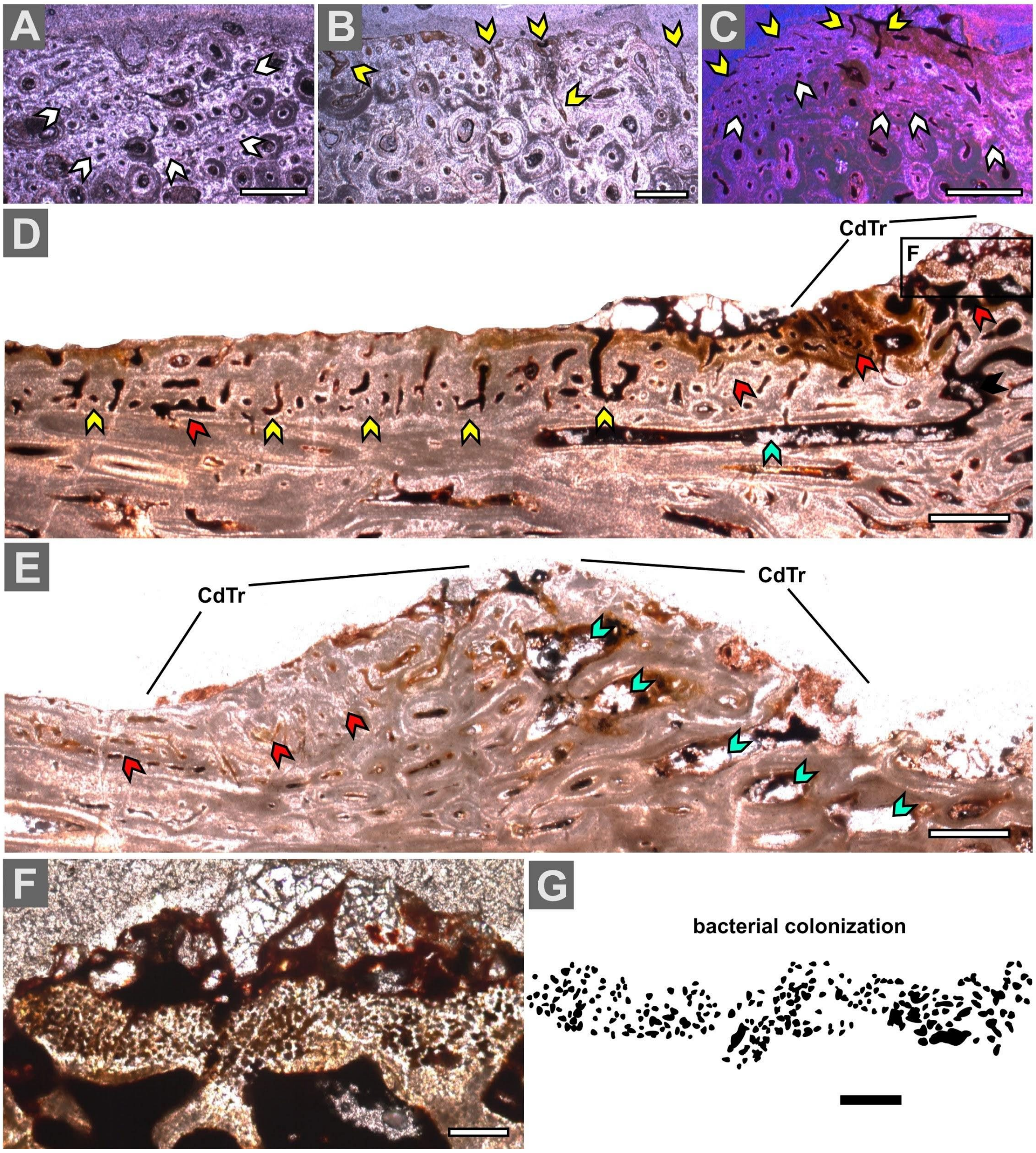

Figure 4. Increasing tissue deformity (bone inflammation) from **A** to **E**. **A,** the early stage of periosteal tissue alteration and bone sequestrum. Localized decomposition of Haversian canals (woven matrix around osteons) in the outer cortex (white arrows). **B**, first radial canals appear from the surface (yellow arrows). **C**, the lesioned area expands on the surface and penetrates the cortex slightly. **D**, lesion spreads all over the surface with dominant Rad (yellow arrows). Some spots containing Ret (red arrows) and ResCav (blue arrows) give rise to a small CdTr. **E**, well-developed CdTr comprises predominantly Ret containing large

ResCav. **F**, grouped iron oxide punctuated structures localized in the CdTr indicate potential secondary infection with bacteria (schematic drawing in **G**). The anteromedial portion in cross section in A-C (polarized light, crossed nicols). The lateral portion in longitudinal view in D and E (polarized light, parallel nicols). Lambda compensator in C. Abbreviations: **CdTr**, Codman's triangle; **Rad**, radial canals; **ResCav**, resorption cavities; **Ret**, reticulated tissue. Scale bar in A, C-E = 500 µm; in B, F, G = 200 µm.

Paleoparasitology

Abundant dark grey to slightly green fusiform shapes (n=64), measuring between 100 and 650 µm in length, and 10-80 µm in width, were observed inside cortical vascular canals and medullary spongiosa of both lesioned area, healthy cortex, and the medulla (Fig.5, 6).

All referred forms have irregular anisotropy (see Fig. 5.D, E), and EDS readings demonstrate they are not chemically uniform, being mostly formed by calcium phosphate with some localized readings of clay minerals and silica (see Fig. S4 in Supplemental information). The morphology of these structures is constant, always showing one subtle more tapered end.

Two dark/more opaque spots, one larger located centrally and one smaller located close to the more tapered end, were observed in several of the analyzed specimens (Fig.6). When visible, these spots were of consistent size and location. Electron microscopy attested their denser nature and distinct chemical composition (Fig. 6.E, F).

The fusiform shapes here described are interpreted as fossilized microorganisms, considered in this work as the promastigote stages of trypanosomatid flagellates (see further in the text). The opaque dots are interpreted as preserved intracellular structures, identified as the nucleus and kinetoplast.

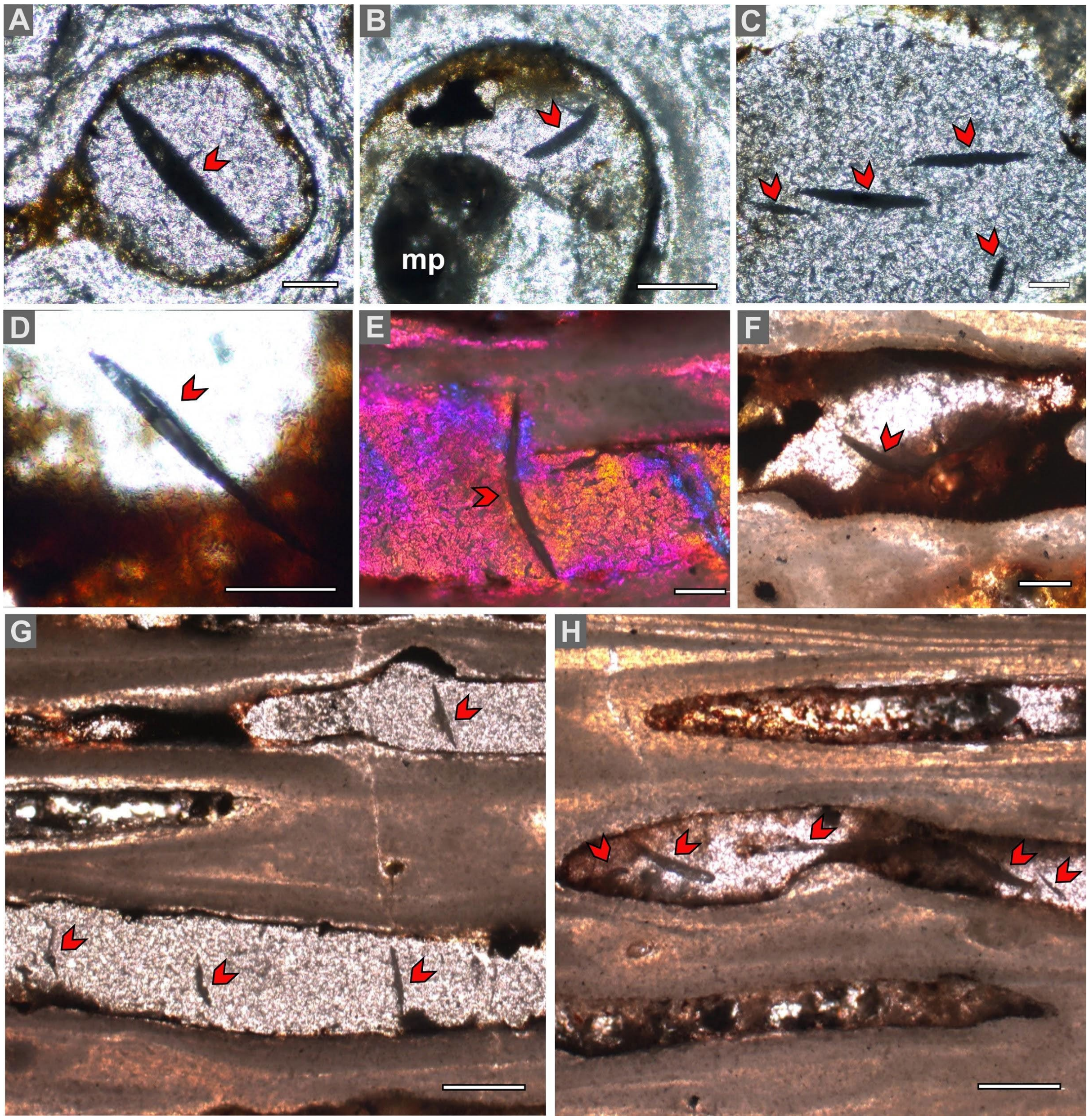

Figure 5. *Brontoleishmania rex* gen. et sp. nov. inside the sauropod vascular canals (A, B, E-H) and bone medulla (C, D). Individuals are indicated by red arrows. Cross-sections in A-D. Longitudinal sections in E-H. Non-filtered light in A-D. Polarized light with crossed nicols in E, and parallel nicols in F-H. Lambda compensator in E. Abbreviation: **mp**, mud pellet. Scale bar in A-D, F = 100 µm; in G, H = 200 µm; in E = 50 µm.

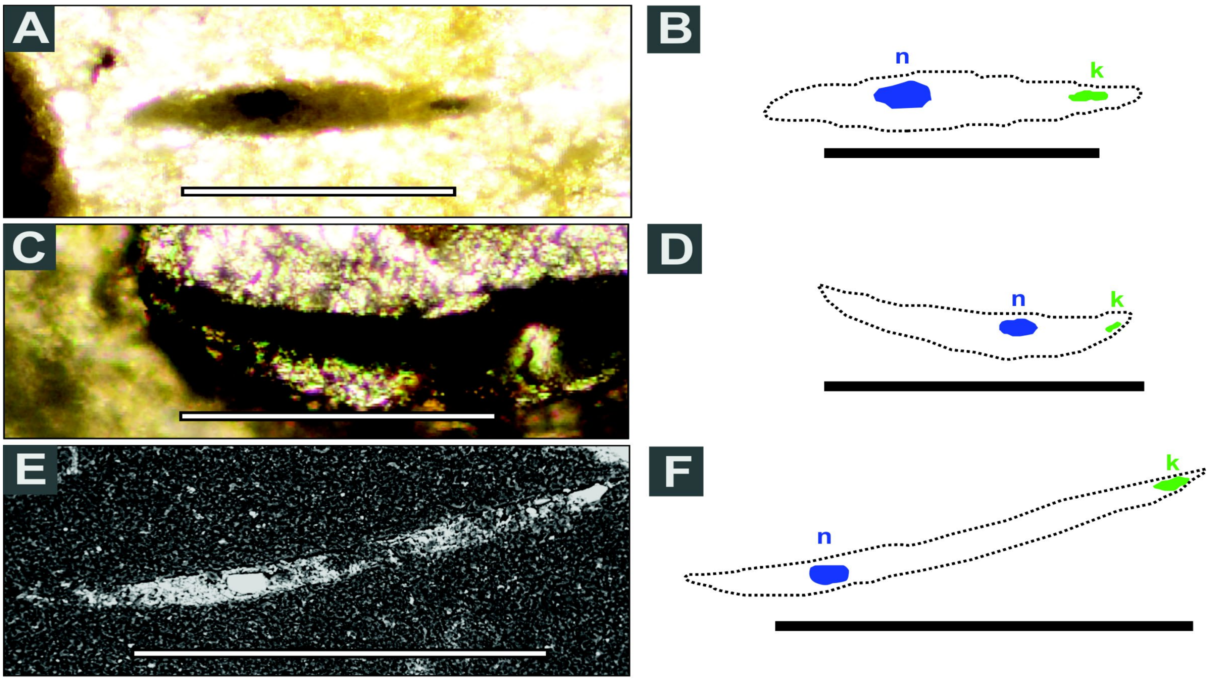

Figure 6. Microanatomy of *Brontoleishmania rex* gen. nov. et sp. nov. parasite of a titanosaur from the Upper Cretaceous Adamantina Formation, Southeast Brazil. Photographs (A, C, E) and their respective schematic drawings (B, D, F). Nucleus and kinetoplast can be seen in A, C, and E. Thin sections under polarized light (parallel nicols) in A, B. Electron microscopy images in E. All cross sections. Abbreviations: **k**, kinetoplast; **n**, nucleus. Scale bar in A-D = 100 µm; in E, F = 500 µm.

The linear regression analysis performed indicated that sample size (n = 64) and the nature of this population fit well in a compatibility model. The resulting equation was: $Y = 6.358 + 0.09884\,X$, where Y is total length, and X is width (both in µm). The relationship between the structure width and total length is mostly compatible with the model ($P < 0.001$; R-sq = 77.38%). The great majority of forms lay between the 95% compatibility intervals. Few lesser compatible elements vary slightly out of these intervals (residual standard deviation = 6.7 µm; Fig. 7).

Data also suggest the proportions of the forms may be correlated with the bone region (cortex/medulla), or available vascular space. Smaller forms were found both in the cortex and the medulla, while the largest individuals (> 500µm) were all found in the medullary region (Fig. 7).

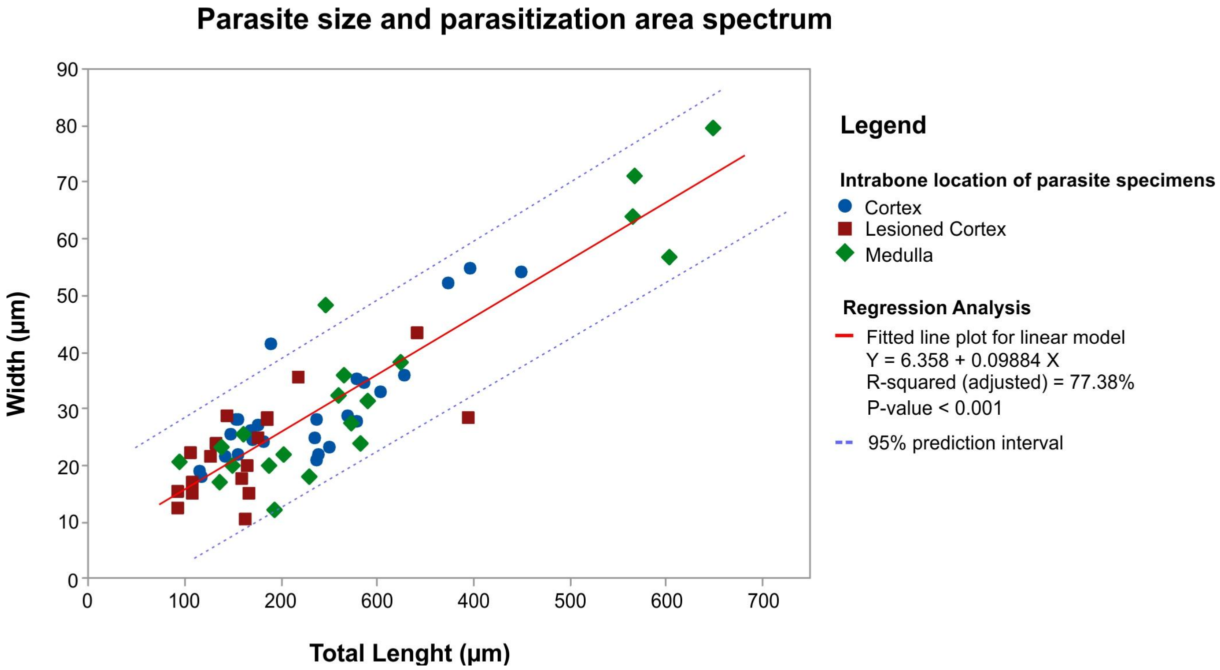

Figure 7. Linear regression analysis relating parasite width and total length (in µm). Point cloud shapes and colors indicate parasitized area spectrum (cortex, medulla, and lesioned cortex). Note that the medulla supports the larger forms and the lesioned cortex is the bone area that mostly restricts parasite dimensions.

Since modern tools used to distinguish recent trypanosomatid species such as molecular or biochemical analyses cannot be applied in this particular case, we decided to describe the fossil form here presented based on its morphology and behavior. The current fossil form is classified in a new collective fossil genus named *Brontoleishmania*.

Brontoleishmania n. gen. (Figs. 5,6,8)

This genus is established as a collective fossil genus for fossil trypanosome-like organisms found *in situ* in non-avian dinosaur tissues.

Brontoleishmania rex n. sp.

Liberforms similar to promastigotes containing nuclei and kinetoplast; ranging from 100-650 µm in length and 10-80 µm in width (Fig.5-7). The nucleus is located in the middle portion of the organism and the kinetoplast is displaced to the anterior end of the cell (Fig.6.A-F). The free flagellum was not preserved.

Diagnosis: The presence of a kinetoplast places *Brontoleishmania* within Kinetoplastea. A small and compact kinetoplast and a single flagellum may place *Brontoleishmania* in the family Trypanosomatidae. The main diagnostic feature of the species is its distinct large size and the association of promastigotes within the bone tissue of an Upper Cretaceous sauropod dinosaur.

Type locality: Ibirá municipality, São Paulo State, uppermost Cretaceous Adamantina Formation, Bauru Basin, Brazil.

Host: The vertebrate host is a sauropod dinosaur. It is not possible to say whether the current parasite was capable of parasitizing other dinosaur species or groups, or if it was a parasite of reptiles in general.

Etymology: *Bronto*, which means 'thunder' in Greek, indirectly refers to sauropods (the 'Thunder Lizards'). *Leishmania* refers to the clade Leishmaniinae. *Rex* is Latin for 'king', referring to the large size of the parasite.

DISCUSSION

Parasite identification

The irregular anisotropy and chemistry of the fusiform structures preserved inside the vascular regions of the fossil bone analyzed, plus the sample morphometry compatibility with an allometric model support the biological origin of the referred structures.

The regularity, size, position and volumetric relationships of the intracellular structures observed are compatible with the nucleus and kinetoplast interpretation. Kinetoplast is a self-replicating organelle present only in Kinetoplastida protozoans [33,34]. The small size and compact nature of the kinetoplast, and the presence of the microorganism inside animal tissue, may indicate an affinity with Trypanosomatidae [35].

On the affinity of *Brontoleishmania* within Trypanosomatidae, we could discard a close relation to *Trypanosoma* and other Juxtaform, forasmuch as *Brontoleishmania* lacks the undulating membrane typical of trypomastigotes and epimastigotes. Based on morphology and behavior, considering the presence of epimastigotes and the capacity to infect a vertebrate host, *Brontoleishmania* may be more closely related to Leishmaniinae *sensu* [36].

When compared to another fossil Leishmaniinae, *Brontoleishmania* essentially differs from *Paleoleishmania* in size and behavior. *Brontoleishmania* (~100-650 µm in length) is much larger than *Paleoleishmania* (5-10 µm in length), even considering the multiple possible morphologies of the latter, and *Brontoleishmania* has promastigote forms infecting vertebrate tissues, behavior not reported for *Paleoleishmania*.

The exceptional preservation of microorganisms and intracellular structures

The occurrence of parasites in paleontological material is rare, especially for the Mesozoic [5,6,11,13]. Most paleoparasitological records consist of helminth eggs and, more rarely, stages of protozoan development preserved either in coprolites or amber [6,11,37]. While most gastrointestinal parasites generally exhibit developmental stages that confer some degree of resistance to their bodies, parasites inhabiting host tissues usually are less prone to fossilization [13]. In the case here described, the exceptional preservation of trypanosomatids possibly occurred through the replication of authigenic minerals [38]. Si, Al, Ca, P, and other elements detected in the SEM/EDS analysis (see supplemental information) would have favored the authigenic mineralization during early diagenesis. In this stage, bone elements come into contact with the geochemical and biological systems leading to tissue decay [39]. Bone decomposition may have provided the ions needed for authigenic mineralization, along with the mineral grains introduced before burial, under the influence of microbial activity.

As for the preservation of intracellular structures, there are precedents in the fossil record for even older fossils that can help us understand what might have occurred in this particular case [40]. A suitable model to explain the observed preservation is the early mineralization of the cytoplasm, before the nucleus and kinetoplast decay. The decay of these intracellular structures, in turn, would have left a void, later filled by diagenetic cement [40]. Both, the nucleus and kinetoplast are structures with condensed DNA, therefore chemically similar. This would explain the fact they were similarly preserved.

Parasite paleobiology, adaptations, and possible further affinities

Fossil trypanosomatids have been reported in the Lower Cretaceous of Myanmar [11,41,42] and the Miocene-Oligocene of Dominican Republic [43,44] in the form of amastigotes, promastigotes, paramastigotes, and trypomastigotes preserved within invertebrate hosts fossilized in amber. Although [5] have described lizard-like *Leishmania*-infected blood cells associated with fossil Phlebotominae flies, trypanosomatids were never reported preserved inside paleovertebrate hosts. The current discovery is, therefore, the first direct evidence of a fossil trypanosomatid preserved inside a vertebrate. It is also the oldest record of Trypanosomatidae in the New World. This finding has implications both for the biogeographic and evolutionary understanding of trypanosomatid protozoans and the maladies caused by them.

Modern trypanosomatids parasites of vertebrates, such as *Leishmania*, *Endotrypanum, Porcisia*, and *Trypanosoma* are all dixenous. They comprise vector-borne species whose life-cycle depends on an invertebrate host, which is also the vector and a vertebrate host. The common ancestor of all dixenous forms, however, is considered to have been monoxenous and dixeny may have evolved at least three times independently in the group [45,46]. *Leishmania* monoxenous common ancestor, for example, is estimated to have lived between 90 and 100 million years ago, during the Early Cretaceous [47–49], which makes the Cretaceous period an interesting time to study the evolution of dixeny in this particular clade.

Since no invertebrate host of *Brontoleishmania rex* is preserved, we cannot confirm whether the studied species was dixenous or monoxenous. However, the monoxeny hypothesis is favored for the abundance of the promastigotes preserved inside the vertebrate host tissue analyzed. Some caution is necessary, however, as we do not yet fully understand the biology and behavior of different species of trypanosomatids, even more about extinct forms. In modern mammalian *Leishmania*, for example, the promastigote stage, generally restricted to the invertebrate host [50], has already been reported in vertebrates [51–53]. Furthermore, in *Sauroleishmania* (subgenera of *Leishmania* which affects modern reptiles), both amastigote and promastigote forms can be commonly found within the vertebrate host [54–57]. In the current case, we were unable to confirm the presence of amastigote forms in the studied sample, although future more comprehensive analyses must be performed.

Monoxenous Leishmaniinae, despite known as insect parasites, have been recurrently reported infecting vertebrates [46,58–64]. These reports include very distinct situations, but generally, the vertebrate host is immunocompromised in some way. These findings have led authors to assume the referred monoxenous forms may be the key to understand the evolution of a dixenous life cycle in Leishmaniinae [46,49]. Indeed adaptations to withstand high temperatures were identified in *Leptomonas seymouri*, and pointed out by the authors as responsible for its capacity to infect homeothermic vertebrates [46]. However, the evolution of dixeny requires another step: surviving the immune system of the vertebrate. This is probably the reason why *L. seymouri* can only infect immunosuppressed vertebrates at its current evolutionary state [46].

Considering purely the behavior of *Brontoleishmania,* since we do not have molecular or biochemical information, one can suggest a putative affinity to monoxenous monogenic Leishmaniinae forms, either basal to the dixenous clade occupied by *Leishmania*, *Endotrypanum*, and *Porcisia* or closely related to Crithidiatae, particularly *Leptomonas*. It is complicated and very tenuous to classify fossil organisms at any greater resolution, but at least, it is plausible to assume similar adaptations to those that allow some monoxenous Leishmaniinae to infect vertebrates nowadays were present in the fossil form reported in this case. Titanosaurs are estimated to have had a body temperature around 38ºC [65,66], so for the parasite to survive, mutations analogous to those highlighted by [46] are fundamentally necessary to *Brontoleishmania*.

The parasite large size

The large proportions of *Brontoleishmania* are very peculiar since modern trypanosomatids are relatively small cells ranging in size from ca. 5 to 70 μm in length and 0.75 to 50 μm in width [67]. Despite the median length and width of individuals attributed to *Brontoleishmania* is 188 μm and 25 μm respectively, and the mean length and width are 232 μm and 29 μm respectively, the largest specimen of the fossil form exceeds 600 μm in length and 70 μm in width, which is quite above expectations.

Size in parasitic microorganisms undergoes selective pressure, regulated mainly by two properties: 1) the physiology of the organism and 2) the host or vector environment. The first is an intrinsic constraint, while the second represents extrinsic selective pressures from a host [67].

Thinking of physiologically possible sizes for single-celled beings, specifically protozoans, we can take modern examples as a comparative parameter. Currently, the largest living parasitic protozoa recorded is *Balantidium coli*, a Ciliate measuring up to about 150 μm [68]. Free-living protozoans, in turn, are known to attain very large sizes, up to 2000 μm in non-testate species. Using the actualism logic, *Brontoleishmania* size is not a problem regarding intrinsic constraints.

Relative to extrinsic constraints, the caliber of the host's vascular environment and the size of its blood cells are the main limiting factors for trypanosomatids [67]. Trypanosomatids need to fit through the capillaries of the host and some must be compatible with the host's erythrocyte dimensions [67]. Since *Brontoleishmania* is not an erythrocyte parasite, the bloodstream caliber may be the main limiting factor for this organism. *Brontoleishmania* host's cortical vascularization (= canal caliber *sensu* [17]) presents a $Can_{min} = 26$ µm and a $Can_{harmean} = 106$ µm. For comparison, one of the largest extant land animals, *Elephas maximus*, has a $Can_{min} = 6$ µm and a $Can_{harmean} = 34$ µm (based on fibula histology from [69]). In fact, the current canal caliber measurement is also greater than any value presented by [17] or [18], the biological implications of which need to be carefully interpreted in the future. Moreover, it is interesting to note, the largest *Brontoleishmania* individuals (i.e. >500 µm in length and >55 µm in width) were all located in the cancellous bone (medulla) (see Fig.7), indicating a size selection linked to vascular space also within the population. Finally, considering the extrinsic selection conditions, it is absolutely feasible that extinct species of trypanosomatids could have been selected to attain larger sizes than the living ones.

Parasite Infection

Regarding the route of infection, rinsing wounds or sores with water contaminated is a possibility, since some trypanosomatids parasitizing the alimentary tracts of insects can be found free-living in the immediate environment [70,71]. Species of Crithidia, for example, normally found in Culicidae undergo a free-living stage in water, as well as *Herpetomonas* spp. infecting Drosophilidae, Phoridae, and Muscidae [41,70].

An alternative hypothesis is transmission through a hematophagous host. Using molecular techniques, a form similar to *Herpetomonas ztiplika*, a gut inhabitant Ceratopogonidae, was found infecting Egyptian rats. The transmission could have happened during the insect blood-feeding [60]. There are also some cases of non-*Leishmania* Leishmaniinae infecting wild Phlebotominae [72–74], and *L. seymouri* was also experimentally found to persist for several days in two species of *Phlebotomus* spp. [46].

All transmission forms reported above are possible since the ill titanosaur analyzed presented an open wound on the lower leg (diagnosed through bone inflammation histology), a possible entry for the parasite; and both families of hematophagous insects mentioned were already present in the Upper Cretaceous [4,41].

Biogeographic implications

Origin and evolution of dixenous parasitism in Leishmaniinae are the sources of an ongoing debate with conflicts between phylogenetic data and historical biogeography reconstructions. Multiple hypotheses have been proposed suggesting different geographic origins and distinct migration times and routes [47–49,75–78]. *Brontoleishmania* discovery may contribute to reinforcing a Gondwanan origin of dixenous parasitism in the Leishmaniinae, since it corresponds to an extinct clade, possibly basal to dixenous forms. As the classification based on morphology and behavior is very tenuous, caution is needed until further discoveries clarify the current interpretation.

Osteomyelitis histological development

Osteomyelitis identification has been historically neglected in dinosaurs due to its rarity in modern-day archosaurs [8]. However, recent findings [3,9] and reanalyses of specimens (e.g. [79] *sensu* [3]) demonstrated this infirmity occurred at least in sauropodomorphs. Unfortunately, previous studies focused on diagnoses strictly based on macroscopical inspections, x-ray charts, and (rarely) tomographies [1,3,9,10]. Here we describe for the first time different stages of bone sequestrum (inflammation) in detail and the histological development of the disease. There is a gradual increase in vascularization and a decrease in bone tissue density during infection stages. Finally, we could establish five histological developmental stages for chronic osteomyelitis:

1) In the early stages of periosteal alteration and secondary bone sequestrum, there is a localized decomposition of Haversian canals in the outer cortex.
2) A few radial canals appear from the surface, perpendicularly.
3) The lesion expands along the surface and penetrates the cortex in a dominant radial pattern.
4) Injured bone proliferates all over the surrounding surface in radial and reticular patterns.
5) Finally, the increase both in the reticular vascularization and resorption cavities results in the rise of Codman’s triangles (CdTr). Additionally, the occurrence of concentrated

horizontally-deposited oxidized bacterial colony traces on CdTr indicates there might have been ulceration and aerial exposure.

Relationship between paleopathology and paleoparasitology

Some Leishmaniinae infections can cause clinical manifestations [80]. The expression of the disease depends on a complex interaction between parasite particularities and host immune responses [80,81]. Some species can cause both systemic and cutaneous infection, while others manifest visceralization [32,81,82]. This may be due to the evolutionary characteristics of each species, which gives them greater affinity and ability to target the skin or other organs [83].

Initial observation suggests that the superficial lesions and elliptical nodules observed in the sauropod LPP-PV-0043 would indicate diffuse cutaneous leishmaniasis [31,32]. However, it was demonstrated that the lesion in this specimen spreads all over to the medulla (Fig.2,4), alongside parasitic forms (Fig.5,8). Added to the presence of *in situ* parasites, infection in the bone marrow is a potential indicator of a visceral leishmaniasis-like condition [32]. There are cases where visceral leishmaniasis develop post-kala-azar dermal leishmaniasis (PKDL) [32]. Furthermore, dermal ulceration may occur in this syndrome [32], as also indicated by the nodular lesions seen in LPP-PV-0043 (Fig.1,2,4). A manifestation of PKDL, or some similar and yet unknown disease, is a potential diagnosis for the case of study. It is unclear whether the chronic osteomyelitis observed in the analyzed specimen was favored or induced by the protozoan infestation described. Pathology could have developed previously by an infestation of other pathogenic organism. Two hypotheses are plausible:

1) Chronic osteomyelitis could have been induced by *Brontoleishmania rex* gen. et sp. nov. infestation. It is possible since modern cases of leishmaniasis occasionally occur associated with chronic osteomyelitis [84–87], essentially in cutaneous and visceral manifestations of the former. However, the latter is usually caused by members of the *Leishmania* genus [84–87]. Nevertheless, there is a recent study reporting non-*Leishmania*, *Crithidia*-related parasites causing pathologies similar to kala-azar in Northeast Brazil [82].

2) *Brontoleishmania rex* gen. et sp. nov. could have developed in a co-infestation scenario. As already mentioned, extant *Leptomonas* infections in vertebrates are usually related to immunosuppressed hosts/individuals, either by a virus or other Leishmaniinae. Hence, it is

possible that the titanosaur developed its pathologies previously from another source. The weakened immune system may have favored the co-infestation.

Despite several records in literature, there is no similar osteohistological description of such pathology, and modern cases generally analyze soft tissues or demineralized bone tissue [87–89], which limits our comparison. Very few is known from non-avian dinosaur immunology to estimate infection duration. However, there is a case study on human patients in the Brazilian Amazon who developed similar pathologies within five months [88]. These latter were contaminated with *Leishmania amazonensis* and presented chronic osteomyelitis associated with cutaneous leishmaniasis. In the case of PKDL, affected individuals develop such deformities in months or years after initial infection with visceral leishmaniasis. Putative life reconstructions of the diseased dinosaur and its parasite are depicted in Fig.8.

Figure 8. A, Life reconstruction of the titanosaur LPP-PV-0043 from the Upper Cretaceous Adamantina Formation, Southeast Brazil. **B**, three-dimensional life reconstruction of *Brontoleishmania rex* gen. et sp. nov. inside sauropod vascular canals (artificial coloration). Artist: Hugo Cafasso.

CONCLUSIONS

It is presented here the first evidence of a vertebrate host of a trypanosomatid-like parasite in the fossil record. This includes the presence of several elements of a new parasitic form, *Brontoleishmania rex* gen. et sp. nov., preserved inside the vascular canals and bone medulla of a senile titanosaur sauropod. Such a record preserved in histological material indicates some dinosaurs were parasitized by a monoxenous form of Leishmaniinae trypanosomatids during the Late Cretaceous of the Southern Hemisphere. The parasite in question may have evolved alongside sauropodomorph dinosaurs and possibly had adaptations to their physiology, with implications to the evolution of dixeny.

This research opened a new possibility for paleontological studies by linking the fields of parasitology, pathology, and histology. The titanosaur analyzed presented chronic osteomyelitis with several characteristics of current leishmaniasis. Elliptical ulcerations, alike to modern-day kala-azar, were present all throughout the bone. Bone inflamation was either caused by the referred parasite or facilitated its infestation. Chronic osteomyelytis histological development was described in detail for the first time.

Finally, we lowered the earliest occurrence of Trypanosomatidae in the New World from the Oligocene-Miocene of Dominican Republic to the Upper Cretaceous of Brazil and perhaps reinforced the hypothesis of a Gondwanan origin for dixenous parasitism in Leishmaniinae. This research contributes substantially to understanding the histology of pathological bone disease, macroevolution and ecology of Leishmaniinae-type parasites, and the early history of tropical diseases.

ACKNOWLEDGMENTS

We would like to acknowledge Paulo Saldiva, Milena Picka Santos, Ellison Cardoso, and the rest of the FM-USP team for conducting fossil tomography and providing nice comments on the material. To Renata Monteiro, for providing insights into osteomyelitis. To Fernanda Aníbal, for her observations regarding parasites. To Erica Tonetto, for conducting electron microscopy analyses. To David Soeiro and Dawid Surmik for kindly accepting to read and comment on a prior version of this manuscript. To Kai Casper, for clarifying the methodology of measuring vascular canal calibers. To Luciana B. Fernandes, for the Corel Draw license. To Paulo, for preparing the thin sections. To *Colecionadores de Ossos*™ and their crowdfunders, for financing thin sections. Author's scholarships and financial aid were provided by the Brazilian National Council for Scientific and Technological Development (CNPq 131777/2018-1) (T.A.), the Brazilian Coordination for the Improvement of Higher Education Personnel (CAPES) (A.M.G. and C.S.I.N.) - Finance Code 001, and FAPESP 2016/20927-0 'Modern accumulation studies and fossil bioclast studies in continental and coastal environments' (F.R.B.).

AUTHOR CONTRIBUTIONS

Dinosaur specimen discovery and preparation by MAF and AMG. Dinosaur taxonomy by TA and AMG. Dinosaur histology, pathology and CT-Scan analysis by TA. Taphonomy by FRB and TA. Parasitology by AMG and CSIN. Earlier paleoparasite discovery by FSRB. Statistical analysis by TA. Wrote by TA, AMG, CSIN, MAF and FRB.

DECLARATION OF INTERESTS

The authors declare no competing interests.

Bibliography

1. Rothschild BM, Martin LD. Skeletal Impact of Disease. New Mexico Museum of Natural History and Science; 2006. Available: https://market.android.com/details?id=book-AGfmCQAAQBAJ
2. Surmik D, Szczygielski T, Janiszewska K, Rothschild BM. Tuberculosis-like respiratory infection in 245-million-year-old marine reptile suggested by bone pathologies. R Soc Open Sci. 2018;5: 180225. doi:10.1098/rsos.180225
3. Xing L, Rothschild BM, Randolph-Quinney PS, Wang Y, Parkinson AH, Ran H. Possible bite-induced abscess and osteomyelitis in Lufengosaurus (Dinosauria: sauropodomorph) from the Lower Jurassic of the Yimen Basin, China. Sci Rep. 2018;8: 5045. doi:10.1038/s41598-018-23451-x
4. Poinar G Jr. Leptoconops nosopheris sp. n.(Diptera: Ceratopogonidae) and Paleotrypanosoma burmanicus gen. n., sp. n.(Kinetoplastida: Trypanosomatidae), a biting midge-trypanosome vector association from the Early Cretaceous. Mem Inst Oswaldo Cruz. 2008;103: 468–471. Available: http://www.scielo.br/scielo.php?pid=S0074-02762008000500010&script=sci_arttext&tlng=es
5. Poinar G, Poinar R. Evidence of Vector-Borne Disease of Early Cretaceous Reptiles. Vector-Borne and Zoonotic Diseases. 2004;4: 281–284. doi:10.1089/vbz.2004.4.281
6. Dentzien-Dias PC, Poinar G Jr, de Figueiredo AEQ, Pacheco ACL, Horn BLD, Schultz CL. Tapeworm eggs in a 270 million-year-old shark coprolite. PLoS One. 2013;8: e55007. doi:10.1371/journal.pone.0055007
7. Ebert D, Herre EA. The evolution of parasitic diseases. Parasitol Today. 1996;12: 96–101. doi:10.1016/0169-4758(96)80668-5
8. Wolff EDS, Salisbury SW, Horner JR, Varricchio DJ. Common avian infection plagued the tyrant dinosaurs. PLoS One. 2009;4: e7288. doi:10.1371/journal.pone.0007288
9. García RA, Cerda IA, Heller M, Rothschild BM, Zurriaguz V. The first evidence of osteomyelitis in a sauropod dinosaur. Lethaia. 2017;50: 227–236. doi:10.1111/let.12189
10. Barbosa FH de S, Marinho T da S, Iori FV, Paschoa L da S. A case of infection in an Aeolosaurini (Sauropoda) dinosaur from the Upper Cretaceous of São Paulo, southeastern Brazil, and the impact on its life. Cretaceous Res. 2018. doi:10.1016/j.cretres.2018.12.004
11. Poinar G Jr, Poinar R. Paleoleishmania proterus n. gen., n. sp., (Trypanosomatidae: Kinetoplastida) from Cretaceous Burmese amber. Protist. 2004;155: 305–310. doi:10.1078/1434461041844259
12. Poinar G. A primitive triatomine bug, Paleotriatoma metaxytaxa gen. et sp. nov. (Hemiptera: Reduviidae: Triatominae), in mid-Cretaceous amber from northern Myanmar. Cretaceous Res. 2019;93: 90–97. doi:10.1016/j.cretres.2018.09.004
13. Poinar G Jr, Boucot AJ. Evidence of intestinal parasites of dinosaurs. Parasitology. 2006;133: 245–249. doi:10.1017/S0031182006000138

14. Fedorov A, Beichel R, Kalpathy-Cramer J, Finet J, Fillion-Robin J-C, Pujol S, et al. 3D Slicer as an image computing platform for the Quantitative Imaging Network. Magn Reson Imaging. 2012;30: 1323–1341. doi:10.1016/j.mri.2012.05.001

15. Lamm E-T. Preparation and Sectioning of Specimens. Bone Histology of Fossil Tetrapods. University of California Press; 2013. doi:10.1525/california/9780520273528.003.0004

16. Padian K, Lamm E-T. Bone Histology of Fossil Tetrapods: Advancing Methods, Analysis, and Interpretation. University of California Press; 2013. Available: https://market.android.com/details?id=book-EBVNmk1nm6MC

17. Huttenlocker AK, Farmer CG. Bone Microvasculature Tracks Red Blood Cell Size Diminution in Triassic Mammal and Dinosaur Forerunners. Curr Biol. 2017;27: 48–54. doi:10.1016/j.cub.2016.10.012

18. Fleischle CV, Sander PM, Wintrich T, Caspar KR. Hematological convergence between Mesozoic marine reptiles (Sauropterygia) and extant aquatic amniotes elucidates diving adaptations in plesiosaurs. PeerJ. 2019;7: e8022. doi:10.7717/peerj.8022

19. Schneider CA, Rasband WS, Eliceiri KW. NIH Image to ImageJ: 25 years of image analysis. Nat Methods. 2012;9: 671–675. Available: https://www.ncbi.nlm.nih.gov/pubmed/22930834

20. Ghilardi AM, Aureliano T, Duque RRC, Fernandes MA, Barreto AMF, Chinsamy A. A new titanosaur from the Lower Cretaceous of Brazil. Cretaceous Res. 2016;67: 16–24. doi:10.1016/j.cretres.2016.07.001

21. García RA, Salgado L, Fernández MS, Cerda IA, Carabajal AP, Otero A, et al. Paleobiology of Titanosaurs: Reproduction, Development, Histology, Pneumaticity, Locomotion and Neuroanatomy from the South American Fossil Record. Ameghiniana. 2015;52: 29–68. doi:10.5710/AMGH.16.07.2014.829

22. Stein K, Csiki Z, Rogers KC, Weishampel DB, Redelstorff R, Carballido JL, et al. Small body size and extreme cortical bone remodeling indicate phyletic dwarfism in Magyarosaurus dacus (Sauropoda: Titanosauria). Proc Natl Acad Sci U S A. 2010;107: 9258–9263. doi:10.1073/pnas.1000781107

23. Klein N, Sander PM, Stein K, Le Loeuff J, Carballido JL, Buffetaut E. Modified laminar bone in Ampelosaurus atacis and other Titanosaurs (Sauropoda): implications for life history and physiology. PLoS One. 2012;7: e36907. doi:10.1371/journal.pone.0036907

24. Aureliano T, Ghilardi AM, Buck PV, Fabbri M, Samathi A, Delcourt R, et al. Semi-aquatic adaptations in a spinosaur from the Lower Cretaceous of Brazil. Cretaceous Res. 2018;90: 283–295. doi:10.1016/j.cretres.2018.04.024

25. Pfretzschner H-U. Pyrite in fossil bone. njgpa. 2001;220: 1–23. doi:10.1127/njgpa/220/2001/1

26. Curry Rogers K, Kulik Z. Osteohistology of Rapetosaurus krausei (Sauropoda: Titanosauria) from the Upper Cretaceous of Madagascar. J Vert Paleontol. 2018; 1–24. doi:10.1080/02724634.2018.1493689

27. Klein N, Sander M. Ontogenetic stages in the long bone histology of sauropod dinosaurs. Paleobiology. 2008;34: 247–263. doi:10.1666/0094-8373(2008)034[0247:OSITLB]2.0.CO;2

28. Mitchell J, Sander PM. The three-front model: a developmental explanation of long bone diaphyseal histology of Sauropoda. Biol J Linn Soc Lond. 2014;112: 765–781. doi:10.1111/bij.12324

29. Huttenlocker AK, Woodward HN, Hall BK. The Biology of Bone. Bone Histology of Fossil Tetrapods. University of California Press; 2013. doi:10.1525/california/9780520273528.003.0002

30. Rothschild BM, Schultze H-P, Pellegrini R. Herpetological Osteopathology: Annotated Bibliography of Amphibians and Reptiles. Springer Science & Business Media; 2012. Available: https://market.android.com/details?id=book-NqVYBAegmA0C

31. Costa AAUML da, Saldanha ACR, Corbett CEP, Barral AMP, Bezerril ACR, Others. Alterações ósseas causadas por Leishmania amazonensis na leishmaniose cutânea difusa (LCD). 2009. Available: https://www.arca.fiocruz.br/handle/icict/9734

32. The Institute for International Cooperation in Animal Biologics and the Center for Food Security and Public Health. Leishmaniasis (cutaneous and visceral). Ames, Iowa: College of Veterinary Medicine, Iowa State University. 2017. Available: http://www.cfsph.iastate.edu/Factsheets/pdfs/leishmaniasis.pdf

33. Shapiro TA, Englund PT. The structure and replication of kinetoplast DNA. Annu Rev Microbiol. 1995;49: 117–143. doi:10.1146/annurev.mi.49.100195.001001

34. Shlomai J. The structure and replication of kinetoplast DNA. Curr Mol Med. 2004;4: 623–647. doi:10.2174/1566524043360096

35. Dwyer DM. Biology of the Kinetoplastida. Am J Trop Med Hyg. 1977;26: 832–833. doi:10.4269/ajtmh.1977.26.832

36. Maslov DA, Votýpka J, Yurchenko V, Lukeš J. Diversity and phylogeny of insect trypanosomatids: all that is hidden shall be revealed. Trends Parasitol. 2013;29: 43–52. doi:10.1016/j.pt.2012.11.001

37. Leung TLF. Fossils of parasites: what can the fossil record tell us about the evolution of parasitism? Biological Reviews. 2015. pp. 410–430. doi:10.1111/brv.12238

38. Briggs DEG. THE ROLE OF DECAY AND MINERALIZATION IN THE PRESERVATION OF SOFT-BODIED FOSSILS. Annu Rev Earth Planet Sci. 2003;31: 275–301. doi:10.1146/annurev.earth.31.100901.144746

39. Keenan SW. From bone to fossil: A review of the diagenesis of bioapatite. Am Mineral. 2016;101: 1943–1951. doi:10.2138/am-2016-5737

40. Yin Z, Cunningham JA, Vargas K, Bengtson S, Zhu M, Donoghue PCJ. Nuclei and nucleoli in embryo-like fossils from the Ediacaran Weng’an Biota. Precambrian Res. 2017;301: 145–151. doi:10.1016/j.precamres.2017.08.009

41. Poinar G Jr. Early Cretaceous trypanosomatids associated with fossil sand fly larvae in Burmese amber. Mem Inst Oswaldo Cruz. 2007;102: 635–637. doi:10.1590/s0074-02762007005000070

42. Poinar G Jr. Leptoconops nosopheris sp. n. (Diptera: Ceratopogonidae) and Paleotrypanosoma burmanicus gen. n., sp. n. (Kinetoplastida: Trypanosomatidae), a biting midge--trypanosome vector association from the Early Cretaceous. Mem Inst Oswaldo Cruz. 2008;103: 468–471. doi:10.1590/s0074-02762008000500010

43. Poinar G Jr. Plasmodium dominicana n. sp. (Plasmodiidae: Haemospororida) from Tertiary Dominican amber. Syst Parasitol. 2005;61: 47–52. doi:10.1007/s11230-004-6354-6

44. Poinar G Jr. Lutzomyia adiketis sp. n. (Diptera: Phlebotomidae), a vector of Paleoleishmania neotropicum sp. n. (Kinetoplastida: Trypanosomatidae) in Dominican amber. Parasit Vectors. 2008;1: 22. doi:10.1186/1756-3305-1-22

45. Kaufer A, Ellis J, Stark D, Barratt J. The evolution of trypanosomatid taxonomy. Parasit Vectors. 2017;10: 287. doi:10.1186/s13071-017-2204-7

46. Kraeva N, Butenko A, Hlaváčová J, Kostygov A, Myškova J, Grybchuk D, et al. Leptomonas seymouri: Adaptations to the Dixenous Life Cycle Analyzed by Genome Sequencing, Transcriptome Profiling and Co-infection with Leishmania donovani. PLoS Pathog. 2015;11: e1005127. doi:10.1371/journal.ppat.1005127

47. Yurchenko VY, Lukes J, Jirku M, Zeledón R, Maslov DA. Leptomonas costaricensis sp. n. (Kinetoplastea: Trypanosomatidae), a member of the novel phylogenetic group of insect trypanosomatids closely related to the genus Leishmania. Parasitology. 2006;133: 537–546. doi:10.1017/S0031182006000746

48. Harkins KM, Schwartz RS, Cartwright RA, Stone AC. Phylogenomic reconstruction supports supercontinent origins for Leishmania. Infect Genet Evol. 2016;38: 101–109. doi:10.1016/j.meegid.2015.11.030

49. Barratt J, Kaufer A, Peters B, Craig D, Lawrence A, Roberts T, et al. Isolation of novel trypanosomatid, Zelonia australiensis sp. nov.(Kinetoplastida: Trypanosomatidae) provides support for a Gondwanan origin of dixenous parasitism in the Leishmaniinae. PLoS Negl Trop Dis. 2017;11: e0005215. Available: https://journals.plos.org/plosntds/article?id=10.1371/journal.pntd.0005215

50. Rey L. REY L. Parasitologia: parasitos e doenças parasitárias do homem nos trópicos ocidentais. Rio de Janeiro: Guanabara Koogan; 2011.

51. Henriques C, de Souza W. Redistribution of plasma-membrane surface molecules during formation of the Leishmania amazonensis-containing parasitophorous vacuole. Parasitol Res. 2000;86: 215–225. Available: https://www.ncbi.nlm.nih.gov/pubmed/10726992

52. Corrêa JR, Soares MJ. Leishmania (Viannia) lainsoni: occurrence of intracellular promastigote forms in vivo and in vitro. Mem Inst Oswaldo Cruz. 2006;101: 923–924. Available: https://www.ncbi.nlm.nih.gov/pubmed/17293989

53. Hamad I, Forestier C-L, Peeters M, Delaporte E, Raoult D, Bittar F. Wild gorillas as a potential

reservoir of Leishmania major. J Infect Dis. 2015;211: 267–273. doi:10.1093/infdis/jiu380

54. Daboul MW. Promastigote existence in infected lesions of cutaneous leishmaniasis. Journal of General Practice. 2014. Available: https://www.researchgate.net/profile/Mohammed_Daboul/publication/280823808_Promastigote_Existence_in_Infected_Lesions_of_Cutaneous_Leishmaniasis/links/564e2f6d08aefe619b0faf8c/Promastigote-Existence-in-Infected-Lesions-of-Cutaneous-Leishmaniasis.pdf

55. Bates PA. Transmission of Leishmania metacyclic promastigotes by phlebotomine sand flies. Int J Parasitol. 2007;37: 1097–1106. doi:10.1016/j.ijpara.2007.04.003

56. Telford SR. Hemoparasites of the Reptilia: Color Atlas and Text. 2008. CRC Press, Taylor & Francis Group, Boca Raton, Florida, USA Google Scholar;

57. Novo SPC, Leles D, Bianucci R, Araujo A. Leishmania tarentolae molecular signatures in a 300 hundred-years-old human Brazilian mummy. Parasit Vectors. 2015;8: 72. doi:10.1186/s13071-015-0666-z

58. Jimenez MI, Lopez-Velez R, Molina R, Canavate C. HIV co-infection with a currently non-pathogenic flagellate. Lancet. 1996. Available: https://www.thelancet.com/journals/lancet/article/PIIS0140-6736(96)90441-9/fulltext

59. Pacheco RS, Marzochi MC, Pires MQ, Brito CM, Madeira M de F, Barbosa-Santos EG. Parasite genotypically related to a monoxenous trypanosomatid of dog’s flea causing opportunistic infection in an HIV positive patient. Mem Inst Oswaldo Cruz. 1998;93: 531–537. doi:10.1590/s0074-02761998000400021

60. Podlipaev SA, Sturm NR, Fiala I, Fernandes O, Westenberger SJ, Dollet M, et al. Diversity of Insect Trypanosomatids Assessed from the Spliced Leader RNA and 5s rRNA Genes and Intergenic Regions1. J Eukaryot Microbiol. 2004;51: 283–290. doi:10.1111/j.1550-7408.2004.tb00568.x

61. Morio F, Reynes J, Dollet M, Pratlong F, Dedet J-P, Ravel C. Isolation of a protozoan parasite genetically related to the insect trypanosomatid Herpetomonas samuelpessoai from a human immunodeficiency virus-positive patient. J Clin Microbiol. 2008;46: 3845–3847. doi:10.1128/JCM.01098-08

62. Srivastava P, Prajapati VK, Vanaerschot M, Van der Auwera G, Dujardin JC, Sundar S. Detection of Leptomonas sp. parasites in clinical isolates of Kala-azar patients from India. Infect Genet Evol. 2010;10: 1145–1150. doi:10.1016/j.meegid.2010.07.009

63. Ghosh S, Banerjee P, Sarkar A, Datta S, Chatterjee M. Coinfection of Leptomonas seymouri and Leishmania donovani in Indian leishmaniasis. J Clin Microbiol. 2012;50: 2774–2778. doi:10.1128/JCM.00966-12

64. Selvapandiyan A, Ahuja K, Puri N, Krishnan A. Implications of co-infection of Leptomonas in visceral leishmaniasis in India. Parasitology. 2015;142: 1657–1662. doi:10.1017/S0031182015001389

65. Eagle RA, Tütken T, Martin TS, Tripati AK, Fricke HC, Connely M, et al. Dinosaur

body temperatures determined from isotopic (^{13}C-^{18}O) ordering in fossil biominerals. Science. 2011;333: 443–445. doi:10.1126/science.1206196

66. Eagle RA, Enriquez M, Grellet-Tinner G, Pérez-Huerta A, Hu D, Tütken T, et al. Isotopic ordering in eggshells reflects body temperatures and suggests differing thermophysiology in two Cretaceous dinosaurs. Nat Commun. 2015;6: 8296. doi:10.1038/ncomms9296

67. Wheeler RJ, Gluenz E, Gull K. The limits on trypanosomatid morphological diversity. PLoS One. 2013;8: e79581. doi:10.1371/journal.pone.0079581

68. Chalmers RM. Chapter Fifteen - Balantidium coli. In: Percival SL, Yates MV, Williams DW, Chalmers RM, Gray NF, editors. Microbiology of Waterborne Diseases (Second Edition). London: Academic Press; 2014. pp. 277–286. doi:10.1016/B978-0-12-415846-7.00015-9

69. Nganvongpanit K, Siengdee P, Buddhachat K, Brown JL, Klinhom S, Pitakarnnop T, et al. Anatomy, histology and elemental profile of long bones and ribs of the Asian elephant (Elephas maximus). Anat Sci Int. 2017;92: 554–568. doi:10.1007/s12565-016-0361-y

70. McGhee RB, Cosgrove WB. Biology and physiology of the lower Trypanosomatidae. Microbiol Rev. 1980;44: 140–173. Available: https://www.ncbi.nlm.nih.gov/pubmed/6997722

71. Chicharro C, Alvar J. Lower trypanosomatids in HIV/AIDS patients. Ann Trop Med Parasitol. 2003;97: 75–78. doi:10.1179/000349803225002552

72. Wallace FG, Hertig M. Ultrastructural comparison of promastigote flagellates (leptomonads) of wild-caught Panamanian Phlebotomus. J Parasitol. 1968;54: 606–612. Available: https://www.ncbi.nlm.nih.gov/pubmed/5757733

73. Bhattarai NR, Das ML, Rijal S, van der Auwera G, Picado A, Khanal B, et al. Natural infection of Phlebotomus argentipes with Leishmania and other trypanosomatids in a visceral leishmaniasis endemic region of Nepal. Trans R Soc Trop Med Hyg. 2009;103: 1087–1092. doi:10.1016/j.trstmh.2009.03.008

74. Machado TDO, Minuzzi-Souza TTC, Ferreira T de S, Freire LP, Timbó RV, Vital TE, et al. The role of gallery forests in maintaining Phlebotominae populations: potential Leishmania spp. vectors in the Brazilian savanna. Mem Inst Oswaldo Cruz. 2017;112: 681–691. doi:10.1590/0074-02760170126

75. Momen H, Cupolillo E. Speculations on the origin and evolution of the genus Leishmania. Mem Inst Oswaldo Cruz. 2000;95: 583–588. Available: https://www.ncbi.nlm.nih.gov/pubmed/10904419

76. Kerr SF. Palaearctic origin of Leishmania. Mem Inst Oswaldo Cruz. 2000;95: 75–80. Available: https://www.ncbi.nlm.nih.gov/pubmed/10656708

77. Noyes HA, Morrison DA, Chance ML, Ellis JT. Evidence for a neotropical origin of Leishmania. Mem Inst Oswaldo Cruz. 2000;95: 575–578. Available: https://www.ncbi.nlm.nih.gov/pubmed/10904417

78. Akhoundi M, Kuhls K, Cannet A, Votýpka J, Marty P, Delaunay P, et al. A Historical Overview of

the Classification, Evolution, and Dispersion of Leishmania Parasites and Sandflies. PLoS Negl Trop Dis. 2016;10: e0004349. doi:10.1371/journal.pntd.0004349

79. Barbosa FH de S, Pereira PVLG da C, Bergqvist LP, Rothschild BM. Multiple neoplasms in a single sauropod dinosaur from the Upper Cretaceous of Brazil. Cretaceous Res. 2016;62: 13–17. doi:10.1016/j.cretres.2016.01.010

80. Boelaert M, Burza S, Romero G. Control and Public Health Aspects. In: Bruschi F, Gradoni L, editors. The Leishmaniases: Old Neglected Tropical Diseases. Cham: Springer International Publishing; 2018. pp. 227–245. doi:10.1007/978-3-319-72386-0_10

81. Pace D. Leishmaniasis. J Infect. 2014;69 Suppl 1: S10–8. doi:10.1016/j.jinf.2014.07.016

82. Sandra R. Maruyama, Alynne K.M. de Santana, Nayore T. Takamiya, Talita Y. Takahashi, Luana A. Rogerio, Caio A.B. Oliveira, et al. Non-Leishmania Parasite in Fatal Visceral Leishmaniasis–Like Disease, Brazil. Emerging Infectious Disease journal. 2019;25: 2088. doi:10.3201/eid2511.181548

83. Zang W-L, Moczydlowska M, Jago JB, Others. Early Cambrian acritarch assemblage zones in South Australia and global correlation. Memoirs of the Association of Australasian Palaeontologists. 2007; 141. Available: https://search.informit.com.au/documentSummary;dn=252017604071310;res=IELNZC

84. Buracco P, Abate O, Guglielmino R, Morello E. Osteomyelitis and arthrosynovitis associated with Leishmania donovani infection in a dog. J Small Anim Pract. 1997;38: 29–30. Available: https://www.ncbi.nlm.nih.gov/pubmed/9121132

85. Infiesta Zulim RM, De Andrade GB, Durante HF, Ribeiro Lachi DC, Mamprim MJ, Sartor R. Canine osteomyelitis caused by Leishmania sp. Medicina Veterinaria-recife. 2011; 63–65. Available: https://repositorio.unesp.br/handle/11449/117763

86. de Souza AI, Juliano RS, Gomes TS, de Araujo Diniz S, Borges AM, Tafuri WL, et al. Osteolytic osteomyelitis associated with visceral leishmaniasis in a dog. Vet Parasitol. 2005;129: 51–54. doi:10.1016/j.vetpar.2005.01.008

87. Costa AAUM, Abreu AL, Gomes CMC, Saldanha ACR, Barral A, Costa JML, et al. Experimental model of chronic osteomyelitis caused by Leishmania (L) amazonensis. Acta Trop. 2006;98: 125–129. doi:10.1016/j.actatropica.2006.02.007

88. Costa AAUML da, da Costa AAUML. Alterações ósseas na leishmaniose cutânea difusa (LCD) no Estado do Maranhão: aspectos clínicos, de imagens e histopatológico. doi:10.11606/t.5.2004.tde-01102014-151600

89. Rathi SK, Pandhi RK, Chopra P, Khanna N. Post-kala-azar dermal leishmaniasis: a histopathological study. Indian J Dermatol Venereol Leprol. 2005;71: 250–253. Available: https://www.ncbi.nlm.nih.gov/pubmed/16394433

Supplementary Information

RESULTS

Paleohistology

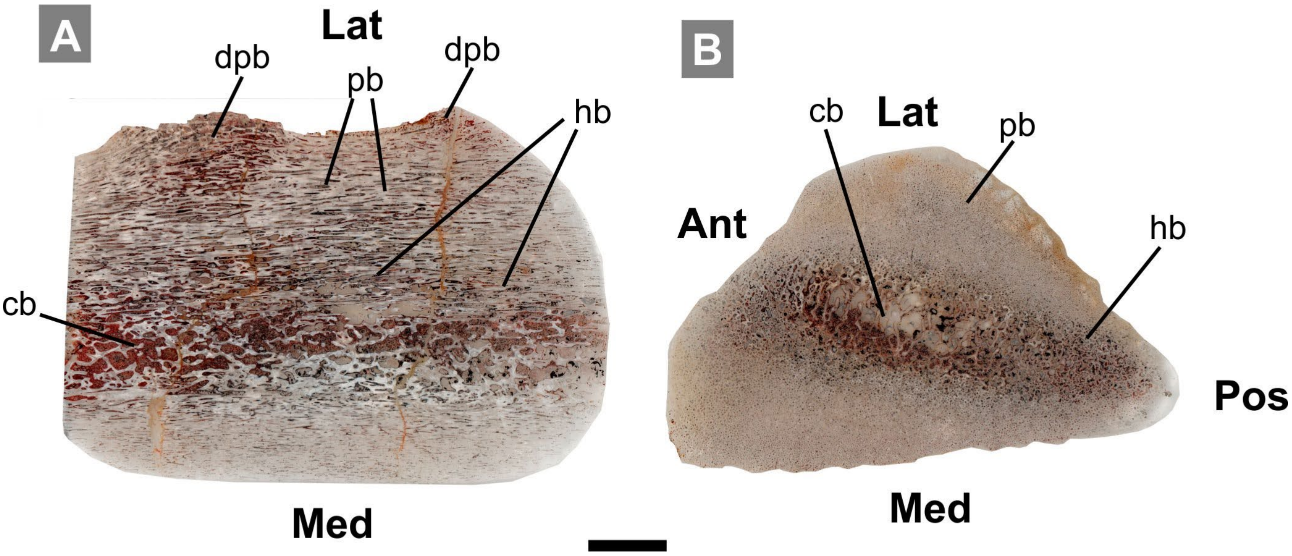

Figure S1. Longitudinal (**A**) and cross (**B**) sections of titanosaur specimen LPP-PV-0043 under normal light. Abbreviations = **Ant**, anterior; **Lat**, lateral; **Med**, medial; **Pos**, posterior; **cb**, cancellous bone; **hb**, Haversian bone, **pb**, periosteal bone; **dpb**, deformed periosteal bone. Scale bar = 1 cm.

Taphonomical remarks

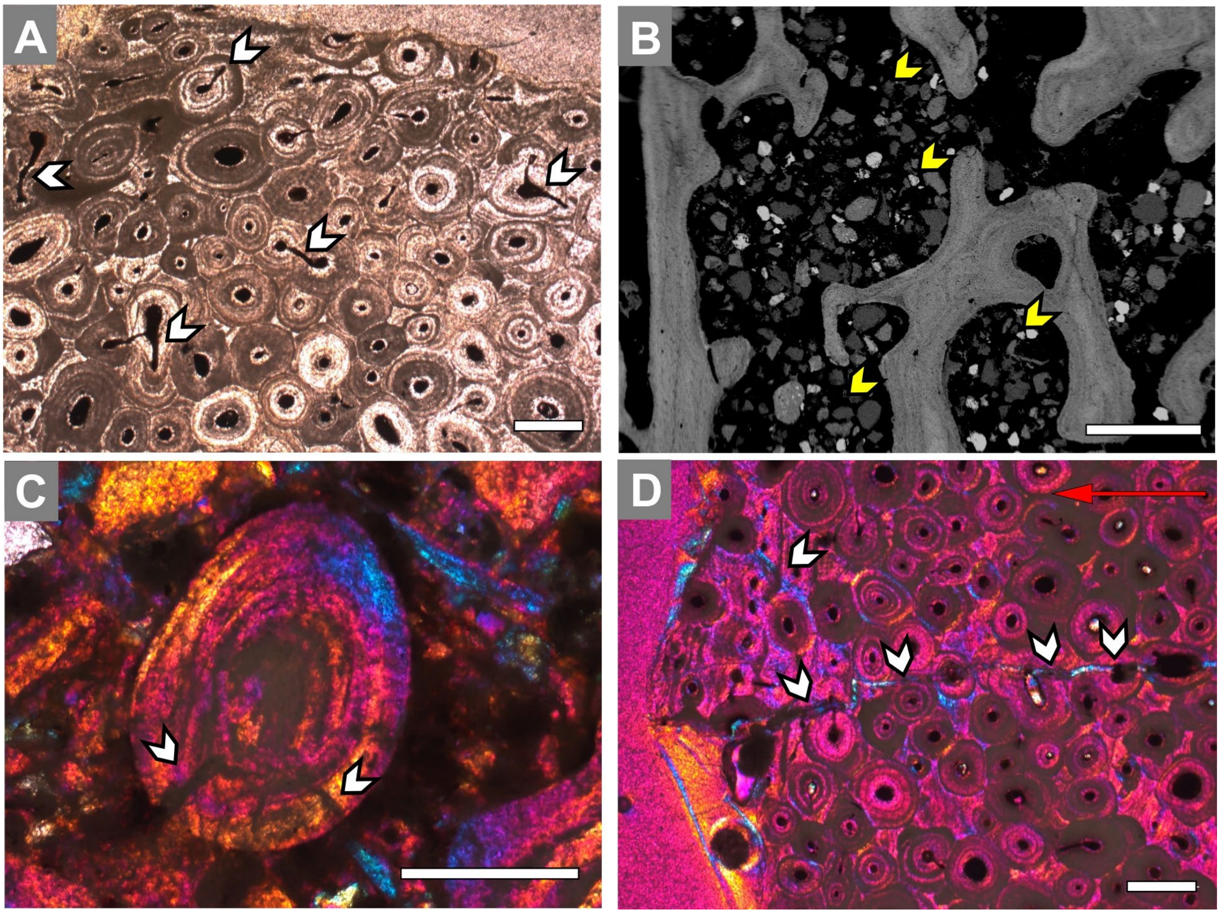

Figure S2. Taphonomical features in the thin sections of the Upper Cretaceous titanosaur LPP-PV-0043. **A**, Iron oxide (white arrows) penetrating secondary osteons longitudinally. **B**, quartz and feldspar sandstone grains infilling medullary spongiosa partially (yellow arrows). **C**, iron oxide infillings in Haversian canals and cracks (white arrows). The red arrow indicates direction towards the cortical surface. **D**, diagenetic cracks across the shaft (white arrows). Photographs under polarized light with parallel (**A**) and crossed (**C**, **D**) nicols. Electron microscopy photograph in **B**. Scale-bar in A = 1 mm; in C, D, and F = 200 µm; B, E = 100 µm.

Geochemistry of LPP-PV-0043

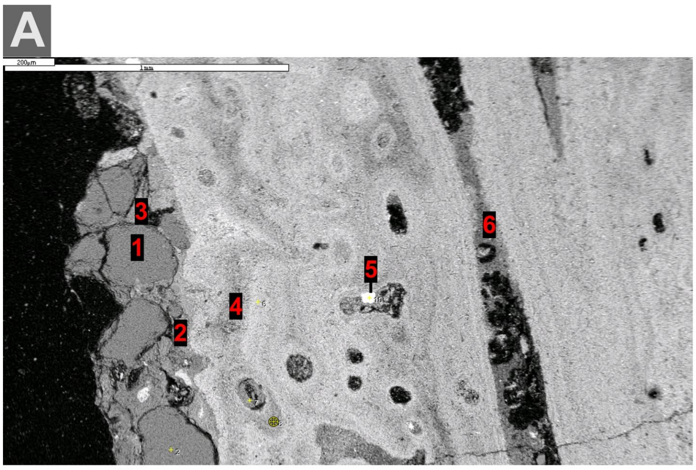

1

Elmt	Spect. Type	Element %	Atomic %
O K	ED	57.72	70.56
Si K	ED	42.28	29.44
Total		100.00	100.00

2

Elmt	Spect. Type	Element %	Atomic %
O K	ED	31.48	51.83
Mg K	ED	1.23	1.33
Al K	ED	4.39	4.29
Si K	ED	15.49	14.53
P K	ED	6.14	5.22
Cl K	ED	0.33	0.24
K K	ED	2.65	1.78
Ca K	ED	13.51	8.88
Ti K	ED	2.48	1.36
Mn K	ED	0.87	0.42
Fe K	ED	21.44	10.11
Total		100.00	100.00

3

Elmt	Spect. Type	Element %	Atomic %
O K	ED	36.49	57.12
Mg K	ED	1.99	2.05
Al K	ED	6.08	5.64
Si K	ED	20.95	18.68
K K	ED	2.95	1.89
Ca K	ED	1.24	0.78
Ti K	ED	3.13	1.63
Mn K	ED	1.72	0.79
Fe K	ED	25.46	11.42
Total		100.00	100.00

4

Elmt	Spect. Type	Element %	Atomic %
O K	ED	60.54	74.76
Na K	ED	1.49	1.28
Mg K	ED	0.69	0.56
Al K	ED	0.93	0.68
P K	ED	34.71	22.14
Fe K	ED	1.65	0.59
Total		100.00	100.00

5

Elmt	Spect. Type	Element %	Atomic %
O K	ED	16.17	34.64
Mg K	ED	1.27	1.80
Al K	ED	4.66	5.92
Si K	ED	12.81	15.63
P K	ED	1.85	2.05
K K	ED	0.89	0.78
Ca K	ED	3.27	2.80
Ti K	ED	1.36	0.97
Fe K	ED	57.71	35.41
Total		100.00	100.00

6

Elmt	Spect. Type	Element %	Atomic %
O K	ED	38.41	68.64
Al K	ED	0.46	0.48
Si K	ED	1.31	1.34
P K	ED	2.29	2.11
Ca K	ED	10.32	7.37
V K	ED	24.14	13.55
Fe K	ED	6.31	3.23
Nd L	ED	11.67	2.31
Sm L	ED	5.09	0.97
Total		100.00	100.00

Figure S3. Electron microscopy of the external-most cortical interface in longitudinal view.

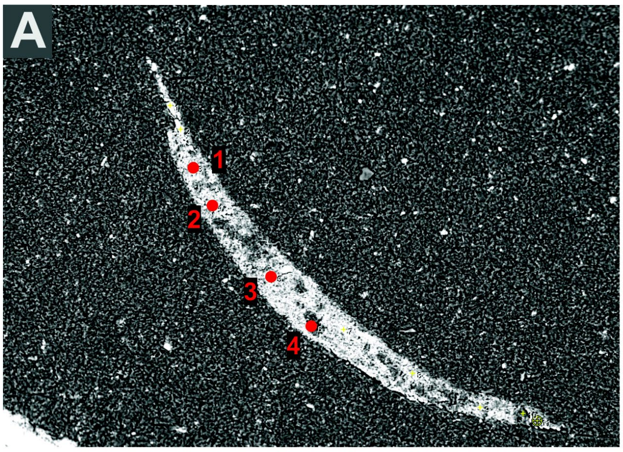

```
1  Elmt    Spect. Element   Atomic
            Type     %        %
   O  K     ED     54.89    70.90
   Na K     ED      7.00     6.29
   Mg K     ED      2.42     2.06
   Al K     ED      7.50     5.74
   P  K     ED      5.56     3.71
   Cl K     ED      0.53     0.31
   K  K     ED      3.24     1.71
   Ca K     ED     15.78     8.13
   Mn K     ED      0.40     0.15
   Fe K     ED      2.70     1.00
   Total          100.00   100.00
```

```
2  Elmt    Spect. Element   Atomic
            Type     %        %
   O  K     ED      2.96     5.08
   Si K     ED     97.04    94.92
   Total          100.00   100.00
```

```
3   Elmt    Spect. Element   Atomic
             Type     %        %
    O  K     ED      8.50    14.06
    Na K     ED      0.29     0.33
    Si K     ED     90.03    84.83
    Ca K     ED      1.19     0.78
    Total          100.00   100.00
```

```
4  Elmt    Spect. Element   Atomic
            Type     %        %
   O  K     ED     25.15    38.54
   Na K     ED      0.81     0.86
   Mg K     ED      0.27     0.27
   Si K     ED     53.94    47.09
   P  K     ED      6.78     5.37
   Cl K     ED      0.23     0.16
   K  K     ED      0.29     0.18
   Ca K     ED     11.65     7.13
   Fe K     ED      0.88     0.39
   Total          100.00   100.00
```

Figure S4. Electron microscopy of a *Brontoleishmania rex* gen. et. sp. Nov. preserved in the medullary spongiosa of a sauropod.

CAPÍTULO IV - ARTIGO CIENTÍFICO

AURELIANO, T., GHILARDI, A. M., SILVA-JÚNIOR, J. C. G., MARTINELLI, A. G., RIBEIRO, C. B., MARINHO, T., FERNANDES, M. F., RICARDI-BRANCO, F. S., MARTIN SANDER, P.. Influence of taphonomy on histological evidence for vertebral pneumaticity in an Upper Cretaceous titanosaur from South America. **Cretaceous Research**, 2020.

Status: Artigo Publicado
Periódico: *Cretaceous Research*
Classificação Qualis: A2

INFLUENCE OF TAPHONOMY ON HISTOLOGICAL EVIDENCE FOR VERTEBRAL PNEUMATICITY IN AN UPPER CRETACEOUS TITANOSAUR FROM SOUTH AMERICA

Tito Aureliano1,2, Aline M. Ghilardi[2], Julian C. G. Silva Junior[3],43, Agustín G. Martinelli5, Luiz Carlos Borges Ribeiro4, Thiago Marinho4, Marcelo A. Fernandes[2], Fresia Ricardi-Branco[1], P. Martin Sander6

[1]Institute of Geosciences, University of Campinas, Campinas, Brazil.

[2]Laboratory of Paleoecology and Paleoichnology, Federal University of São Carlos, São Carlos, São Paulo State, Brazil.

3Laboratório de Paleontologia de Ribeirão Preto, Faculdade de Filosofia, Ciências e Letras de Ribeirão Preto, Universidade de São Paulo, Ribeirão Preto, São Paulo State, Brazil.

4Centro de Pesquisas Paleontológicas “Llewellyn Ivor Price”, Universidade Federal do Triângulo Mineiro, Peirópolis, Uberaba, Minas Gerais State, Brazil.

5CONICET-Sección Paleontología de Vertebrados, Museo Argentino de Ciencias Naturales 'Bernardino Rivadavia', Av. Ángel Gallardo 470, Buenos Aires, C1405DJR, Argentina.

6 Division of Paleontology, University of Bonn, Nussallee 8, 53115, Bonn, Germany.

ABSTRACT

There is a necessity to systematically sample taxa to enlighten our knowledge on the presence of histological correlates of avian-like air sacs among dinosaurs. This work expands the studies on the occurrence of pneumosteum in sauropods to the Brazilian lithostrotian titanosaur *Uberabatitan ribeiroi*. This confirms previous hypotheses on the insertion of an air sacs system on titanosaurian vertebrae based on external observation and CT-scans. We also highlight that diagenesis can obliterate traces of pneumosteal bone. Caution is required to have a good understanding of the diagenetic history of the studied specimens. This could avoid false negatives, especially when sampling pneumatic histological traces in stem taxa. Additionally, we describe a new workflow for manipulating CT-scan data using open-source software. The goal is to make this technology more accessible to research groups with limited funding and potentialize the achievement of more paleontological data.

Keywords: pneumosteum, diagenesis, histology, Sauropoda, tomography

INTRODUCTION

Saurischian dinosaurs are model organisms for the understanding of evolutionary extremes (Sander et al. 2011; Aureliano et al. 2018; Xu et al. 2015; Cerda et al. 2012; Sander 2013), ranging from the mechanical sustaining of extremely large sauropod bodies to the lightness and agility of derived theropods (Sander et al. 2011; Perry et al. 2009; Bates et al. 2010; Dyke et al. 2013). Their biomineralized remains indicate a diverse array of adaptations in response to environmental changes in deep time. Accelerated dinosaurian metabolism is evidenced through long bone tissue deposition rates (Sander et al. 2011; Cerda et al. 2017; Mitchell & Sander 2014; Curry Rogers & Kulik 2018). However, that would imply in gigantothermal overheating in sauropods, at least in theory (Perry et al. 2009; Wedel 2003; Sander et al. 2011). In order to revert this situation, one of the evolutionary innovations that appeared in this group was their highly effective respiratory capacity, part and parcel of which was a system of air sacs (i.e. diverticula projected from the lungs) that permeated the body cavities and certain bones (Wedel 2003; Wedel 2009; Lambertz et al. 2018). In sauropodomorphs, several macrostructures in the axial skeleton (eg. fossae, laminae, and certain foramina) have been indicated also as attachment evidence of those structures (Yates et al. 2012; Wedel 2003; Wedel 2009; Wedel 2007; Wilson et al. 2011; Wilson 2012). However, research on fossil pneumaticity before 2018 was limited to indirect evidence either from direct observation of structures or from their computed tomographies. Very few is known on the histological equivalents of pneumaticity: the pneumosteum (Lambertz et al. 2018). Only two non-avian taxa have been sampled since: the basal neosauropods *Europasaurus* and *Diplodocus sp.* (Lambertz et al. 2018). However, new data is needed to obtain a better understanding on which occasions such tissue might be preserved in the fossil record. Therefore, there is an urge to sample more taxa across strata, wider geographical locations, and distinct phylogenetic contexts.

The titanosaurs from the Upper Cretaceous Bauru Basin, Southeast Brazil, have the potential to provide more data on this matter. Not only because of the abundance of sauropod material and taxonomic diversity, but also for presenting distinct taphonomy across individuals, units and outcrops. In this paper, we sampled a posterior cervical vertebra of a young individual of the derived neosauropod *Uberabatitan ribeiroi* (Salgado & Carvalho 2008; Silva Junior et al. 2019) from Serra da Galga Member of the Marília Formation, in southwestern Minas Gerais. A combination of computed tomography, petrography and histology was conducted to study pneumaticity in this taxon and the micropreservation of fossil tissue.

Additionally, here we present a novel workflow for the three-dimensional reconstruction of fossils from CT-scan slices using strictly multi-system open source softwares. The goal is to make this technology more accessible to other research groups with limited to no funding. Hopefully, this will potentialize the extraction of novel computed tomography paleontological data from these less privileged but highly competent teams.

MATERIAL AND METHODS

Institutional abbreviations: CPPLIP, Centro de Pesquisas Paleontológicas "Llewellyn Ivor Price", Universidade Federal do Triângulo Mineiro, Peirópolis, Uberaba, Minas Gerais, Brazil; **HU-UFSCar**, Hospital Universitário, Universidade Federal de São Carlos, São Carlos, São Paulo, Brazil; **PVL**, Paleovertebrate Collection, Instituto "Miguel Lillo", San Miguel de Tucumán, Argentina; **MCT**, Museu de Ciências da Terra, Rio de Janeiro, Brazil.

Material

The studied specimen (CPPLIP-1024; Fig. 1) corresponds to a posterior cervical vertebra, deposited at the Centro de Pesquisas Paleontológicas "Llewellyn Ivor Price", Universidade Federal do Triângulo Mineiro, Peirópolis, Brazil. It was found in the site known as "BR-050 Km 153" by personnel of the CPPLIP and it was included in the description of Carvalho & Salgado (2008) and Silva Junior et al. (2019).

Anatomical terminology and measurements

Here we employ the nomenclature proposed by Wilson et al. (2011) for vertebral fossae; Wilson (2012) for laminae, and Wedel et al. (2000) and Wedel (2003, 2007) for pneumatic structures. The histological nomenclature used herein is in accordance with Padian & Lamm (2013). We also employ the terms anterior and posterior instead of cranial and caudal.

Anatomical Abbreviations: c, centrum; **cdf**, centrodiapophyseal fossa; **cpol**, centrodiapophyseal lamina; **nc**, neural center; **pcdl**, posterior centrodiapophyseal lamina; **po**, postzygapophysis; **pocdf**, postzygapophyseal centrodiapophyseal fossa; **podl**, postzygodiapophyseal lamina; **spof**, spinopostzygapophyseal fossa; **tpol**, intrapostzygapophyseal lamina.

Computer tomography acquisition

A CT-scan of the specimen was obtained using a Philips Diamond Select Brilliance CT 16-slice medical scanner with more than 200 slices and a voxel size of 0.75 mm at the HU-UFSCar.

A new workflow for three-dimensional reconstruction and refinement using free software

The medical program *3D Slicer* v4.10.2 (Fedorov et al. 2012) was used to import DICOM slices and analyze the data. This is usually enough for imaging tomographic slices. However, depending on the taphonomical peculiarities of the specimen, further filters may be applied for visualization. For example, in the vertebra of CPPLIP-1024 the contrast between sedimentary matrix and the camellate bone walls was very low. A volume filter using a preset for PET volume in rainbow colors was applied to highlight the pneumatic structures (Fig.2). Afterwards, the volume is exported as a model at the desired format (eg. *.obj* or *.ply*). At this stage, one should use the model editor to cut out every unnecessary bias outside the specimen, such as eventual remnant tomographer table pieces.

Structures such as sutures, fenestrae, fossae, and laminae are very relevant when describing characters. Therefore, figure plates must be as clear as possible when highlighting those features. Sometimes, neither photograph of the fossil or the 3D model with 'metallic shade' make it clear enough to avoid misinterpretations. There is a further step in order to produce photorealistic figures highlighting the actual relevant data. We use another software, traditionally applied to the study of trace fossils: *CloudCompare* 2.9.1 (CloudCompare 2018). The model is imported in *CloudCompare* and one applies the Ambient Occlusion plugin (Tarini et al. 2003) to produce a photorealistic monochromatic with homogenized texture. Finally, one may take pictures at the desired views within software and export as high-resolution images (see Fig.1 for an example).

Bone histology

We followed the methodology presented by Lamm (2013) and Padian & Lamm (2013). The specimen was tomographed before sectioned. Pneumosteum is the histological correlates to the respiratory system, including the lungs, air sacs, and their diverticula (Lambertz et al. 2018).

When pneumosteum tissue was first described, authors sampled the prezygapophysis of a cervical vertebra of the German basal neosauropod *Europasaurus holgeri* (Lambertz et al. 2018). In this work, we cross-sectioned the postzygapophysis of the cervical vertebra of *Uberabatitan ribeiroi* in order to explore a different element. See Fig.1 for the plane of section. Thin section was produced by following standard procedures (Lamm 2013; Padian & Lamm 2013) and grounded to a thickness of around 40-50 µm. Thin section was observed and photographed by using a petrographic ZEISS Axioscope microscope with coupled AxioCam MRc 5 camera, and imaging software ZEISS Application Suite v.4.4. Pictures were corrected for brightness and contrast in Adobe Photoshop CC 20.0.1 and composite images were prepared in Corel Draw X6.

Specimen: CPPLIP-1024 (posterior cervical vertebra). The presence of other specimens up to three times larger (e.g. CPPLIP-1690) implies that CPPLIP-1024 was a young subadult individual (Silva Junior et al. 2019).

Locality and horizon: "BR-050 km 153" site, Serra da Galga area, about 25 km north of Uberaba city, Minas Gerais state of Brazil; Serra da Galga Member (da Fonseca Sampaio & Dal'Bó 2017), Marília Formation (Salgado & Carvalho 2008), Bauru Basin, upper-most Cretaceous.

Diagnosis

This vertebra constitutes one of several specimens found on the type-locality of *Uberabatitan ribeiroi* (Silva Junior et al. 2019; Salgado & Carvalho 2008). Only the left posterior portion is preserved (Fig.1). It features a deep cotyle with subcircular shape and well-defined margins when seen in the posterior view. The volume between the neural spine and the spinopostzygapophyseal fossa is not preserved. This latter fossa deepens until close to the neural center and is posteroventrally delimited by the intrapostzygapophyseal lamina. The postzygapophysis bears a large and flat articular facet and is connected with the centrum by a columnar centropostzygapophyseal lamina and with the neural spine by the eroded spinopostzygapophyseal lamina. On the lateral view, the postzygapophysis is connected to the eroded diapophysis by the compact postzygodiapophyseal lamina, which delimits the postzygapophyseal centrodiapophyseal fossa. This fossa excavates medially until close to the neural canal and is limited ventrally by the posterior centrodiapophyseal lamina. Foramina are absent throughout preserved volume.

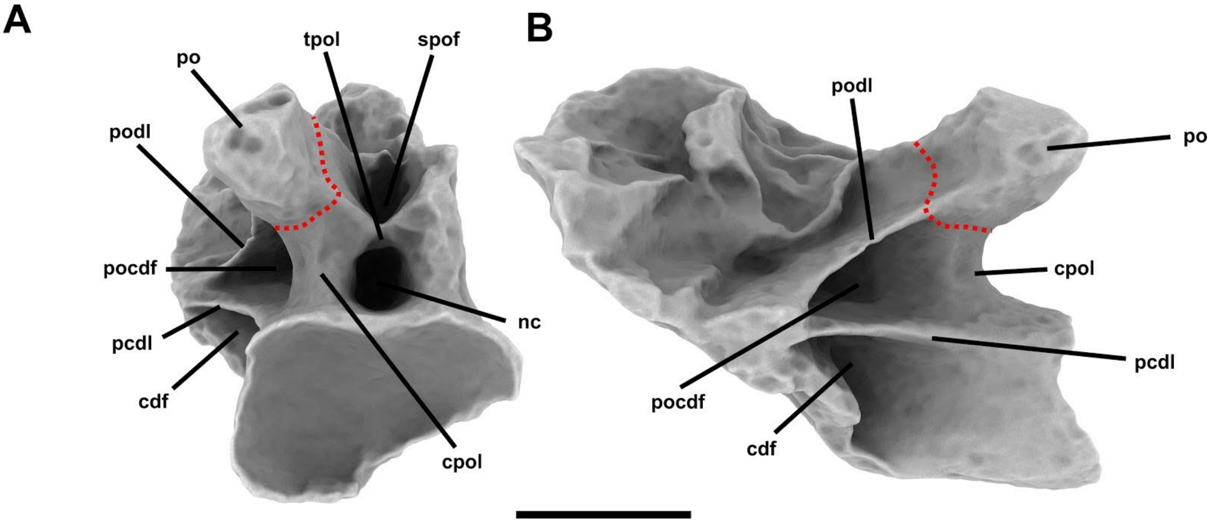

Figure 1. Posterior cervical vertebra of the Upper Cretaceous Brazilian lithostrotian titanosaurian *Uberabatitan ribeiroi* (CPPLIP-1024). Three-dimensional reconstruction from CT-scan in proximal (**A**) and left lateral (**B**) views. Red line shows sampling plane. This photorealistic image table applies a novel technique of CT-scan data processing and refinement using open source software (see methods for details). **Abbreviations: c**, centrum; **cdf**, centrodiapophyseal fossa; **cpol**, centrodiapophyseal lamina; **nc**, neural center; **pcdl**, posterior centrodiapophyseal lamina; **po**, postzygapophysis; **pocdf**, postzygapophyseal centrodiapophyseal fossa; **podl**, postzygodiapophyseal lamina; **spof**, spinopostzygapophyseal fossa; **tpol**, intrapostzygapophyseal lamina. Scale bar = 100 mm.

RESULTS

CT-Scan

Tomography slices and the reconstructed three dimensional model allowed a successful observation of the internal pneumatic structures of *Uberabatitan ribeiroi* specimen CPPLIP-1024. The postzygapophysis is denser at the base and increases pneumaticity distally (Fig.2.1-3, 6). It is also more pneumatized than the laminae. The middle infradiapophyseal fossa shows greater pneumatization than both laminae and postzygapophysis base (Fig.2.6). In the neural center, camellae are smaller distally and increase inwards. Camellae follow slightly radial pattern within centrum distally, perpendicular to the cotyle internal surface (in lateral and ventral views; see Fig.2.7,8). These are subhorizontally elongated throughout centrum (in lateral and ventral views; Fig.2.4,5,7,8).

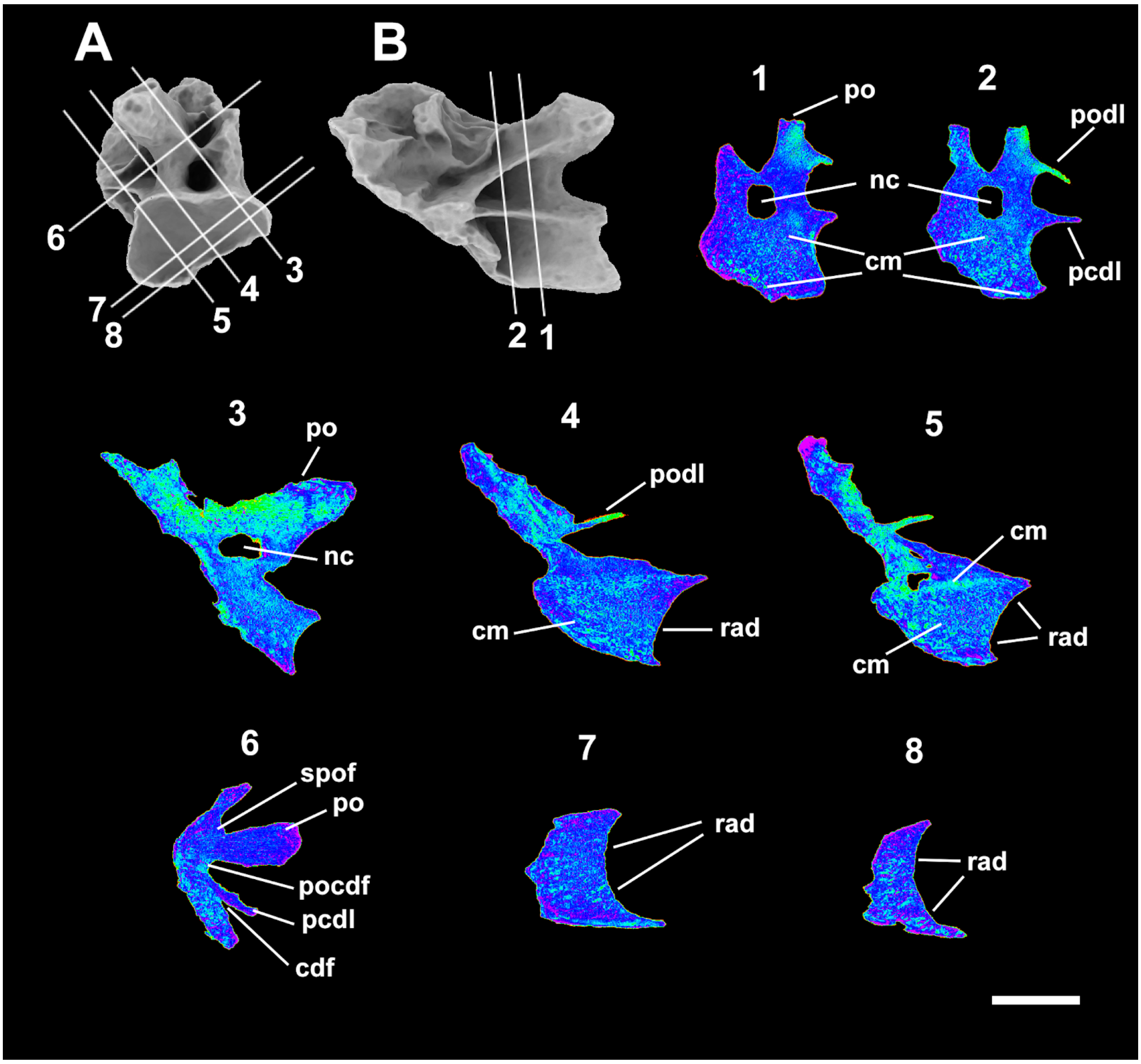

Figure 2. Internal structures of the cervical vertebra of CPPLIP-1024 of *Uberabatitan ribeiroi*. Reconstructed three dimensional model in proximal (**A**) and lateral (**B**) views presenting inverted tangencial CT-scan slices (1-8). Purple and darker blue indicate lower densities (eg. pneumatic cavities). Lighter blue and green demonstrate denser structures (eg. camellate bone). In this particular case, the latter might also indicate infilled sedimentary matrix and imaging artifacts. Excessively bright areas (eg. lighter green) are probably taphonomical artifacts (caused by localized diagenetic calcite percolation). **Abbreviations: cm**, camella; **nc**, neural canal; **po**, postzygapophysis; **rad**, radial camellae. Scale bar = 50 mm.

Taphonomy and petrography

The vertebra preserves only its mid-posterior volume. This loss might have happened either during pre-burial transport. There are cracks all over the vertebral surface and internally to the microscopic level (Fig.3.A). These fractures are usually filled with diagenetic calcite. These are evidenced through minerals featuring high birefringence with rainbow aspect and typical crystallographic acute twinning (Fig.3.B). Calcite also occur as subangular grains amidst matrix. Localized areas of the trabeculae were substituted and recrystallized by carbonate matrix (Fig.3.C). There are also mineral grains composed of quartz, K-feldspar, and fractured hydroxyapatite camellate bone. Moderately unsorted subrounded quartz grains abound in every infilled cavity (Fig.3.D).

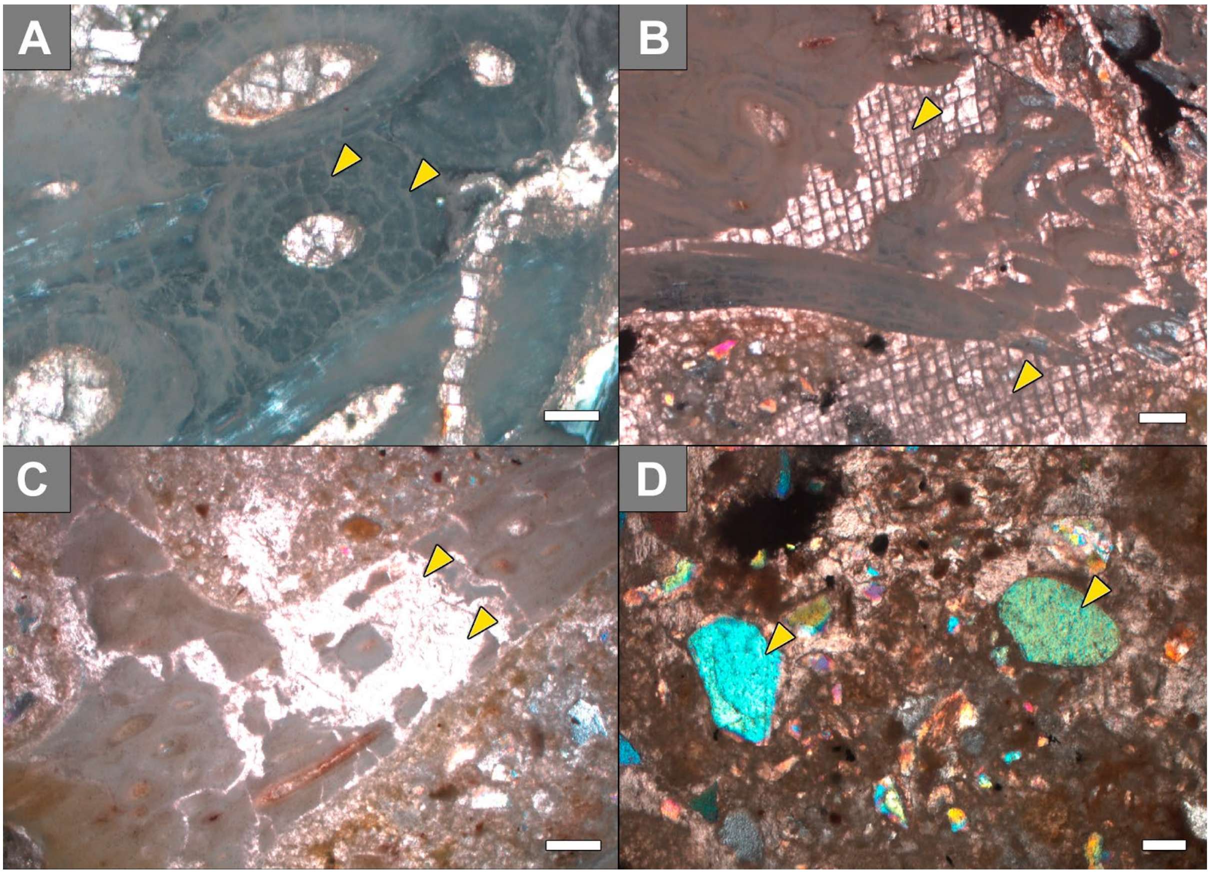

Figure 3. Petrography picturing diagenetic features of CPPLIP-1024 of *Uberabatitan ribeiroi*. **A**, microscopic calcite cracks in trabeculae. **B**, Fractures infilled with diagenetic calcite. Note typical crystallographic acute twinning. **C**, localized trabeculae substituted and recrystallized by carbonate matrix. **D**, moderately unsorted subrounded to subangular quartz grains abound in a cavity. The high quartz birefrigence shown in this photograph was caused

because this thin section is higher than the petrographic standard (> 32 µm). Polarized light under crossed nicols. Scale bar in **A, C, D** = 200 µm; in **B** = 100 µm.

Histology

The postzygapophysis cross-section reveals a moderately preserved internal camellate pattern (Fig.4). Bone walls present a conservative thickness of 1 mm (ranging between 0.5 and 2.0 mm). The camellate pockets vary greatly in size (from 1.5 to 7 mm wide) and shape, from subquadrangular to trapezoid forms. Smaller cavities are closer to the bone surface and get larger inwards.

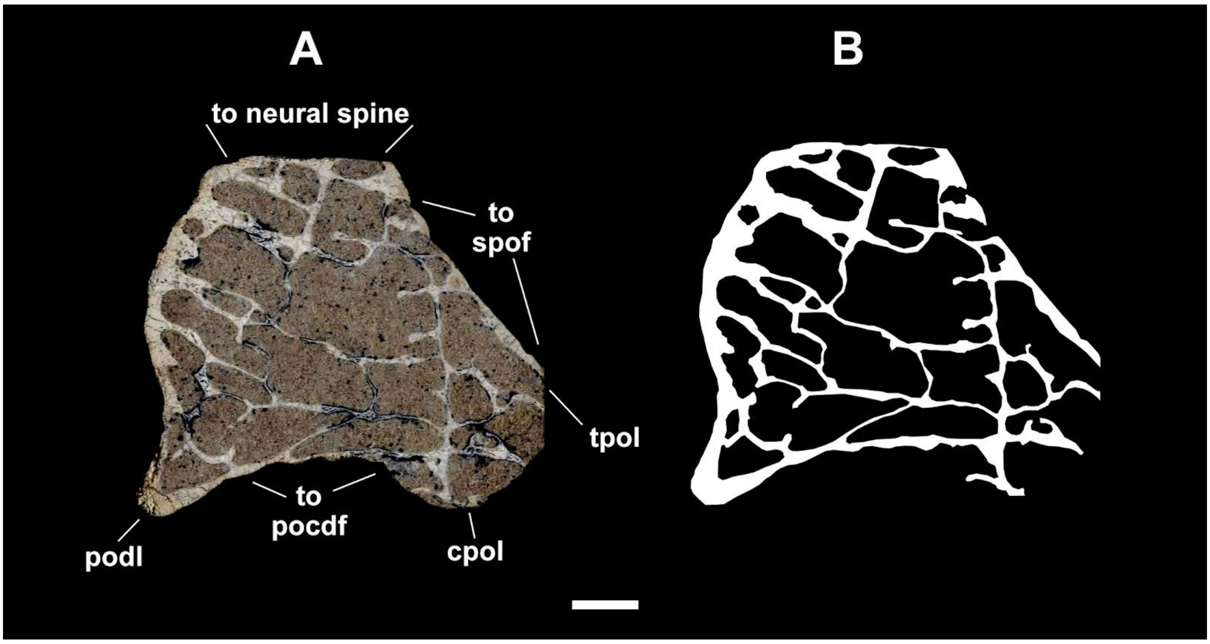

Figure 4. Camellate bone structure in the postzygapophysis cross-section of *Uberabatitan ribeiroi* (CPPLIP-1024). **A**, photograph of the polished cross-section indicating laminae (cpol, podl, and tpol) and surfaces leading to fossae (pocdf, spof). The surface linked to the neural spine is eroded. **B**, manually delineated camellate bone walls from the cross-section. Note the majority of subquadrangular and subtrapezoidal shapes. Smaller cavities are closer to the bone surface. Scale bar = 10 mm.

The bone comprises regular trabeculae in most of its extension. Internally, camellate walls comprise tightly packed secondary lamellar bone in their longer axes. The intersection between chambers presents localized secondary osteons. Laminae (podl, cpol, tpol) feature secondary remodeling up to the cortical surface. About 95% of the entire microstructure was compromised by diagenetic calcite, giving a ‘milky’ texture covering most of the observable areas. Even after these destructive events, there are isolated spots where pneumosteum has survived diagenetic destruction (Fig.5). Except by the podl, pneumosteal tissue preservation was more common in interior camellae closer to the neural spine, the cpol, tpol, and in the surface to the spof. Pneumosteal tissue is recognized by and distinguished from the secondary lamellar trabecular tissues by presenting an undulose extinction and a densely packed fabric of tiny ‘hair-like’ fibers. The appearance of these resembles the asbestiform parallel fibrous aggregates of serpentines (Da Mommio 2018). Nonetheless, pneumosteum present a smaller scale compared to serpentines. The eroded crenulated surface facing the pocdf, and the surrounding camellae, did not preserve any pneumosteum due to diagenetic destruction. However, some are preserved in loose trabeculae and primary tissue in the camella closer to the neural spine, spof. In the podl, there is pneumosteal tissue in both the external and internal surfaces of the lamina.

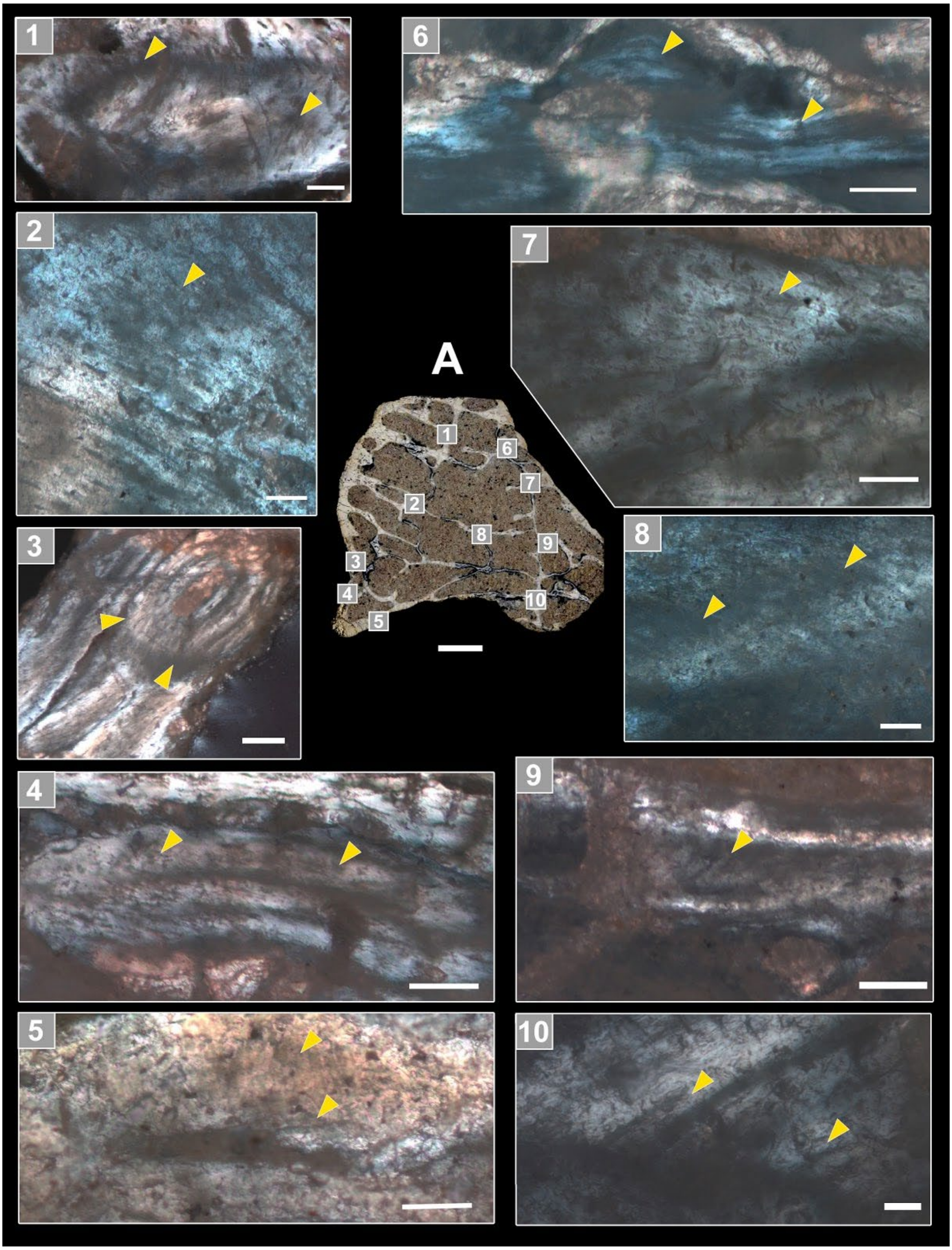

Figure 5. Pneumosteum (light yellow arrows) in the posterior cervical vertebra of the titanosaur *Uberabatitan ribeiroi* (CPPLIP-1024). **A**, polished cross-section illustrating sample locations (1-10). Despite bad microstructural preservation, pneumosteal bone still endured

diagenesis better in some areas (eg. 1, 3, 4, 6) than the others. Pneumosteum distinguishes from regular primary fibrolamellar and secondary trabecular tissues by presenting an undulose extinction of asbestiform densely-packed fabrics of tiny 'hair-like' fibers. Polarized light under crossed nicols. Scale bar in **A** = 10 mm; in **10** = 20 µm; in **1**, **2**, **4-8** = 50 µm; in **3**, **9** = 100 µm.

DISCUSSION

There are several features in the *Uberabatitan ribeiroi* vertebra indicating attachment to pneumatic structures. Several laminae delineate large deep fossae in which diverticula anchored. Foramina are absent, however. This is probably because CPPLIP-1024 was a young individual and foramina develop later in ontogeny (Wedel 2007; Wedel 2003; Wedel 2009). Nevertheless, Ct-scan images also reveal a complex array of smaller cavities that abound inside the centrum and in the postzygaphophysis. These internal pneumatic cavities are elongated posteriorly and slightly radial to the cotyle internal surface, similar to *Austroposeidon magnificus* cervicals (MCT 1628-R; Bandeira et al. 2016). The camellate fabric of CPPLIP-1024 shows a subquadrangular to subtrapezoidal shape. This is similar to the cervical of *Saltasaurus loricatus* (PVL 4017-214) and differs from the pattern seen in dorsals (eg. PVL 4017-47) and caudals (eg. PVL 4017-37) of the Argentinean taxon (Cerda et al. 2012). Dorsals and caudals present an even more chaotic array of camellae. Both *Saltasaurus* specimens from Cerda et al. (2012) belonged to adult individuals of approximately the same ontogenetic stage. Although not commented on by those authors, it is possible that the camellate architecture may indicate which air sacs system has influenced them. Therefore, further samples would contribute to solve questions about the pneumatization development along the axial skeleton (see Wedel 2003). The similarities between the pattern across derived titanosaurs CPPLIP-1024 and PVL 4017-214 may indicate the influence of the cervical air sac system. However, further samples in more taxa are necessary to test this hypothesis.

Pneumatic structures are relevant in dinosauriform phylogeny (Yates et al. 2012; Wedel 2007; Wedel 2006; O'Connor 2006). Pneumosteal tissue is indirect evidence of the contact of air-sac diverticula with the skeleton (Lambertz et al. 2018). Within non-avian dinosaurs, this tissue has been confirmed in the Jurassic neosauropods *Europasaurus holgeri* and *Diplodocus* sp.. We now report vertebral pneumosteum in the derived non-saltasaurine lithostrotian titanosaur *Uberabatitan ribeiroi*. In the spots with the best preservation, pneumosteum in the Brazilian taxon has shown the exact pattern observed in *Europasaurus holgeri* and *Diplodocus sp.*. Our observations indicate that all trabeculae in the postzygapophysis are composed of pneumosteum, corroborating the evidence from the camellate structure. Since derived titanosaurs have demonstrated to be an extreme in pneumaticity (Cerda et al. 2012; Wedel 2003; Wedel 2007), this histological result confirms previous hypotheses for the clade (Cerda et al. 2012; Wedel 2003; Bandeira et al. 2016). However, our results also have shown that pneumosteum is destroyed before complete obliteration of trabeculae in a destructive diagenesis scenario. Therefore, caution is needed when selecting relevant specimens for sampling. Especially when studying stem taxa, one may end up in a false negative absence of pneumosteum in a case where diagenesis had played a destructive role.

CONCLUSIONS

We presented a new workflow for manipulating CT-scan data to produce photorealistic figure charts using open source multi-system software. The goal is to make this technology more accessible to research groups with limited funding and to potentialize the availability of novel computed tomography paleontological data.

The CT-scan of the cervical vertebra revealed a complex array of smaller cavities that abound inside the centrum and in the postzygaphophysis. It is possible that the camellate architecture is directly influenced by the air-sacs system that surrounds the vertebra. The posterior cervical CPPLIP-1024 shows a subquadrangular to subtrapezoidal camellate pattern. It may be indicative of the cervical system. This condition differs from the even more chaotic subrounded fabric from the dorsals and caudals of closely related taxa.

We expanded the occurrence of pneumosteum in sauropods to the Brazilian titanosaur *Uberabatitan ribeiroi*. This confirmed previous hypotheses on the insertion of bird-like air sacs system on titanosaurian vertebrae based on external observation and CT-scans. We also highlighted that diagenesis can obliterate traces of pneumosteal bone. One must be cautious to have a good understanding of the diagenetic history of the studied specimen. This could avoid false negatives, especially when sampling pneumatic histological traces in stem taxa.

ACKNOWLEDGMENTS

We would like to acknowledge Oswaldo Jorge and the rest of the HU-UFSCar team for conducting fossil tomography. To Arthur Brum for providing insights into pneumosteum. To Filippo Bertozzo for his observations regarding sampling spots. To the anonymous reviewers for their comments. To *Colecionadores de Ossos*TM for funding the thin section. Authors research grants, scholarships and financial aid were provided by the Brazilian National Council for Scientific and Technological Development (CNPq) (T.A., T.S.M., and FRB-303527/2017-0), the Brazilian Coordination for the Improvement of Higher Education Personnel (CAPES) (A.M.G) - Finance Code 001, Fundação de Amparo à Pesquisa do Estado de Minas Gerais (T.S.M.) and FAPESP 2016/20927-0 'Modern accumulation studies and fossil bioclast studies in continental and coastal environments' (F.R.B.) and FAPESP 2018/21094-7 (J.C.G.S.J.).

Bibliography

Aureliano, T. et al., 2018. Semi-aquatic adaptations in a spinosaur from the Lower Cretaceous of Brazil. *Cretaceous Research*, 90, pp.283–295. Available at: http://www.sciencedirect.com/science/article/pii/S0195667117305153.

Bandeira, K.L.N. et al., 2016. A new giant Titanosauria (Dinosauria: Sauropoda) from the Late Cretaceous Bauru Group, Brazil. *PloS one*, 11(10), p.e0163373. Available at: http://dx.doi.org/10.1371/journal.pone.0163373.

Bates, K.T. et al., 2010. Sensitivity analysis in evolutionary robotic simulations of bipedal dinosaur running. *Journal of Vertebrate Paleontology*, 30(2), pp.458–466. Available at: https://doi.org/10.1080/02724630903409329.

Cerda, I.A. et al., 2017. Novel insight into the origin of the growth dynamics of sauropod dinosaurs. *PloS one*, 12(6), p.e0179707. Available at: http://dx.doi.org/10.1371/journal.pone.0179707.

Cerda, I.A., Salgado, L. & Powell, J.E., 2012. Extreme postcranial pneumaticity in sauropod dinosaurs from South America. *Paläontologische Zeitschrift*, 86(4), pp.441–449. Available at: https://doi.org/10.1007/s12542-012-0140-6.

CloudCompare, 2018. Version 2.9. 1 [GPL software]. Available at: http://www.cloudcompare.org/.

Curry Rogers, K. & Kulik, Z., 2018. Osteohistology of *Rapetosaurus krausei* (Sauropoda: Titanosauria) from the Upper Cretaceous of Madagascar. *Journal of Vertebrate Paleontology*, pp.1–24. Available at: https://doi.org/10.1080/02724634.2018.1493689.

Da Mommio, A., 2018. ALEX STREKEISEN: Serpentine. *Alex Strekeisen*. Available at: http://www.alexstrekeisen.it/english/meta/serpentine.php [Accessed June 28, 2019].

Dyke, G. et al., 2013. Aerodynamic performance of the feathered dinosaur *Microraptor* and the evolution of feathered flight. *Nature communications*, 4, p.2489. Available at: http://dx.doi.org/10.1038/ncomms3489.

Fedorov, A. et al., 2012. 3D Slicer as an image computing platform for the Quantitative Imaging Network. *Magnetic resonance imaging*, 30(9), pp.1323–1341. Available at:

http://dx.doi.org/10.1016/j.mri.2012.05.001.

da Fonseca Sampaio, L. & Dal'Bó, P.F., 2017. Interpretação paleoambiental dos calcretes da Formação Marília na região de Uberaba (MG). *Geologia USP. Série*. Available at: https://www.revistas.usp.br/guspsc/article/view/134871.

Lambertz, M., Bertozzo, F. & Sander, P.M., 2018. Bone histological correlates for air sacs and their implications for understanding the origin of the dinosaurian respiratory system. *Biology letters*, 14(1). Available at: http://dx.doi.org/10.1098/rsbl.2017.0514.

Lamm, E.-T., 2013. Preparation and Sectioning of Specimens. In *Bone Histology of Fossil Tetrapods*. University of California Press. Available at: http://california.universitypressscholarship.com/10.1525/california/9780520273528.001.0001/upso-9780520273528-chapter-4.

Mitchell, J. & Sander, P.M., 2014. The three-front model: a developmental explanation of long bone diaphyseal histology of Sauropoda. *Biological journal of the Linnean Society. Linnean Society of London*, 112(4), pp.765–781. Available at: https://academic.oup.com/biolinnean/article/112/4/765/2415870 [Accessed December 17, 2018].

O'Connor, P.M., 2006. Postcranial pneumaticity: an evaluation of soft-tissue influences on the postcranial skeleton and the reconstruction of pulmonary anatomy in archosaurs. *Journal of morphology*, 267(10), pp.1199–1226. Available at: https://onlinelibrary.wiley.com/doi/abs/10.1002/jmor.10470.

Padian, K. & Lamm, E.-T., 2013. *Bone Histology of Fossil Tetrapods: Advancing Methods, Analysis, and Interpretation*, University of California Press. Available at: https://market.android.com/details?id=book-EBVNmk1nm6MC.

Perry, S.F. et al., 2009. Implications of an avian-style respiratory system for gigantism in sauropod dinosaurs. *Journal of experimental zoology. Part A, Ecological genetics and physiology*, 311(8), pp.600–610. Available at: https://onlinelibrary.wiley.com/doi/abs/10.1002/jez.517.

Salgado, L. & Carvalho, I.S., 2008. UBERABATITAN RIBEIROI, A NEW TITANOSAUR

FROM THE MARÍLIA FORMATION (BAURU GROUP, UPPER CRETACEOUS), MINAS GERAIS, BRAZIL. *Palaeontology*. Available at: https://onlinelibrary.wiley.com/doi/abs/10.1111/j.1475-4983.2008.00781.x.

Sander, P.M., 2013. An evolutionary cascade model for sauropod dinosaur gigantism--overview, update and tests. *PloS one*, 8(10), p.e78573. Available at: http://dx.doi.org/10.1371/journal.pone.0078573.

Sander, P.M. et al., 2011. Biology of the sauropod dinosaurs: the evolution of gigantism. *Biological reviews of the Cambridge Philosophical Society*, 86(1), pp.117–155. Available at: http://dx.doi.org/10.1111/j.1469-185X.2010.00137.x.

Silva Junior, J.C.G. et al., 2019. Osteology and systematics of *Uberabatitan ribeiroi* (Dinosauria; Sauropoda): a Late Cretaceous titanosaur from Minas Gerais, Brazil. *Zootaxa*, 4577(3), pp.401–438. Available at: https://www.researchgate.net/profile/Julian_Silva_Junior/publication/332274953_Osteology_and_systematics_of_Uberabatitan_ribeiroi_Dinosauria_Sauropoda_a_Late_Cretaceous_titanosaur_from_Minas_Gerais_Brazil/links/5cab507d92851c64bd581393/Osteology-and-systematics-of-Uberabatitan-ribeiroi-Dinosauria-Sauropoda-a-Late-Cretaceous-titanosaur-from-Minas-Gerais-Brazil.pdf.

Tarini, M., Cignoni, P. & Scopigno, R., 2003. Visibility Based Methods and Assessment for Detail-recovery. In *Proceedings of the 14th IEEE Visualization 2003 (VIS'03)*. VIS '03. Washington, DC, USA: IEEE Computer Society, p. 60–. Available at: https://doi.org/10.1109/VISUAL.2003.1250407.

Wedel, M.J., 2009. Evidence for bird-like air sacs in saurischian dinosaurs. *Journal of experimental zoology. Part A, Ecological genetics and physiology*, 311(8), pp.611–628. Available at: https://onlinelibrary.wiley.com/doi/abs/10.1002/jez.513.

Wedel, M.J., 2006. Origin of postcranial skeletal pneumaticity in dinosaurs. *Integrative zoology*, 1(2), pp.80–85. Available at: http://dx.doi.org/10.1111/j.1749-4877.2006.00019.x.

Wedel, M.J., 2003. Vertebral pneumaticity, air sacs, and the physiology of sauropod dinosaurs. *Paleobiology*, 29(2), pp.243–255. Available at:

https://www.cambridge.org/core/journals/paleobiology/article/vertebral-pneumaticity-air-sacs-and-the-physiology-of-sauropod-dinosaurs/22C8C9E2378D8DCCD32BE689459EF620 [Accessed June 20, 2019].

Wedel, M.J., 2007. What pneumaticity tells us about “prosauropods”, and vice versa. *Special Papers in Palaeontology*, 77, pp.207–222. Available at: https://www.researchgate.net/profile/Mathew_Wedel/publication/272152712_What_pneumaticity_tells_us_about_prosauropods'_and_vice_versa/links/57d2e0e108ae5f03b48cd10c/What-pneumaticity-tells-us-about-prosauropods-and-vice-versa.pdf.

Wilson, J.A. et al., 2011. A nomenclature for vertebral fossae in sauropods and other saurischian dinosaurs. *PloS one*, 6(2), p.e17114. Available at: http://dx.doi.org/10.1371/journal.pone.0017114.

Wilson, J.A., 2012. New vertebral laminae and patterns of serial variation in vertebral laminae of sauropod dinosaurs. Available at: https://deepblue.lib.umich.edu/bitstream/handle/2027.42/92460/Contributions32no7-HR-c08-15-2012.pdf?sequence=2.

Xu, X. et al., 2015. A bizarre Jurassic maniraptoran theropod with preserved evidence of membranous wings. *Nature*, 521(7550), pp.70–73. Available at: http://dx.doi.org/10.1038/nature14423.

Yates, A.M., Wedel, M.J. & Bonnan, M.F., 2012. The early evolution of postcranial skeletal pneumaticity in sauropodomorph dinosaurs. *Acta palaeontologica Polonica*, 57(1), pp.85–100. Available at: http://www.app.pan.pl/article/item/app20100075.html.

CAPÍTULO V - ARTIGO CIENTÍFICO

AURELIANO, T., GHILARDI, A. M., FERNANDES, M. F., RICARDI-BRANCO, F. S., MARTIN SANDER, P.. Novel insights on the nature of pneumosteum: distinction between soft tissue traces in the bone.

Status: Manuscrito a ser submetido

NOVEL INSIGHTS ON THE NATURE OF PNEUMOSTEUM: DISTINCTION BETWEEN SOFT TISSUE TRACES IN THE BONE

Tito Aureliano[1,2], Aline M. Ghilardi[2], Marcelo A. Fernandes[3], P. Martin Sander[4], Fresia Ricardi-Branco[1]

[1]Institute of Geosciences, University of Campinas. Campinas, Brazil.

[2]Dinosaur Ichnology and Osteohistology Laboratory (DINOlab), Department of Geology, Federal University of Rio Grande do Norte (URFN). Natal, Brazil.

[3]Laboratory of Paleoecology and Paleoichnology, Federal University of Sao Carlos. Sao Carlos, Brazil.

[4]Division of Paleontology, University of Bonn, Nussallee 8, 53115. Bonn, Germany.

ABSTRACT

There is an urge in paleontology to expand paleohistological sampling in order to improve our understanding of the evolution of avian-like air sacs in archosaurs. This work expands the occurrence of pneumosteal bone tissue in dinosaurs to the lithostrotian titanosaur *Aeolosaurus maximus* Santucci & Arruda-Campos 2011 from the Upper Cretaceous of Brazil. CT scan of a posterior dorsal vertebral neural arch revealed a complex arrangement between fossae and laminae associated with pulmonary diverticula. Despite the absence of any camellate architecture in the laminae, pneumosteum tissue was identified. This observation corroborates the previous hypothesis that diverticula would be appended to vertebrae fossae. Furthermore, we conclude that the nonexistence of camellae is not definitive evidence to discard the pneumatization of bone. Additionally, we established a solid criterion for histological comparison to distinguish pneumosteal bone fibers from Sharpey's fibers (muscle and tendon insertions). Here we brought characters from optical mineralogy to differentiate those biomineralized tissue types. We hope this will assist colleagues to collect more data for the expansion of the knowledge on the evolution of the respiratory system in archosaurs.

Keywords: pneumosteum, respiratory system, histology, Sauropoda, postcranial skeletal pneumaticity

INTRODUCTION

Archosaurs comprise a diverse and long-lived clade. They adapted to colonize a variety of ecosystems since the Triassic (Fiorillo and Gangloff, 2001; Claessens, O'Connor and Unwin, 2009; Dyke, 2010; Nesbitt, 2011; Brusatte, O'Connor and Jarvis, 2015; Godoy, 2019; Dias *et al.*, 2020). One of their innovations was the postcranial skeletal pneumaticity (O'Connor, 2006; Wedel, 2006; Cerda, Salgado and Powell, 2012; Buchmann and Rodrigues, 2019). These pneumatic structures in the skeleton are a reflection of a permeating system of diverticula originating from the lungs (Wedel, 2003, 2009; Lambertz, Bertozzo and Sander, 2018). This adaptation coevolved with the increased metabolic rates, gigantism, partial thermal regulation, and even flight in saurischian dinosaurs (O'Connor, 2004, 2006; Perry *et al.*, 2009; Sander *et al.*, 2011; Mitchell and Sander, 2014; Cerda *et al.*, 2017). Structures such as fossae, laminae, and foramina have been used as evidence of air sacs attaching to the dinosaur axial skeleton (Wedel, 2003, 2007, 2009; O'Connor, 2006; Wilson *et al.*, 2011; Wilson, 2012; Yates, Wedel and Bonnan, 2012). Nonetheless, modern paleontological approaches go beyond macroscopic observations and computed tomography. Although very little is currently known, histological indicators of this interaction between bone and lung diverticula have been reported for some sauropods and fossil birds (Lambertz, Bertozzo and Sander, 2018; Aureliano *et al.*, 2020). Consequently, there is a need to sample more taxa from different phylogenetic contexts, across space and time.

In this paper, we sampled a posterior dorsal vertebra of an adult individual of the lithostrotian titanosaur *Aeolosaurus maximus* (Santucci and Arruda-Campos, 2011) from the Upper Cretaceous Adamantina Formation, western São Paulo state, Brazil. CT scan and histology were conducted to unveil the interaction between the neural arch laminae and their surrounding air sacs. Moreover, we established a solid histological base to distinguish pneumosteal bone fibers from the Sharpey's fibers (muscle and tendon insertions), which can sometimes be confused during histological observation.

MATERIALS AND METHODS

Institutional abbreviations: CPPLIP, Centro de Pesquisas Paleontológicas "Llewellyn Ivor Price", Universidade Federal do Triângulo Mineiro, Peirópolis (Uberaba), Brazil; **DINOlab**, Dinosaur Ichnology and Osteohistology Laboratory, Federal University of Rio Grande do

Norte, Natal, Brazil; **HU-UFSCar**, Hospital Universitário, Universidade Federal de São Carlos, São Carlos, Brazil; **PVL**, Paleovertebrate collection, Instituto “Miguel Lillo”, San Miguel de Tucumán, Argentina; **MCT**, Museu de Ciências da Terra, Rio de Janeiro, Brazil; **MPMA**, Museu Paleontológico de Monte Alto, Monte Alto, Brazil.

Material

The studied specimen (MPMA 12-0001-97; Fig. 1) corresponds to the neural arch of a posterior titanosaur dorsal vertebra. It was rescued from a site on the outskirts of Monte Alto municipality, São Paulo State, Brazil, by Antonio Arruda Campos, Sandra Tavares, Fabiano Iori, and Cledinei Francisco. The neural arch is part of the holotype of *Aeolosaurus maximus* Santucci and Arruda-Campos 2011 and is housed at the Museu Paleontológico de Monte Alto, Monte Alto city, São Paulo state, Brazil.

Anatomical and histological nomenclature and measurements

We follow the anatomical nomenclature proposed by Wilson et al. (2011) for vertebral fossae; Wilson (2012) for laminae, and Wedel et al. (2000) and Wedel (2003, 2007) for pneumatic structures. Histological terms are in accordance with the standard literature (Francillon-Viellot *et al.*, 1990; Padian and Lamm, 2013). ‘Pneumosteum’ is in accordance with Lambertz et al. (2018). The terms ‘anterior’ and ‘posterior’ were used instead of cranial and caudal.

Anatomical Abbreviations:

General: **c**, centrum; **d**, diapophysis; **fr**, foramen; **pa**, paraphophysis; **po**, postzygaphophysis; **pr**, prezygapophysis; **s**, neural spine.

Laminae: **acdl**, anterior centrodiapophyseal lamina; **cprl**, centroprezygapophyseal lamina; **pcdl**, posterior centrodiapophyseal lamina; **pcpl**, posterior centroparapophyseal lamina; **prpl**, prezygoparapophyseal lamina; **spdl**, spinodiapophyseal lamina; **sprl**, spinoprezygaphoseal lamina.

Fossae: **cpaf**, centroparapophyseal fossa; **pacdf**, parapophyseal centrodiapophyseal fossa; **pocdf**, postzygapophyseal centrodiapophyseal fossa; **prpadf**, prezygapophyseal parapodiapophyseal fossa; **prsdf**, prezygapophyseal spinodiapophyseal fossa; **spof**, spinopostzygapophyseal fossa.

Mineralogical description

Mineralogical terms are in accordance with the standard literature (Klein and Dutrow, 2007; Raith, Raase and Reinhardt, 2011).

Computed tomography

A CT scan of the specimen was obtained before histological sampling using a Philips Diamond Select Brilliance CT 16-slice medical scanner with more than 200 slices and a voxel size of 0.75 mm at the HU-UFSCar. Acceleration voltage varied between 90 and 120 kV in a current of 367 mA. The methodology by Aureliano et al. (2020) was followed for data management and generating three-dimensional reconstruction with the software *3D Slicer* v. 4.10 (Fedorov *et al.*, 2012).

Bone histology

The main objective of histological sampling was to detect and describe the presence of 'pneumosteal bone'. Pneumosteum is a peculiar type of secondary bone that correlates with postcranial skeletal pneumaticity and, thus, to the lungs and their diverticula (Lambertz, Bertozzo and Sander, 2018). To test for the presence of pneumosteum, we cross-sectioned the acdl and the pcdl of the neural arch of a posterior dorsal vertebra attributed to *A. maximus* (MPMA 12-0001-97). Additionally, we sampled the surface of the prezygapophysis for histological control in an area where pneumosteum was not expected. See Fig.1 for the planes of section. Sections from the laminae were produced following standard procedures (Lamm, 2013). The prezygapophysis sample was obtained from a core drill (Stein and Sander, 2009). The samples were pruned to a thickness of ~40-50 µm. Thin sections were observed and photographed by using a petrographic ZEISS Axioscope microscope with an AxioCam MRc 5 camera attached and imaging software ZEISS Application Suite v. 4.4. Pictures were corrected for brightness and contrast in Adobe Photoshop CC 20.0.1, and composite images were prepared in Corel Draw X6.

Specimen: MPMA 12-0001-97-1024 (neural arch of a posterior dorsal vertebra). The specimen is part of the holotype of *Aeolosaurus maximus* Santucci & Arruda-Campus (2011).

Features of other elements of this specimen indicate this was an adult individual (Santucci and Arruda-Campos, 2011). However, no skeletochronological histology has been published so far.

Locality and horizon: Monte Alto municipality, São Paulo State, Turonian-Santonian Adamantina Formation (Santucci and Arruda-Campos, 2011; Castro *et al.*, 2018), Bauru Group, Southeast Brazil.

Diagnosis

This vertebra is part of the holotype of *Aeolosaurus maximus* (Santucci and Arruda-Campos, 2011). The specimen was considerably compromised by taphonomic processes. Only the neural arch was sampled in this study (Fig.1), although there is a partially preserved mechanically detached vertebral center associated with the arch. Santucci & Arruda-Campos (2011) recovered the phylogenetic position of MPMA 12-0001-97 as an Aeolosaurini, sister group of *Aeolosaurus* (*A. comahuensis* + *A. rionegrinus*). However, further analyses recovered this taxon as sister-group of Rinconsauria, either as a non-Aeolosaurini (Bandeira *et al.*, 2016) or as an Aeolosaurini (Silva Junior *et al.*, 2019). In both cases, *Aeolosaurus maximus* was recovered as a separate taxon apart from *A. comahuensis* and *A. rionegrinus* (against Santucci & Arruda-Campos, 2011). Notwithstanding, it is possible that *A. maximus* may be reassigned to a new genus in future research.

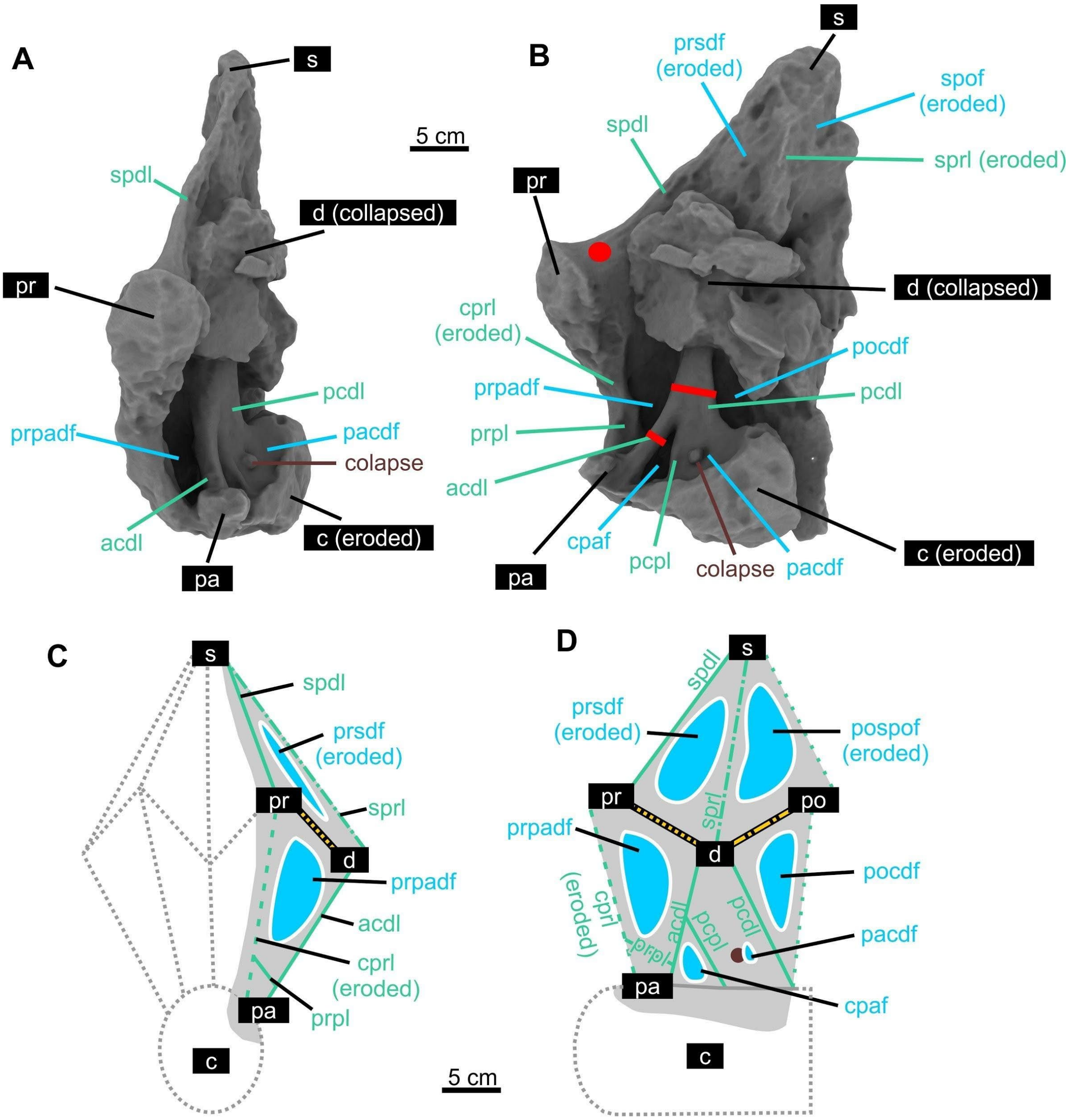

Figure 1. Neural arch of a posterior dorsal vertebra of the Late Cretaceous Brazilian titanosaur *Aeolosaurus maximus* (MPMA 12-0001-97-1024). Three-dimensional reconstruction from CT scan (A, B) and schematic morphological diagrams (C, D) in anterior (A, C) and left lateral (B, D) views. Red lines and dot show sampling planes. **Abbreviations: acdl**, anterior centrodiapophyseal lamina; **c**, centrum; **cpaf**, centroparapophyseal fossa; **cprl**, centroprezygapophyseal lamina; **d**, diapophysis; **pacdf**, parapophyseal centrodiapophyseal fossa; **pa**, paraphophysis; **pcdl**, posterior centrodiapophyseal lamina; **pcpl**, posterior centroparapophyseal lamina; **po**, postzygapophysis; **pocdf**, postzygapophyseal

centrodiapophyseal fossa; **pr**, prezygapophysis; **prpl**, prezygoparapophyseal lamina; **prpadf**, prezygapophyseal parapodiapophyseal fossa; **prsdf**, prezygapophyseal spinodiapophyseal fossa; **s**, neural spine; **spdl**, spinodiapophyseal lamina; **spof**, spinopostzygapophyseal fossa; **sprl**, spinoprezygaphoseal lamina.

RESULTS

Morphology of neural arch MPMA 12-0001-97-1024

The vertebra is considerably fragmented (Fig.1.A-D). Several parts are badly preserved and have collapsed during early burial or diagenesis, probably due to the highly pneumatized nature of the bone. The anterior-most portion of the neural arch is slightly eroded in lateral view (Fig.1.D) and very compromised in proximal view (>50% loss of material; see Fig.1.C). Only the left lateral portion has been preserved. Foramina are absent throughout the preserved volume. The diapophysis has collapsed but can be identified. Part of the vertebral center is preserved but has been mistakenly identified as the prezygapophysis by Santucci & Arruda-Campos (2011). The prezygapophysis has been deformed by a smooth proximal twist. The prezygapophysis has a subcircular articulation, sizeable and convex. The parapophysis is dislocated anteriorly towards the center and bears a thick and flat articular facet that connects to the latter. It is surrounded by two deep fossae (cpaf and prpadf) and is connected to three laminae (cprl, prpl and acdl). A further two laminae (pcpl and pcdl) connect to the mid-posterior portion of the vertebral center. The fossae prpadf, cpaf, and pocdf are very deep, but pacdf is subtle and partially covered by collapsed bone. The neural spine is more abraded than the region between the diapophysis and the center. However, traces of collapsed laminae (spdl and sprl) and two fossae (prsdf and spof) can be detected. The dorsal vertebra MPMA 12-0001-97-1024 shows an advanced degree of complexity (*sensu* Wilson et al. 2011), which leads us to conclude it is was placed more posteriorly than originally proposed by Santucci & Arruda-Campos (2011).

CT scanning of neural arch MPMA 12-0001-97-1024

The tomography slices allowed a 3D reconstruction of the *Aeolosaurus maximus* neural arch MPMA 12-0001-97-1024. However, internal preservation was too poor, and artifacts abound in the images throughout the neural arch (Fig.2.A.1-3). These might be the reasons why most of the internal pneumatic structures could not be assessed through the tomographic images. However, the CT scans show that there is an array of elongated cavities arranged in parallel extending from the prezygapophysis to the neural spine throughout the spdl. Camellae are smaller at the prezygapophysis and the spdl (average diameter = 2.4 mm) but increase towards the neural spine (average diameter = 5.9 mm). The prezygapophysis shows a subcircular camellate architecture in proximal view which projects radially towards the spdl (Fig.2.3). The laminae pcdl and acdl (Fig.2.1-3) showed a continuum of uniform lower density along their long axis. The preserved portion of the vertebral center showed no pneumatic bone structures most possibly due to diagenetic deformation.

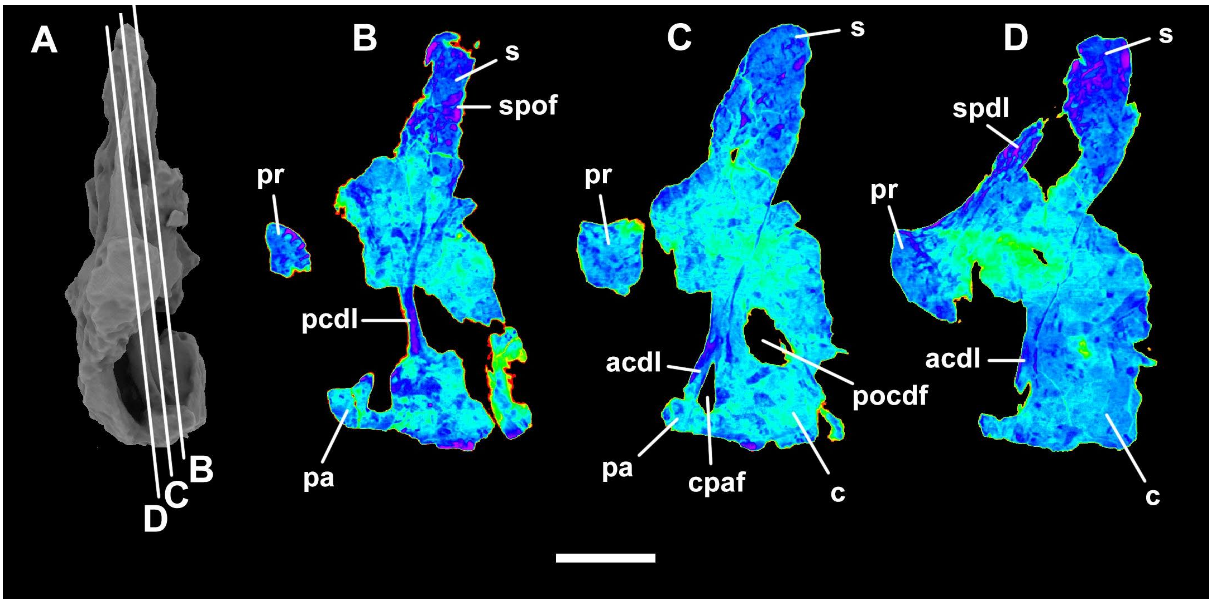

Figure 2. Internal structures of the dorsal neural arch of MPMA 12-0001-97-1024. **A**, 3D surface model in proximal view illustrating the location of three subvertical tangential virtual sections (B-D). Virtual sections with density plotted in false color. Purple and darker blue indicate areas of lower density (i.e., pneumatic cavities). The lighter blue and green indicate denser structures (i.e., bone walls). The sections show that only a few pneumatic structures survived taphonomic processes. In this particular case, the green colors might also indicate sediment infill and imaging artifacts. **Abbreviations: acdl**, anterior centrodiapophyseal lamina; **c**, centrum; **cpaf**, centroparapophyseal fossa; **pa**, paraphophysis; **pcdl**, posterior centrodiapophyseal lamina; **pocdf**, postzygapophyseal centrodiapophyseal fossa; **pr**,

prezygapophysis; **spdl**, spinodiapophyseal lamina; **spof**, spinopostzygapophyseal fossa. Scale bar = 10 cm.

Taphonomy and petrography

The neural arch preserves only its left lateral mid-anterior region. The specimen shows evidence of mechanical abrasion and bone collapse that occurred before or soon after embedding with sediments. There are abraded osteons on the surface indicating pre-burial mechanical transportation (Fig.3.A). Empty spaces and the concave bottom surface of the laminae were filled by clastic sediment (Fig.3.A-B). These mostly comprise mineral grains of quartz, K-feldspar, and clay (illite). Very poorly sorted angular to subrounded grains abound (Fig.3.B). Originally open spaces are also filled in by bone fragments originating from collapsed trabeculae (see supplementary material). There is more Ca than P in the fossilized bone. Ca usually is the infilling material and most analytical people are unable to know what they are shooting at, matrix or bone, and no F counts at all. Late diagenesis alteration is substantiated by microcracks throughout the trabeculae (Fig.3.A, C). Post-exhumation weathering signs are validated by the presence of opaque oxide minerals (rich in Fe, Mn, and Mg) infilling the secondary osteons centripetally (Pfretzschner, 2004) (Fig.3.D; see supplementary material). Nonetheless, the microanatomy is well-preserved to the microscopic level and histology could be accessed. The fact that the bone is birefringent in cross-polarized light indicates good preservation of the bone apatite.

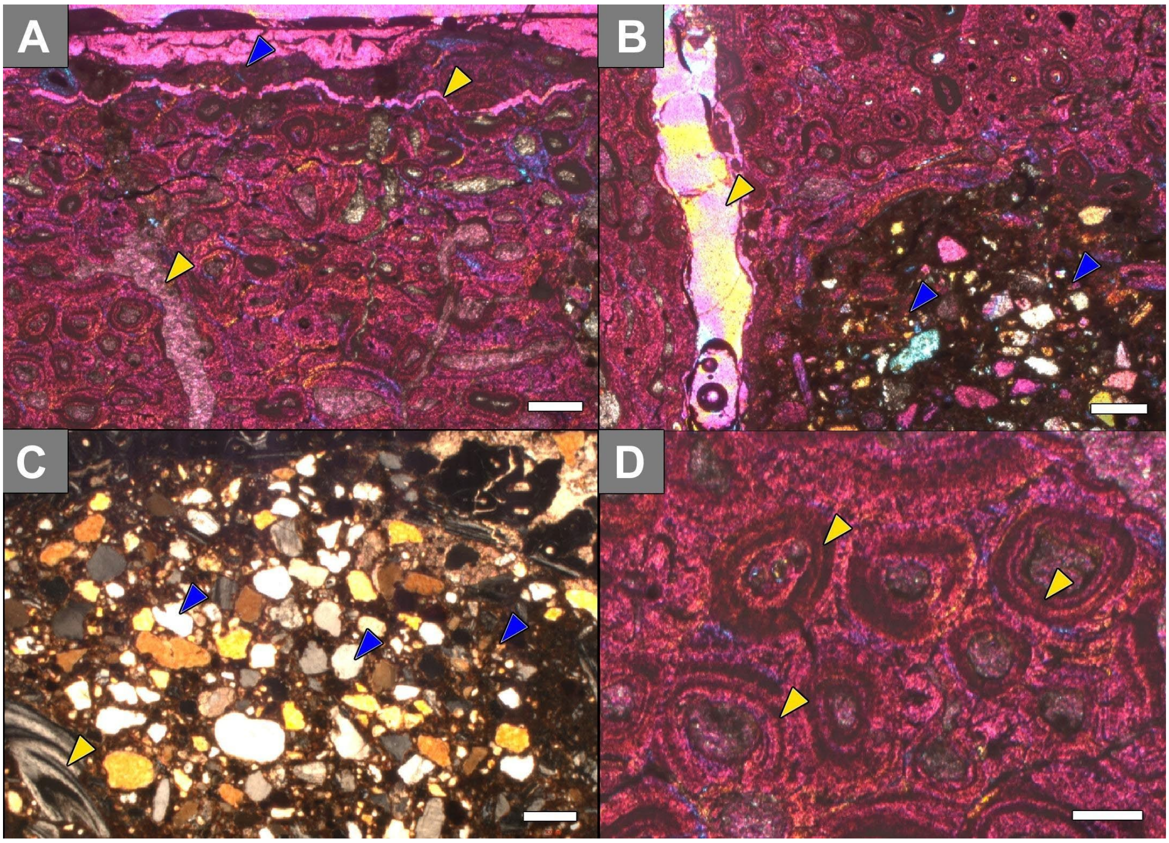

Figure 3. The taphonomy of MPMA 12-0001-97-1024 seen in the petrographic thin sections. **A**, abraded osteons at the surface (dark blue arrow) and microcracks in the trabeculae (light yellow arrows). **B**, late diagenetic fracture crossing the trabeculae of pcpl (light yellow arrow), and clastic sedimentary grains in contact with the internal surface of the lamina (dark blue arrow). **C**, very poorly sorted subrounded to angular mineral grains (blue arrow) and fragments of collapsed bone trabeculae (yellow arrow) amidst the sedimentary matrix. Note the well preserved birefringence of the bone apatite crystallites. The unusually high quartz and feldspar birefringence was caused because by thin sections being thicker than the petrographic standard (> 32 μm). D, opaque oxide minerals infilled the lamellar bone in secondary osteons centripetally (arrows) during weathering. Cross-polarized light in **A-D** with the lambda compensator in **A**, **B**, **D**. Scale bar in **A, B, C** = 500 μm; in **D** = 200 μm.

Histology

The thin sections of the vertebral laminae comprise bone compacta with no visible pneumatic architecture (e.g. camellae; see Fig. 4) except for a foramen between the pcdl and the acdl (Fig.4.A). The acdl features an acute convexity closer to the parapophysis. Pcdl and acdl fuse to form a larger table towards the diapophysis Pcdl projects deeper inwards. There are collapsed bone and ossified tendon fragments amidst the sedimentary matrix that fills both fossae. The bone of the lamina encompasses secondary trabeculae in most of its extension. Either the bone tissue is compact (see above) it is cancellous, made up by trabeculae. I (and the readers) would need intermediate magnification images to check. Despite the lack of any camellate fabric, pneumosteal bone is widespread throughout laminae (Fig.5.1-7 and Fig.6.2-4.2). Pneumosteum is distinguishes from regular trabeculae by comprising an array of tiny asbestiform densely-packed fibers, usually shorter than 60 µm. These fibers feature low relief and undulose extinction. Pneumosteal bone was found to be present both in the external (Fig.5.1,5,6) and internal (Fig.5.2-4) surfaces of the fused laminae (pcdl and acdl) closer to the diapophysis. It was also present surrounding the foramen floor (Fig.5.7).

There is no pneumosteum on the external surface of the lower acdl (the sample closer to the parapophysis) (Fig.6.1). However, there is pneumosteum in the convex internal surface of this region (Fig.6.2,3) and in trabecular fragments in the acdl (Fig.6.4). A chaotic (oblique) ossified tendon agglomerate appears nearby the internal laminar surface of the lower acdl and comprises a plastic tissue with undulose extinction and abundant Sharpey's fibers (Fig.6.**5**). These latter are larger, show higher relief (*sensu* Klein & Dutrow, 2007), and greater lengths when directly compared to pneumosteal fibers.

The thin section cut from the core sample of the prezygapophysis provides a fair base for a comparison between Sharpey's fibers and the pneumosteal bone (Fig.7.1-3). This sample location features a dense regular and irregular collagenous connective tissue insertion and any pneumosteal bone traces. Additionally, a dense irregular connective tissue sheath envelops tendons laterally (Fig.7.4). Secondary lamellar bone underlie the dense regular connective tissue insertions. This allowed the unique opportunity to observe in detail the Sharpey's fibers insertion in the interface between bone and tendon (Fig.7.2,3). As noted before, the Sharpey's fibers here also showed a high relief, undulose extinction, and insertion angles of approximately 60° (Fig.7.1,2.2,3.3). Each of these fibers is much longer (>200 µm) and wider than the pneumosteum packs (<60 µm). Sharpey's fibers also exhibit an organized parallel pattern in contrast to the chaotic asbestiform organization of the pneumosteal fibers. A list discerning the optical features between pneumosteal bone and Sharpey's fibers is presented in Table 1.

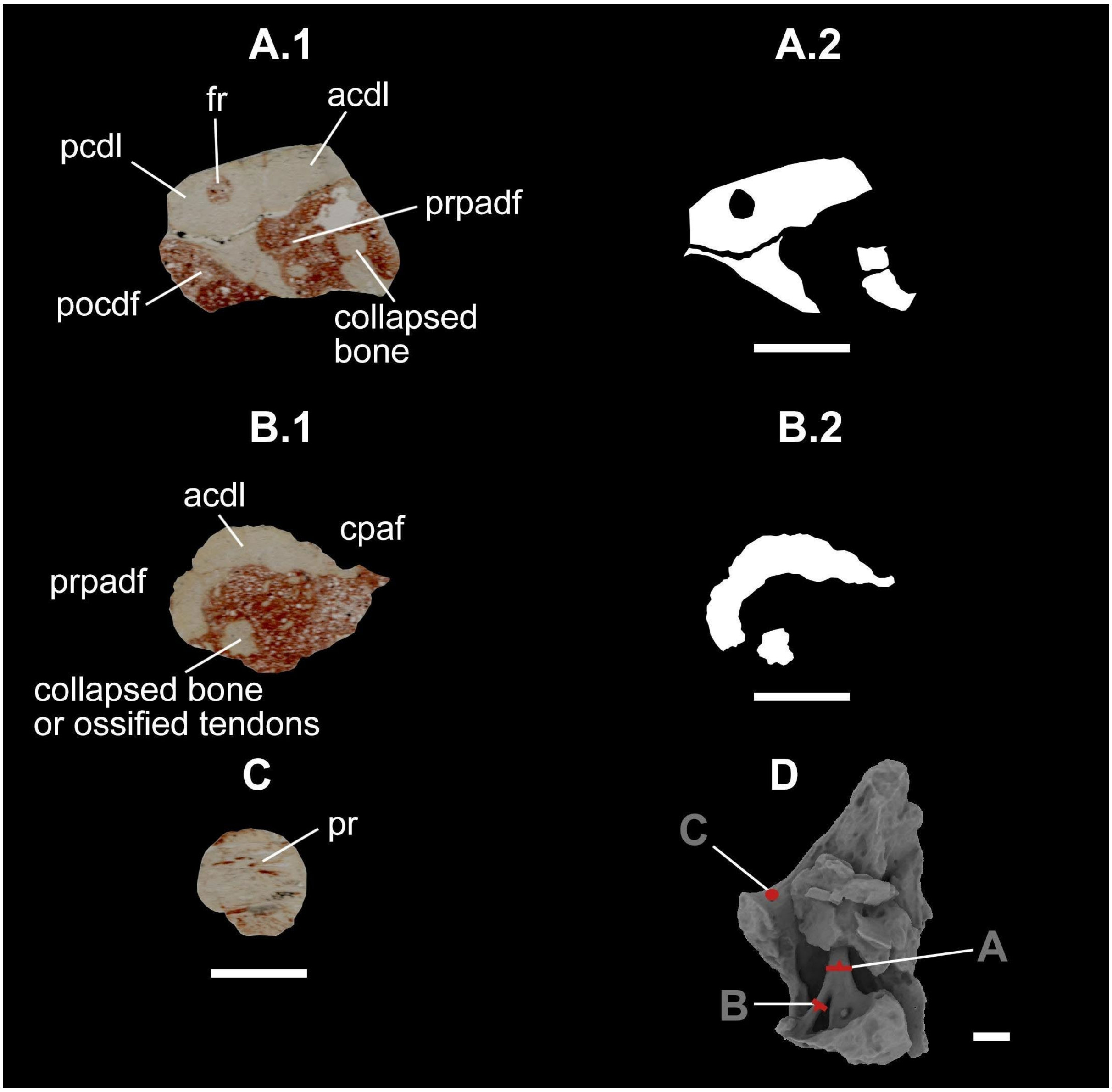

Figure 4. Bone samples from the lamina and prezygapophysis cross section of a posterior dorsal vertebra of *Aeolosaurus maximus* (MPMA 12-0001-97-1024). **A.1**, **B.1** polished section scans of the laminae and **A.2**, **B.2** show manually delineated schematic drawings of their respective preserved bone tissue. Bone compacta shows no visible pneumatic structures (camellae). **A**, pcdl and acdl fuse to form a large table closer to the diapophysis. Pcdl projects deeper inwards. **B**, acdl comprises a thick compact bone with acute convexity and no visible pneumatic architecture. There are collapsed bone fragments amidst the sedimentary matrix that fill both fossae. **C** shows a thin-section scan of the prezygapophysis. **D**, vertebral neural arch indicating sample sites and orientation. Sections: **A**, DINOlab-TS-0105; **B**, DINOlab-TS-0106; **C**, DINOlab-TS-0107; **Abbreviations: acdl**, anterior centrodiapophyseal lamina;

cpaf, centroparapophyseal fossa; **fr**, foramen; **pcdl**, posterior centrodiapophyseal lamina; **pocdf**, postzygapophyseal centrodiapophyseal fossa; **pr**, prezygapophysis; **prpadf**, prezygapophyseal parapodiapophyseal fossa. Scale bar in A-C = 10 mm; in D = 5 cm.

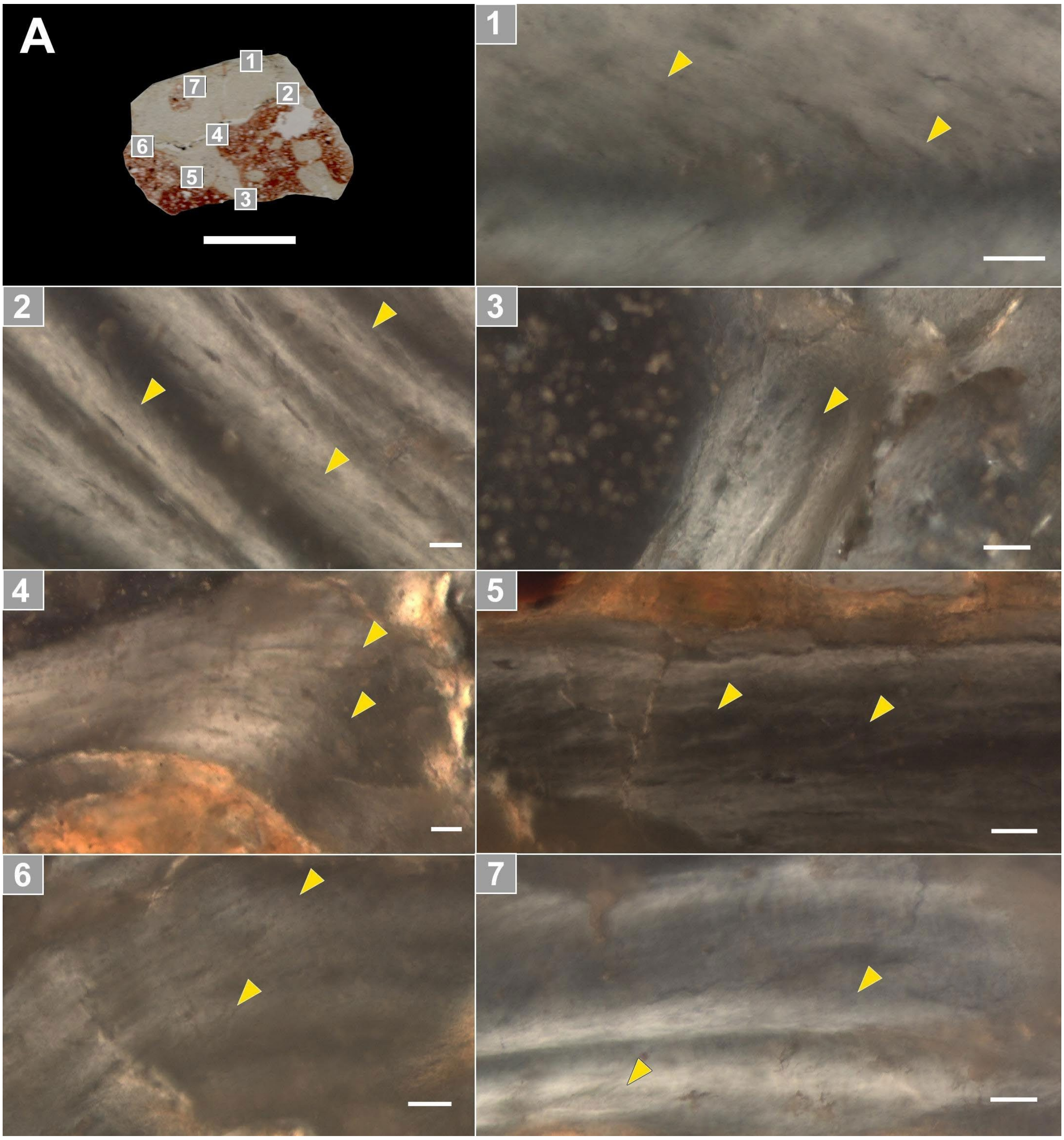

Figure 5. Pneumosteum in the fused laminae closer to the diapophysis (acdl and pcdl) of a posterior dorsal vertebra of the titanosaur *Aeolosaurus maximus* (MPMA 12-0001-97-1024; section DINOlab-TS-0105). **A**, polished section scans with locations of images in **B to I**). Pneumosteum is distinguished from regular trabeculae consisting of lamellar bone tissue by comprising an array of tiny asbestiform densely packed fibers (usually shorter than 60 µm).

These feature low contrast and undulose extinction. Pneumosteal bone was found to be present both in the external (**1**, **5**, **6**) and internal (**2**-**4**) surfaces of the laminae. It was also present surrounding the foramen floor (**7**). **Abbreviations: acdl**, anterior centrodiapophyseal lamina; **pcdl**, posterior centrodiapophyseal lamina. Polarized light under crossed nicols. Scale bar in A = 10 mm; in 1-7 = 20 µm.

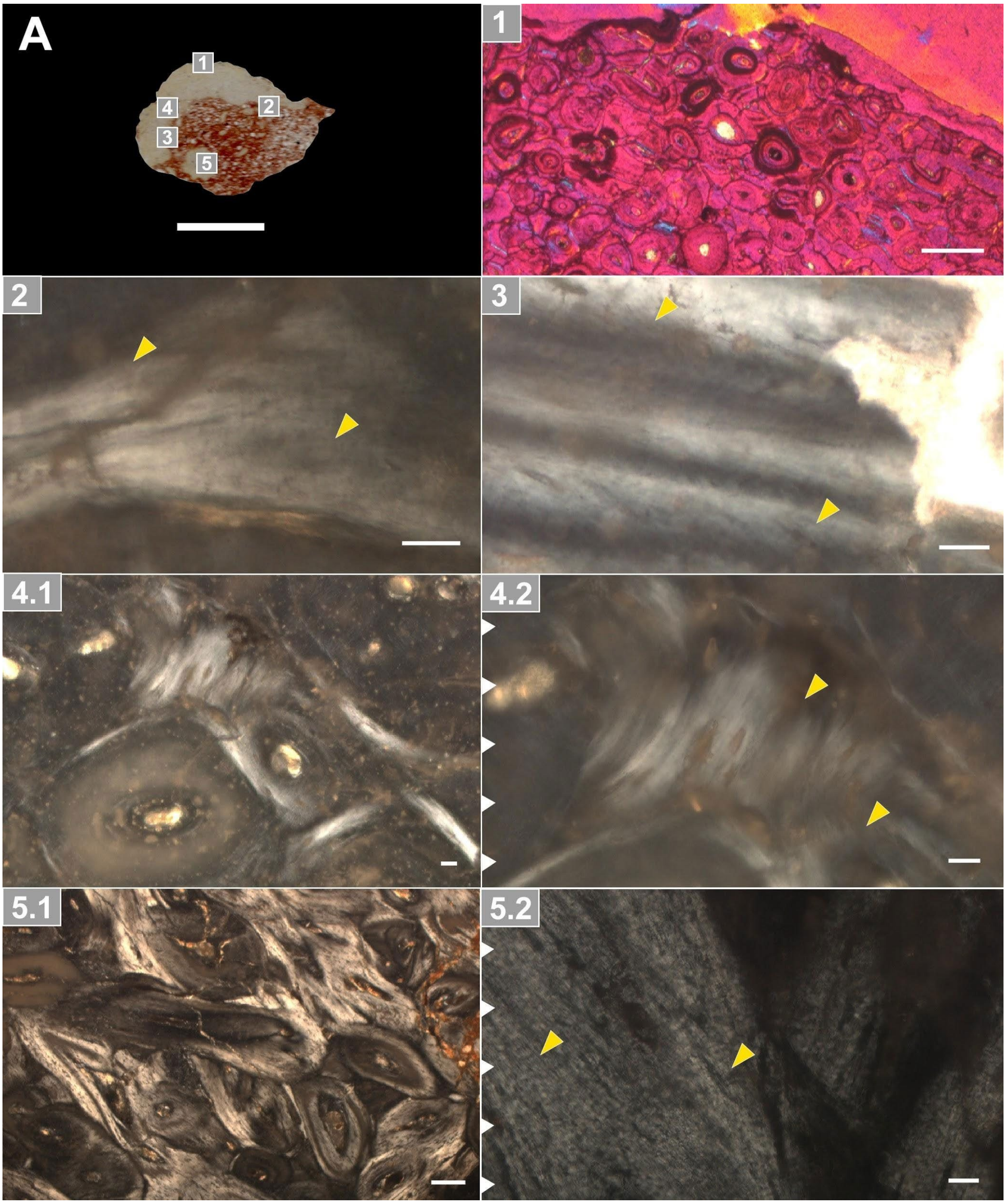

Figure 6. Photomicrographs of pneumosteal bone and Sharpey's fibers in the acdl (closer to the pa) of a posterior dorsal vertebra of the titanosaur *Aeolosaurus maximus* (MPMA 12-0001-97-1024; section DINOlab-TS-0106). **A**, polished cross section indicating image locations (**1**-**7**). Pneumosteum in this sample is distinguished from regular trabeculae by featuring an array of tiny asbestiform densely-packed fibers (usually shorter than 60 μm). These show low-contrast and undulose extinction. There is no pneumosteal bone on the external surface of the acdl (**1**). However, pneumosteum exists in the convex internal surface (**2**, **3**) and in the acdl trabeculae (**4**). A chaotic (oblique) ossified tendon agglomerate appears nearby the internal laminar surface and comprises a plastic tissue with undulose extinction and abundant Sharpey's fibers (**5**). The latter are larger, show higher relief, and longer lengths when directly compared to pneumosteal fibers (see Table 1 for details). Polarized light under crossed nicols **1-5.2** with lambda compensator in **1**. **Abbreviations: acdl**, anterior centrodiapophyseal lamina; **pa**, parapophysis. Scale bar in **A** = 10 mm; in **1** = 500 μm; in **2-4.2, 5.2** = 20 μm; in **5.1** = 200 μm.

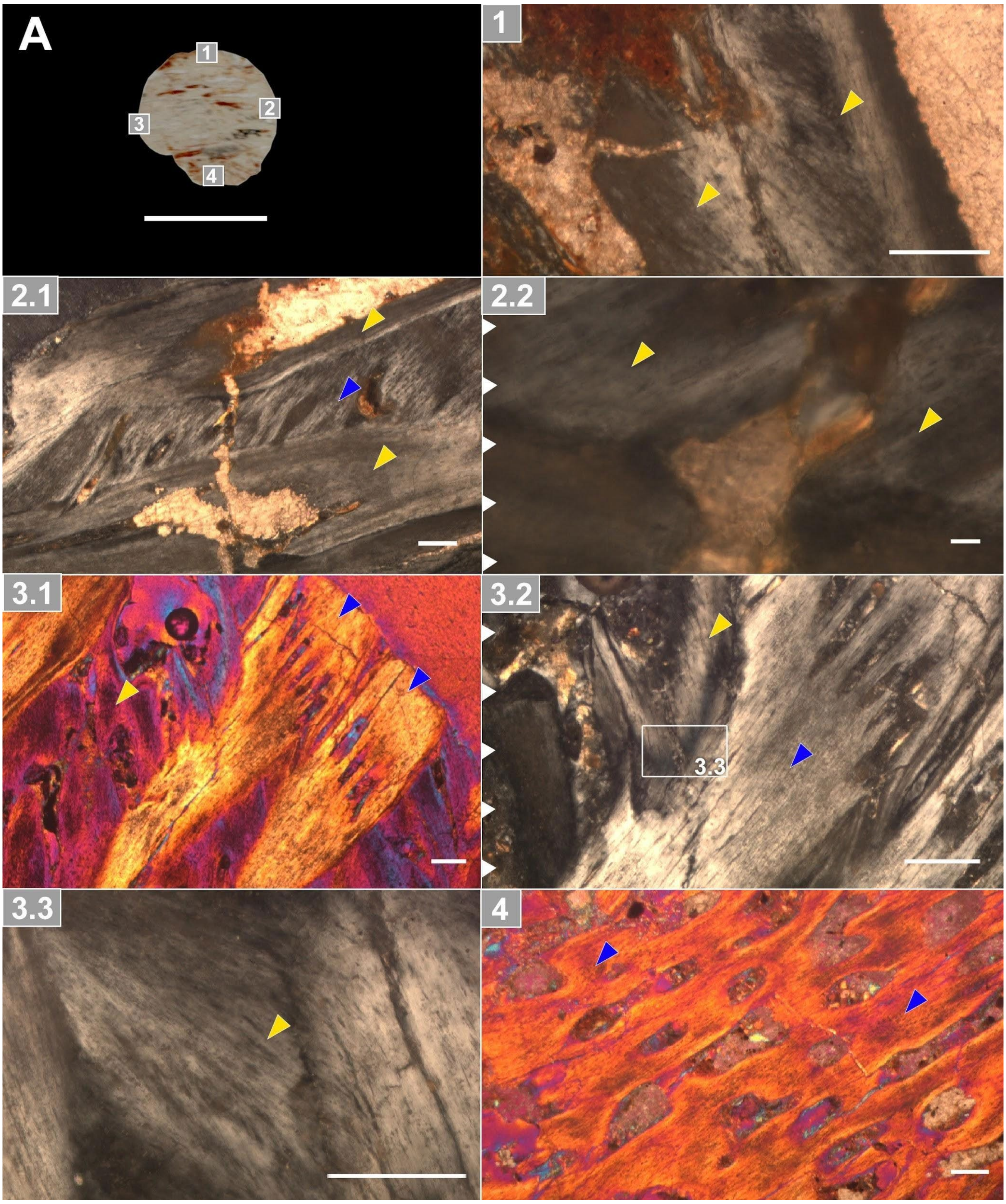

Figure 6. Dense regular and irregular collagenous connective tissue complex on the prezygapophysis of a posterior dorsal vertebra of the titanosaur *Aeolosaurus maximus* (MPMA 12-0001-97-1024; section DINOlab-TS-0107). **A**, polished cross-section illustrating image locations (**1**-**4**). Pneumosteal bone was absent in this sample. **1**, Sharpey's fibers showing high relief and insertion angles of approximately 60°. **2.1**, dense regular connective

tissue (tendons; yellow arrows) and underlying bone trabeculae (dark blue arrow). **2.2**, detail of the Sharpey's fibers acute angle of insertion in the interface between bone and tendon. **3.1**, connective tissue (blue arrows) attaching to the bone (yellow arrow) with detail of the appendage (**3.2**, **3.3**). **3.3**, Sharpey's fibers These also feature a 60° insertion angle. **4**, a dense irregular connective tissue sheath envelops tendons laterally. Polarized light under crossed nicols in **1-4** with lambda compensator in **3.1** and **4**. Scale bar in **A** = 10 mm; in **2.2** = 20 μm; in **1**, **2.1**, **3.1-4** = 200 μm.

Table 1. Distinct optical mineralogical properties between pneumosteal bone tissue and Sharpey's fibers.

Fossilized tissue	**Minimum magnification required**	**Fiber length**	**Optical relief**	**Extinction**	**Texture / Pattern**
Pneumosteum	40 X	usually shorter than 60 μm	shorter	always undulose	asbestiform (chaotic)
Sharpey's fibers	10 X	usually longer than 200 μm	higher	may be undulose or absent	inclined parallel lines at specific angles

DISCUSSION

Comments on fossilization

The composition of the *A. maximus* fossilized bone showed high concentrations of calcium and phosphor but no fluor counts. REE were also absent throughout the section. This contrasts with other samples from the Adamantina Formation (Marchetti *et al.*, 2019). Fortunately, this variation in the chemistry of recrystallization did not prevent the preservation of delicate structures originating from soft tissues, including the pneumosteal bone and ossified tendons and cartilage. Nevertheless, calcite dissolution has shown to be a more harmful diagnetic event for paleohistology (Aureliano et al., 2020).

Redescription of the neural arch of *Aeolosaurus maximus*

The original description of MPMA 12-0001-97-1024 by Santucci & Arruda-Campos (2011) has mistakenly identified the center as the prezygapophysis. Consequently, the latter has been wrongly identified as the diapophysis. However, the actual diapophysis was destroyed during diagenesis. Furthermore, the complexity of the laminae/fossae arrangement indicates the specimen is a posterior dorsal vertebra (Wilson *et al.*, 2011; Wilson, 2012) instead of an anterior one (contra Santucci & Arruda-Campos, 2011). Therefore, considering that *A. maximus* has been a problematic taxon in recent phylogenetic analyses (Bandeira *et al.*, 2016; Silva Junior *et al.*, 2019), redescription of the holotype matrix the rescoring of the characters for the holotype in phylogenetic matrix used to assess its phylogenetic affinities? suggested.

Pneumatic macroscopic structures in *Aeolosaurus maximus*

Despite the extensive diagenetic destruction, several pneumatic structures in a neural arch of the *Aeolosaurus maximus* holotype are preserved associated with the organism's respiratory system. A complex arrangement between fossae and laminae once gave support to pulmonary diverticula. The acdl and pcdl laminae contain no camellae, but there is a single foramen in their fused table. CT scan images showed that the specimen was diagenetic compromised and few data could be extracted from the images. Nonetheless, they reveal a camellate architecture in the neural arch, spdl, spof, and in the prezygapophysis. These internal pneumatic cavities are elongated between the prezygapophysis and the neural spine, and slightly radial to the prezygapophysis articulation surface. A similar pattern has been observed in the cervical cotyles of *Austroposeidon magnificus* MCT 1628-R (Bandeira *et al.*, 2016) and *Uberabatitan ribeiroi* CPPLIP-1024 (Aureliano *et al.*, no date in%20press). Therefore, this pattern may correlate to the structural needs of the vertebral articulation surfaces instead of being restricted to any specialized area. Elongated cylindrical bone walls perpendicular to the surfaces may have been a histological adaptation to sustain axial mechanical stresses (Christian and Dzemski, 2011; Hohn, 2011; Padian *et al.*, 2013). The neural spinal camellate fabric of MPMA 12-0001-97-1024 shows no continuous shape and size. The architecture of the latter could not be directly compared to *Saltasaurus loricatus* (Cerda, Salgado and Powell, 2012), *Austroposeidon magnificus* (Bandeira *et al.*, 2016), and *Uberabatitan ribeiroi* (Aureliano *et al.*, 2020) because of lack of CT data.

New insights on the pneumosteum

The evolution of pneumatic structures played a definitive role in archosaur phylogeny (O'Connor, 2006; Wedel, 2006, 2007; Butler, Barrett and Gower, 2009, 2012; Claessens, O'Connor and Unwin, 2009). Classically, the association between the skeleton and the respiratory system has been limited to macroscopic observations and tomographies (Wilson *et al.*, 2011; Cerda, Salgado and Powell, 2012; Wilson, 2012; Yates, Wedel and Bonnan, 2012). Fortunately, it is also possible to investigate the histology of the air-sac diverticula contact with the skeleton throughout the identification of a specific secondary bone tissue called pneumosteum (Lambertz, Bertozzo and Sander, 2018). This tissue has been reported for very few taxa, however. The pneumosteal bone in the neural arch of *Aeolosaurus maximus* has confirmed several characteristics found in *Uberabatitan* (Aureliano *et al.*, no date), *Europasaurus*, and *Diplodocus* (Lambertz, Bertozzo and Sander, 2018). Additionally, by applying descriptive concepts from optical mineralogy, we could go further with the description of this tissue in this study. Pneumosteum is distinguished from the lamellar bone tissue making up regular bone trabeculae by constituting an array of tiny asbestiform densely-packed fibers (usually shorter than 60 µm). These fibers depicted a low optical relief in every rotation angle, and exhibited undulose extinction. Our study also indicated that despite the absence any camellate structure in the laminae, pneumosteal bone was present. The latter was found to be present both in the external and internal surfaces of the laminae (pcdl and acdl), in the trabeculae fragments, and also surrounding the foramen floor. This observation corroborates the hypothesis that diverticula would be attached to their surrounding fossae (cpaf, prpadf, and pocdf) (O'Connor, 2006; Wilson *et al.*, 2011).

Furthermore, it may be quite challenging to distinguish pneumosteal bone fibers from the ones resulted from muscle and tendon insertions (Sharpey's fibers). We established a solid base for histological comparison between these tissues (see Table 1). All Sharpey's fibers found in this approach are in accordance with previous observations from other taxa (Petermann and Sander, 2013; Sanchez *et al.*, 2013; Pereyra *et al.*, 2019). They exhibit a high relief, undulose extinction, and insertion angles of approximately 60° relative to the cortical surface. These fibers are considerably longer (>200 µm) and thicker (<60 µm) than the pneumosteum ones. Another difference is that the former show an organized parallel pattern in contrast to the chaotic asbestiform organization of the latter.

CONCLUSIONS

We expanded the occurrence of pneumosteum in dinosaurs to the Brazilian titanosaur *Aeolosaurus maximus*. We detected mistakes in the original description of *A. maximus* vertebra and suggest a careful redescription of the holotype specimen. CT scanning of the neural arch revealed a complex arrangement between fossae and laminae associated with an air-sac system. Despite the absence of any camellate architecture in the laminae, pneumosteal bone tissue was present. This observation corroborates the hypothesis that diverticula would be attached to the fossae. Furthermore, we also conclude that the nonexistence of camellae is not definitive evidence to discard the pneumatization of the bone.

Additionally, we established a solid base for histological comparison to distinguish pneumosteal bone fibers from the Sharpey's fibers (muscle and tendon insertions) using the polarizing microscope. We hope this will assist colleagues to collect more data for the expansion of the knowledge on the evolution of the respiratory system in archosaurs.

ACKNOWLEDGEMENTS

We would like to acknowledge Oswaldo Jorge and the rest of the HU-UFSCar team for conducting fossil tomography. To Sandra Tavares and Fabiano Iori for their assistance at the Monte Alto Paleontological Museum collection. To the Departamento de Pós-Graduação do Instituto de Geociências, Unicamp, and to *Colecionadores de Ossos*$^{\text{TM}}$, for funding transportation and thin sections. Authors research grants, scholarships, and financial aid were provided by the Brazilian National Council for Scientific and Technological Development (CNPq) (T.A.), the Brazilian Coordination for the Improvement of Higher Education Personnel (CAPES - Finance Code 001) (A.M.G), and FAPESP 2016/20927-0 'Modern accumulation studies and fossil bioclast studies in continental and coastal environments' (F.R.B.).

Bibliography

Aureliano, T. *et al.* (2020) ‘Influence Of Taphonomy On Histological Evidence For Vertebral Pneumaticity In An Upper Cretaceous Titanosaur From South America’, *Cretaceous Research*, p. 104337. doi: 10.1016/j.cretres.2019.104337.

Bandeira, K. L. N. *et al.* (2016) ‘A New Giant Titanosauria (Dinosauria: Sauropoda) from the Late Cretaceous Bauru Group, Brazil’, *PloS one*, 11(10), p. e0163373. doi: 10.1371/journal.pone.0163373.

Brusatte, S. L., O’Connor, J. K. and Jarvis, E. D. (2015) ‘The Origin and Diversification of Birds’, *Current biology: CB*. Elsevier, 25(19), pp. R888–98. doi: 10.1016/j.cub.2015.08.003.

Buchmann, R. and Rodrigues, T. (2019) ‘The Evolution of Pneumatic Foramina in Pterosaur Vertebrae’, *Anais da Academia Brasileira de Ciencias*, 91Suppl. 2(Suppl. 2), p. e20180782. doi: 10.1590/0001-3765201920180782.

Butler, R. J., Barrett, P. M. and Gower, D. J. (2009) ‘Postcranial skeletal pneumaticity and air-sacs in the earliest pterosaurs’, *Biology letters*, 5(4), pp. 557–560. doi: 10.1098/rsbl.2009.0139.

Butler, R. J., Barrett, P. M. and Gower, D. J. (2012) ‘Reassessment of the evidence for postcranial skeletal pneumaticity in Triassic archosaurs, and the early evolution of the avian respiratory system’, *PloS one*. journals.plos.org, 7(3), p. e34094. doi: 10.1371/journal.pone.0034094.

Castro, M. C. *et al.* (2018) ‘A Late Cretaceous mammal from Brazil and the first radioisotopic age for the Bauru Group’, *Royal Society open science*, 5(5), p. 180482. doi: 10.1098/rsos.180482.

Cerda, I. A. *et al.* (2017) ‘Novel insight into the origin of the growth dynamics of sauropod dinosaurs’, *PloS one*. journals.plos.org, 12(6), p. e0179707. doi: 10.1371/journal.pone.0179707.

Cerda, I. A., Salgado, L. and Powell, J. E. (2012) ‘Extreme postcranial pneumaticity in sauropod dinosaurs from South America’, *Paläontologische Zeitschrift*. Springer, 86(4), pp. 441–449. doi: 10.1007/s12542-012-0140-6.

Christian, A. and Dzemski, G. (2011) ‘Neck posture in sauropods’, *Biology of the sauropod dinosaurs: understanding the life of giants. Indiana University Press, Bloomington*. books.google.com, pp. 251–260. Available at: https://books.google.com/books?hl=pt-BR&lr=&id=1GOYYwqctxMC&oi=fnd&pg=PA251&dq=neck+posture+in+sauropods+andreas+christian&ots=meSfmsN39K&sig=_5TwBNwH0k9iFzrbdlSqGSkbPHY.

Claessens, L. P. A. M., O’Connor, P. M. and Unwin, D. M. (2009) ‘Respiratory evolution facilitated the origin of pterosaur flight and aerial gigantism’, *PloS one*, 4(2), p. e4497. doi: 10.1371/journal.pone.0004497.

Dias, W. A. F. *et al.* (2020) ‘The pterygoid region and cranial airways of Caipirasuchus paulistanus and Caipirasuchus montealtensis (Crocodyliformes, Sphagesauridae), from the Upper Cretaceous Adamantina Formation, Bauru Basin, Brazil', *Cretaceous Research*. Elsevier, 106, p. 104192. Available at: https://www.sciencedirect.com/science/article/pii/S0195667118304051.

Dyke, G. J. (2010) 'Palaeoecology: different dinosaur ecologies in deep time?', *Current biology: CB*, 20(22), pp. R983–5. doi: 10.1016/j.cub.2010.10.001.

Fedorov, A. *et al.* (2012) '3D Slicer as an image computing platform for the Quantitative Imaging Network', *Magnetic resonance imaging*, 30(9), pp. 1323–1341. doi: 10.1016/j.mri.2012.05.001.

Fiorillo, A. R. and Gangloff, R. A. (2001) 'Theropod teeth from the Prince Creek Formation (Cretaceous) of northern Alaska, with speculations on Arctic dinosaur paleoecology', *Journal of Vertebrate Paleontology*. Taylor & Francis, 20(4), pp. 675–682. doi: 10.1671/0272-4634(2000)020[0675:TTFTPC]2.0.CO;2.

Francillon-Viellot, H. *et al.* (1990) 'Microstructure and mineralization of vertebrate skeletal tissues. In (J. Carter, Ed.) Skeletal Biomineralization: Patterns, Processes and Evolutionary Trends, vol. 1'. New York: Van Nostrand Reinhold.

Godoy, P. L. (2019) 'Crocodylomorph cranial shape evolution and its relationship with body size and ecology', *Journal of evolutionary biology*. Wiley Online Library. doi: 10.1111/jeb.13540.

Hohn, B. (2011) 'Walking with the shoulder of giants: biomechanical conditions in the tetrapod shoulder girdle as a basis for sauropod shoulder reconstruction', *Biology of the sauropod dinosaurs: understanding the life of giants*. Indiana University Press, 182, p. 196. Available at: https://books.google.com/books?hl=pt-BR&lr=&id=1GOYYwqctxMC&oi=fnd&pg=PA182&dq=walking+with+the+shoulder+of+giants+bianca+hohn&ots=meSfmsN29S&sig=UqV7ltdhyjds5pd02PeCDbIxGTQ.

Klein, C. and Dutrow, B. (2007) *Manual of mineral science*. Wiley.

Lambertz, M., Bertozzo, F. and Sander, P. M. (2018) 'Bone histological correlates for air sacs and their implications for understanding the origin of the dinosaurian respiratory system', *Biology letters*. rsbl.royalsocietypublishing.org, 14(1). doi: 10.1098/rsbl.2017.0514.

Lamm, E.-T. (2013) 'Preparation and Sectioning of Specimens', in *Bone Histology of Fossil Tetrapods*. University of California Press. doi: 10.1525/california/9780520273528.003.0004.

Marchetti, I. *et al.* (2019) 'Fossildiagenesis and ontogenetic insights of crocodyliform bones from the Adamantina Formation, Bauru Basin, Brazil', *Journal of South American Earth Sciences*. Elsevier, 96, p. 102327. doi: 10.1016/j.jsames.2019.102327.

Mitchell, J. and Sander, P. M. (2014) 'The three-front model: a developmental explanation of long bone diaphyseal histology of Sauropoda', *Biological journal of the Linnean Society. Linnean Society of London*. Oxford University Press, 112(4), pp. 765–781. doi:

10.1111/bij.12324.

Nesbitt, S. J. (2011) ‘The Early Evolution of Archosaurs: Relationships and the Origin of Major Clades’, *Bulletin of the American Museum of Natural History*. BioOne, 352, pp. 1–292. doi: 10.1206/352.1.

O’Connor, P. M. (2004) ‘Pulmonary pneumaticity in the postcranial skeleton of extant aves: a case study examining Anseriformes’, *Journal of morphology*. Wiley Online Library, 261(2), pp. 141–161. doi: 10.1002/jmor.10190.

O’Connor, P. M. (2006) ‘Postcranial pneumaticity: an evaluation of soft-tissue influences on the postcranial skeleton and the reconstruction of pulmonary anatomy in archosaurs’, *Journal of morphology*. Wiley Online Library, 267(10), pp. 1199–1226. Available at: https://onlinelibrary.wiley.com/doi/abs/10.1002/jmor.10470.

Padian, K. *et al.* (2013) ‘Research applications and integration’, in *Bone Histology of Fossil Tetrapods: Advancing Methods, Analysis, and Interpretation*. University of California Press, pp. 265–285. Available at: https://books.google.com/books?hl=pt-BR&lr=&id=EBVNmk1nm6MC&oi=fnd&pg=PA265&dq=research+applications+and+integration+kevin+padian&ots=c_VYtfOM1V&sig=rY2NJt3cCJ4cT_WN2O2gj1rAbm8.

Padian, K. and Lamm, E.-T. (2013) *Bone Histology of Fossil Tetrapods: Advancing Methods, Analysis, and Interpretation*. University of California Press. Available at: https://market.android.com/details?id=book-EBVNmk1nm6MC.

Pereyra, M. E. *et al.* (2019) ‘Osteohistological correlates of muscular attachment in terrestrial and freshwater Testudines’, *Journal of anatomy*, 234(6), pp. 875–898. doi: 10.1111/joa.12975.

Perry, S. F. *et al.* (2009) ‘Implications of an avian-style respiratory system for gigantism in sauropod dinosaurs’, *Journal of experimental zoology. Part A, Ecological genetics and physiology*. Wiley Online Library, 311(8), pp. 600–610. Available at: https://onlinelibrary.wiley.com/doi/abs/10.1002/jez.517.

Petermann, H. and Sander, M. (2013) ‘Histological evidence for muscle insertion in extant amniote femora: implications for muscle reconstruction in fossils’, *Journal of anatomy*, 222(4), pp. 419–436. doi: 10.1111/joa.12028.

Pfretzschner, H.-U. (2004) ‘Fossilization of Haversian bone in aquatic environments’, *Comptes rendus. Palevol*. Elsevier, 3(6), pp. 605–616. doi: 10.1016/j.crpv.2004.07.006.

Raith, M. M., Raase, P. R. and Reinhardt, J. R. (2011) *Guide to thin section microscopy*. University of Bonn.

Sanchez, S. *et al.* (2013) ‘3D microstructural architecture of muscle attachments in extant and fossil vertebrates revealed by synchrotron microtomography’, *PloS one*. journals.plos.org, 8(2), p. e56992. doi: 10.1371/journal.pone.0056992.

Sander, P. M. *et al.* (2011) ‘Biology of the sauropod dinosaurs: the evolution of gigantism’, *Biological reviews of the Cambridge Philosophical Society*. Wiley Online Library, 86(1), pp. 117–155. doi: 10.1111/j.1469-185X.2010.00137.x.

Santucci, R. M. and Arruda-Campos, A. C. de (2011) ‘A new sauropod (Macronaria, Titanosauria) from the Adamantina Formation, Bauru Group, Upper Cretaceous of Brazil and the phylogenetic relationships of Aeolosaurini’, *Zootaxa*. zanzara.fondazionemcr.it, 3085, pp. 1–33. Available at: http://www.zanzara.fondazionemcr.it/UploadDocs/4037_Santucci_ArrudaCampos_2011.pdf.

Silva Junior, J. C. G. *et al.* (2019) ‘Osteology and systematics of Uberabatitan ribeiroi (Dinosauria; Sauropoda): a Late Cretaceous titanosaur from Minas Gerais, Brazil’, *Zootaxa*. researchgate.net, 4577(3), pp. 401–438. Available at: https://www.researchgate.net/profile/Julian_Silva_Junior/publication/332274953_Osteology_and_systematics_of_Uberabatitan_ribeiroi_Dinosauria_Sauropoda_a_Late_Cretaceous_titanosaur_from_Minas_Gerais_Brazil/links/5cab507d92851c64bd581393/Osteology-and-systematics-of-Uberabatitan-ribeiroi-Dinosauria-Sauropoda-a-Late-Cretaceous-titanosaur-from-Minas-Gerais-Brazil.pdf.

Stein, K. and Sander, P. M. (2009) ‘Histological core drilling: a less destructive method for studying bone histology’, in *Methods in fossil preparation: proceedings of the first annual Fossil Preparation and Collections Symposium*. ebook]: Petrified Forest National Park, pp. 69–80. Available at: http://www.academia.edu/download/44573693/Histological_core_drilling_a_less_destru20160409-9077-3nz6af.pdf.

Wedel, M. J. (2003) ‘Vertebral pneumaticity, air sacs, and the physiology of sauropod dinosaurs’, *Paleobiology*. Cambridge University Press, 29(2), pp. 243–255. doi: 10.1017/S0094837300018091.

Wedel, M. J. (2006) ‘Origin of postcranial skeletal pneumaticity in dinosaurs’, *Integrative zoology*, 1(2), pp. 80–85. doi: 10.1111/j.1749-4877.2006.00019.x.

Wedel, M. J. (2007) ‘What pneumaticity tells us about “prosauropods”, and vice versa’, *Special Papers in Palaeontology*. researchgate.net, 77, pp. 207–222. Available at: https://www.researchgate.net/profile/Mathew_Wedel/publication/272152712_What_pneumaticity_tells_us_about_prosauropods'_and_vice_versa/links/57d2e0e108ae5f03b48cd10c/What-pneumaticity-tells-us-about-prosauropods-and-vice-versa.pdf.

Wedel, M. J. (2009) ‘Evidence for bird-like air sacs in saurischian dinosaurs’, *Journal of experimental zoology. Part A, Ecological genetics and physiology*. Wiley Online Library, 311(8), pp. 611–628. Available at: https://onlinelibrary.wiley.com/doi/abs/10.1002/jez.513.

Wilson, J. A. *et al.* (2011) ‘A nomenclature for vertebral fossae in sauropods and other saurischian dinosaurs’, *PloS one*. journals.plos.org, 6(2), p. e17114. doi: 10.1371/journal.pone.0017114.

Wilson, J. A. (2012) ‘New vertebral laminae and patterns of serial variation in vertebral laminae of sauropod dinosaurs’. Museum of Paleontology, The University of Michigan. Available at:

https://deepblue.lib.umich.edu/bitstream/handle/2027.42/92460/Contributions32no7-HR-c08-15-2012.pdf?sequence=2.

Yates, A. M., Wedel, M. J. and Bonnan, M. F. (2012) 'The Early Evolution of Postcranial Skeletal Pneumaticity in Sauropodomorph Dinosaurs', *Acta palaeontologica Polonica*. BioOne, 57(1), pp. 85–100. doi: 10.4202/app.2010.0075.**SUPPLEMENTARY MATERIAL**

METHOD

Electron microscopy

Electron Dispersive X-Ray Spectroscopy analysis was conducted in MPMA 12-0001-97-1024 and its sedimentary infills to investigate its taphonomy. Sample was photographed and analyzed with an Oxford Instruments INCA x-act with Aztec software attached to a high vacuum FEI Quanta 250.

TAPHONOMY AND GEOCHEMISTRY

Sedimentary clasts and matrix

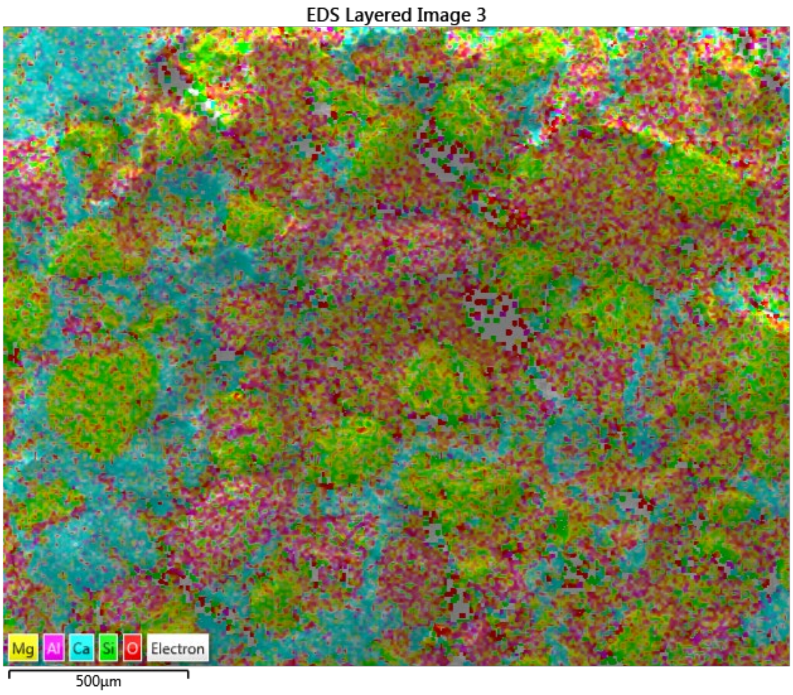

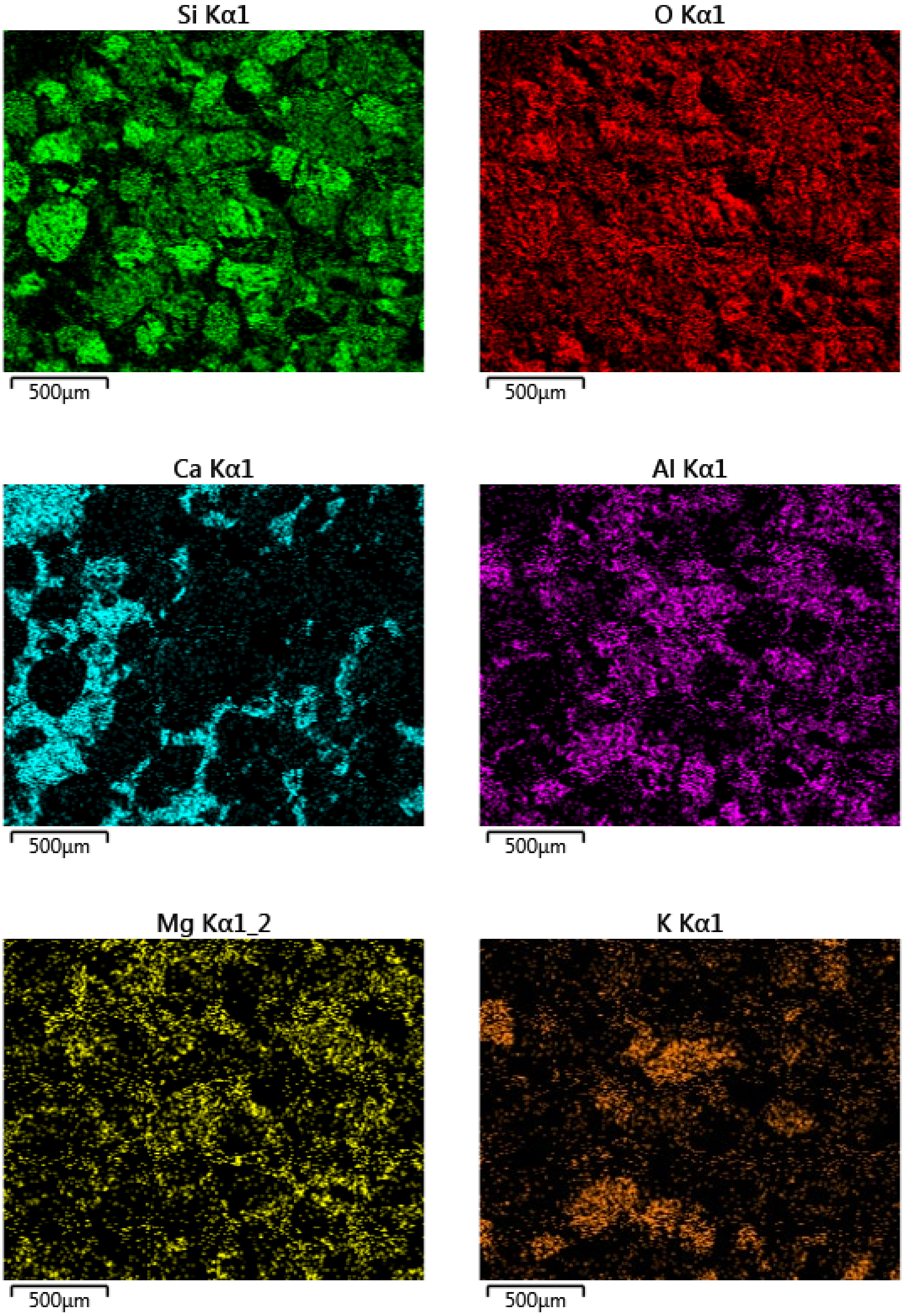
Si Kα1
500µm
O Kα1
500µm
Ca Kα1
500µm
Al Kα1
500µm
Mg Kα1_2
500µm
K Kα1
500µm

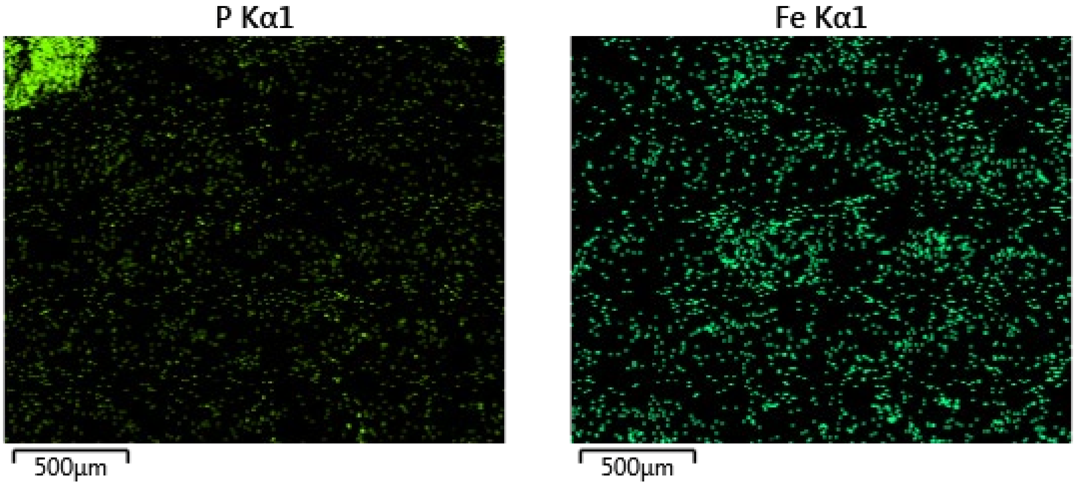

Figure S1. EDS elemental maps illustrating the distribution of elements of the infilled sedimentary matrix in a vertebral lamina of the titanosaur *Aeolosaurus maximus* (MPMA 12-0001-97-1024).

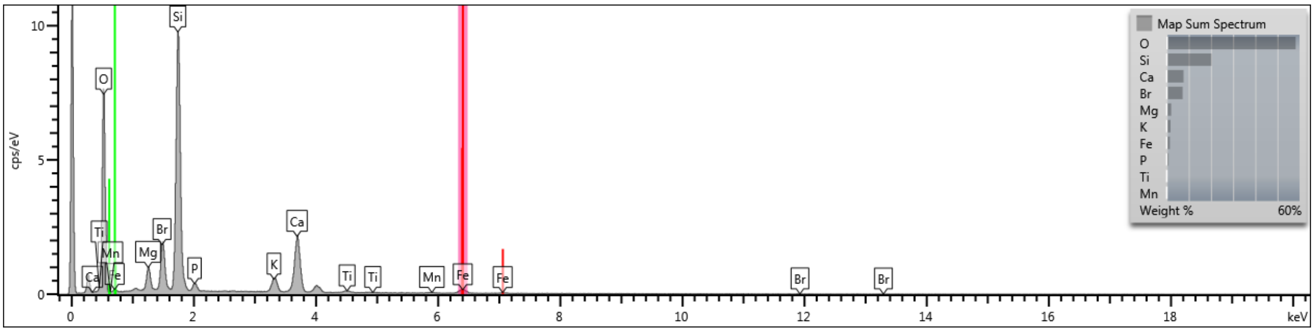

Figure S2. EDS elemental map spectrum showing the general composition of the sedimentary matrix of Fig.S1.

Bone fossilization chemistry

Sample site 1

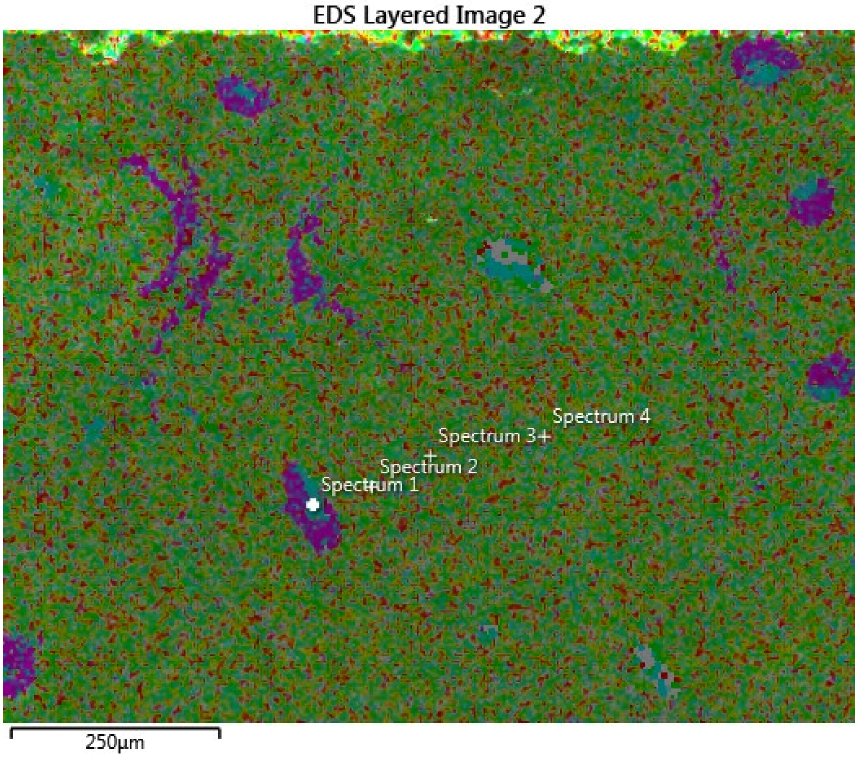
EDS Layered Image 2
Spectrum 4
Spectrum 3
Spectrum 2
Spectrum 1
250µm

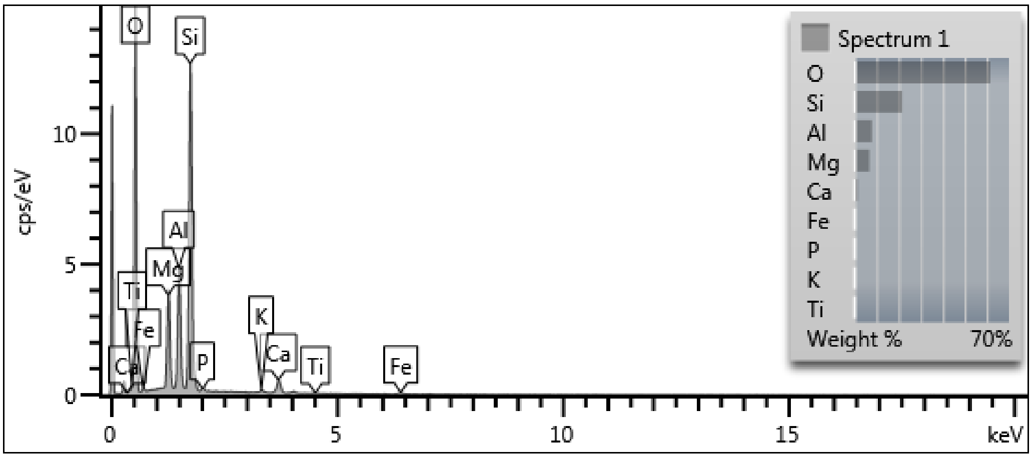
Spectrum 1
O
Si
Al
Mg
Ca
Fe
P
K
Ti
Weight %
70%
cps/eV
10
5
0
keV
15
O
Si
Al
Mg
Ti
Fe
Ca
P
K
Ca
Ti
Fe

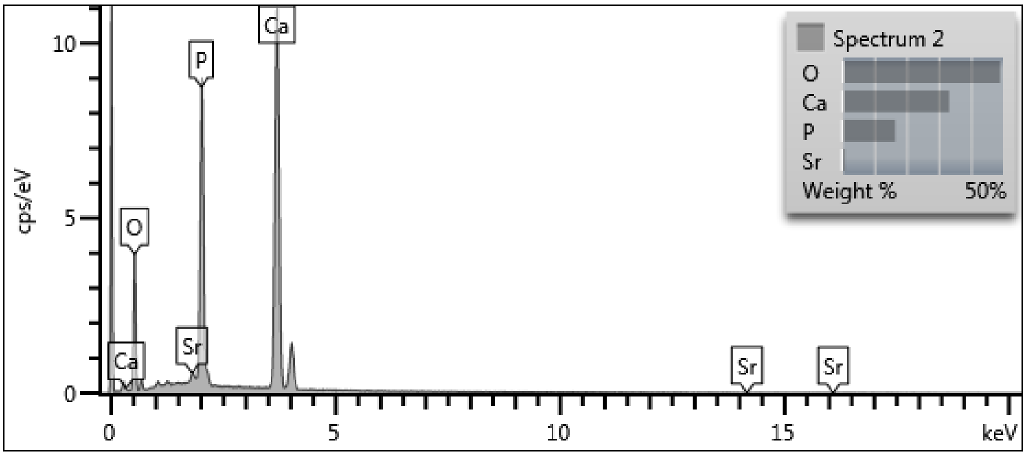
Spectrum 2
O
Ca
P
Sr
Weight %
50%
cps/eV
10
5
0
keV
15
Ca
P
O
Sr
Ca
Sr
Sr

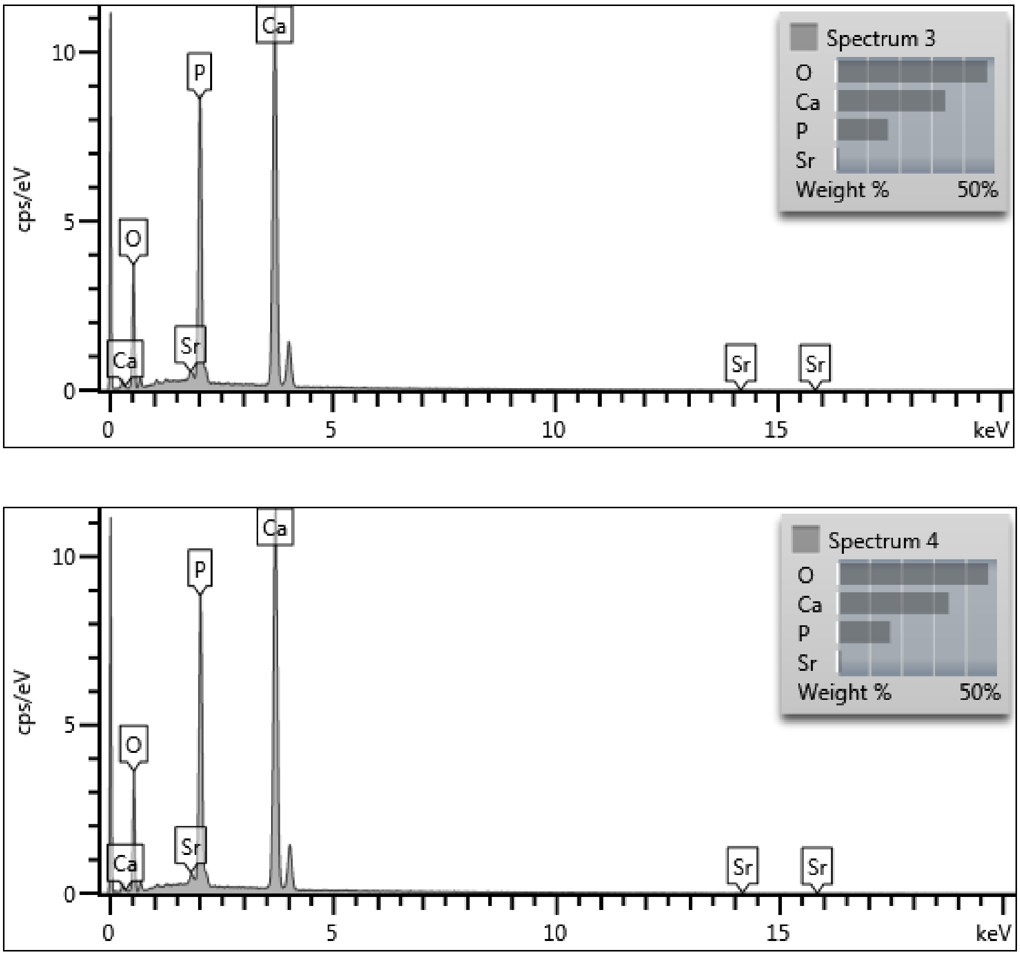

Figure S3. EDS elemental map (top) illustrating the distribution of elements in the fossilized bone trabeculae and composition spectra in a vertebra of the *Aeolosaurus maximus* (MPMA 12-0001-97-1024).

Sample site 2

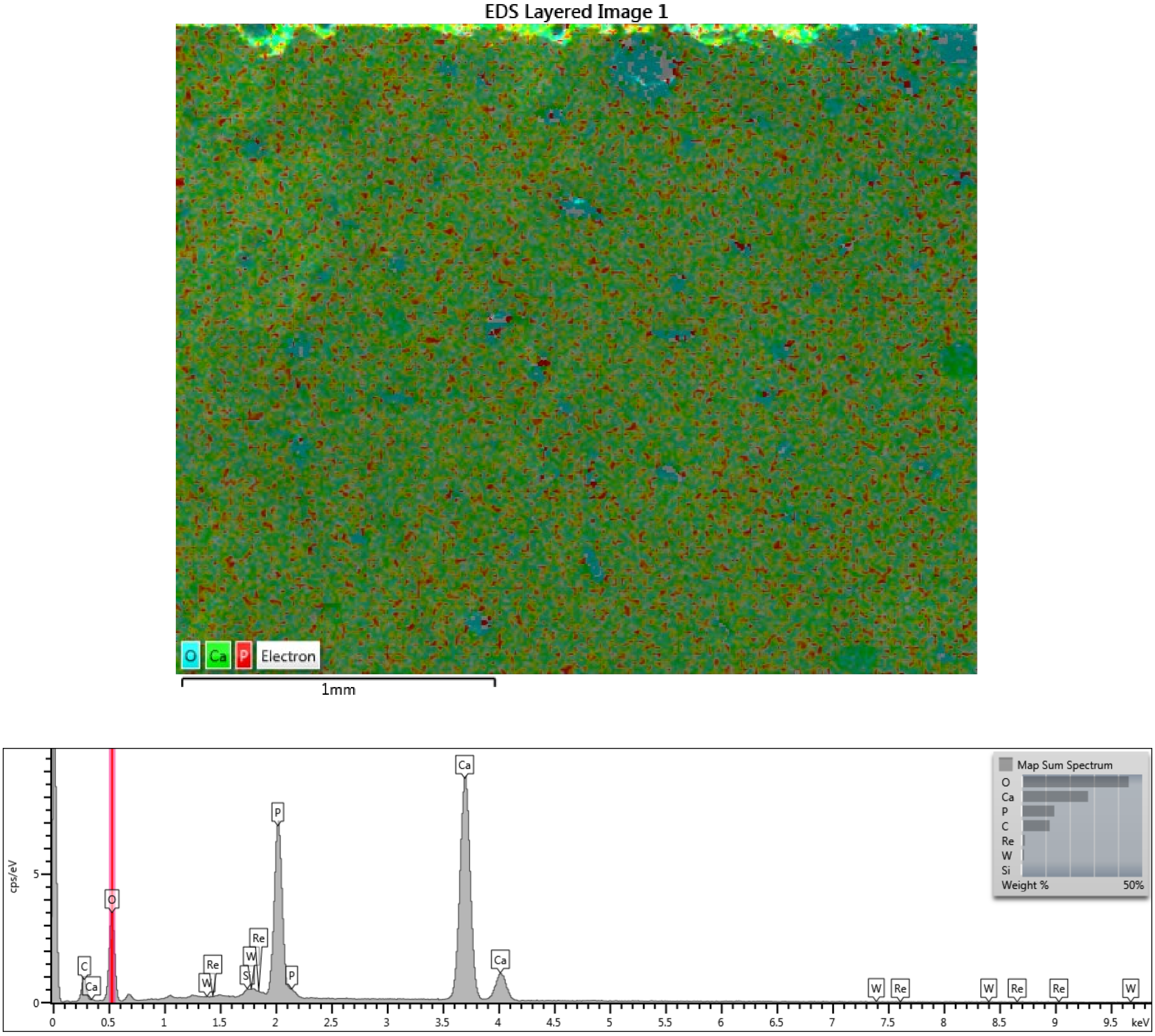

Figure S4. EDS elemental map (top) illustrating the distribution of elements in the fossilized bone tissue and its composition spectrum in a vertebra of the *Aeolosaurus maximus* (MPMA 12-0001-97-1024).

CAPÍTULO VI - ARTIGO CIENTÍFICO

AURELIANO, T., GHILARDI, A. M., FERNANDES, M. F., NAVARRO, B., MARTIN SANDER, P., RICARDI-BRANCO, F. S.. Exquisite air sacs histological traces in a hyperpneumatized saltasaur from South America.

Status: Manuscrito a ser submetido

EXQUISITE AIR SACS HISTOLOGICAL TRACES IN A HYPERPNEUMATIZED SALTASAUR FROM SOUTH AMERICA

Tito Aureliano[1,2,3], Aline M. Ghilardi[2], Marcelo A. Fernandes[3], Bruno Navarro[4], P. Martin Sander[5], Fresia Ricardi-Branco[1]

[1]Institute of Geosciences, University of Campinas (Unicamp). Campinas, Brazil.

[2]Dinosaur Ichnology and Osteohistology Laboratory (DINOlab), Department of Geology, Federal University of Rio Grande do Norte (URFN). Natal, Brazil.

[3]Laboratório de Paleoecologia e Paleoicnologia (LPP), Departamento de Ecologia e Biologia Evolutiva (DEBE), Federal University of São Carlos (UFSCar). Sao Carlos, Brazil.

[4]Laboratório de Paleontologia, Museu de Zoologia, University of Sao Paulo, Avenida Nazaré, 481, 04263-000. Sao Paulo, Brazil.

[5]Division of Paleontology, University of Bonn, Nussallee 8, 53115. Bonn, Germany.

ABSTRACT

This study reports the occurrence of pneumosteum (osteohistological correlates of an avian-like air sacs system) in a Saltasauridae sauropod from the Upper Cretaceous Adamantina Formation in Southeast Brazil. We corroborate the hypotheses of an air sacs system on titanosaurian vertebrae based on external observation and computed tomographies. This is the fourth non-avian dinosaur taxon in which histological traces of air sacs have been found. We provided a detailed description of pneumatic structures from the CT scan of a dorsal vertebra of the specimen as a parameter for comparison with other taxa. The camellate pattern found in the vertebral center of the LPP-PV-0200 and other titanosaurs show distinct architectures. Subtrapezoidal architecture might be related to the cervical air sacs system. A chaotic arrangement may me related to the lung air sacs system. Further sampling in more taxa is necessary to test this hypothesis. The extreme pneumaticity observed in this Saltasauridae contrasts with previous assumptions that this feature is correlated with the evolution of giant sizes in sauropodomorphs. This study reinforces that even small-bodied sauropod clades could be hyperpneumatized.

Keywords: pneumosteum, respiratory system, histology, Sauropoda, pneumaticity

INTRODUCTION

Dinosaurs developed a varied array of adaptations throughout more than 230 million years of evolution (Wedel, Cifelli and Sanders, 2000; Mateus, Maidment and Christiansen, 2009; Norman *et al.*, 2011; Li *et al.*, 2012; Ibrahim *et al.*, 2014; Bandeira *et al.*, 2016; Delcourt, 2018; Müller, Langer and Dias-da-Silva, 2018; Pacheco *et al.*, 2019). Sauropods are often highlighted for their morphological adaptations to gigantism and increasingly high metabolic rates in derived clades (Stein *et al.*, 2010; Sander *et al.*, 2011; Cerda, Salgado and Powell, 2012; Sander, 2013; Mitchell and Sander, 2014; Curry Rogers and Kulik, 2018). The postcranial skeletal pneumaticity (PSP) is one of their most remarkable adaptations shared between theropods and sauropods (Wedel, 2003, 2006, 2007; Cerda, Salgado and Powell, 2012; Yates, Wedel and Bonnan, 2012; Brum *et al.*, 2018). These pneumatic structures in the axial skeleton (eg. fossae, laminae) are a reflection of a permeating system of diverticula originating from the lungs (Wedel, 2003, 2006, 2007, 2009; O'Connor, 2006; Wilson *et al.*, 2011; Wilson, 2012). Most of the approaches to study PSP in dinosaurs were limited to the observation of either macroscopic structures or their computed tomographies (CT scans). More recently there has been histological approaches to detect PSP throughout the detection of pneumosteum, but few taxa have been sampled so far (Lambertz, Bertozzo and Sander, 2018; Aureliano *et al.*, 2020). Therefore, there is an urge to sample more taxa across space and time.

Saltasauridae titanosaurs had already been highlighted for their hyperpneumaticity in the axial skeleton in comparison to sauropodomorphs (Wedel, 2003; Cerda, Salgado and Powell, 2012). We sampled a posterior dorsal vertebra of an adult individual of a Saltasauridae titanosaur from the Upper Cretaceous Adamantina Formation, Southeast Brazil. Computer tomography and histology were conducted throughout the vertebral center to unveil the interaction between the pleurocoels and their attached air sacs. Therefore, our results provided another piece for understanding the evolution of the respiratory system in derived sauropod dinosaurs.

MATERIAL AND METHODS

Institutional abbreviations: CPPLIP, Centro de Pesquisas Paleontológicas "Llewellyn Ivor Price", Universidade Federal do Triângulo Mineiro, Peirópolis (Uberaba), Brazil; **DINOlab**, Dinosaur Ichnology and Osteohistology Laboratory, Federal University of Rio Grande do Norte, Natal, Brazil; Centro de Pesquisas Paleontológicas "Llewellyn Ivor Price", Federal University of Triângulo Mineiro, Peirópolis (Uberaba), Brazil; **LPP-PV**, Laboratório de Paleoecologia e Paleoicnologia (UFSCar), Federal University of São Carlos (UFSCar), São Carlos, Brazil; **HU-UFSCar**, Hospital Universitário, Federal University of São Carlos, São Carlos, Brazil; **PVL**, Paleovertebrate collection, Instituto "Miguel Lillo", San Miguel de Tucumán, Argentina; **MCT**, Museu de Ciências da Terra, Rio de Janeiro, Brazil.

Material

Specimen: The studied specimen (LPP-PV-0200; Fig. 1) corresponds to a posterior dorsal vertebra of a titanosaur. It was rescued by Marcelo and Luciana Fernandes from a site in a farm at the Ibirá municipality, São Paulo midwest, Southeast Brazil. Aline Ghilardi prepared and restored the specimen. It is included in the description of the holotype of a new Saltasauridae taxon still under description by Bruno Navarro and colleagues separately. It was a small-bodied adult titanosaur (~6 m long). The specimen is housed at the Laboratory of Paleoichnology and Paleoecology at the Federal University of São Carlos, São Carlos city, São Paulo, Brazil.

Locality and horizon: Ibirá municipality, São Paulo State, Turonian-Santonian (Castro *et al.*, 2018) Adamantina Formation, Bauru Group, Southeast Brazil. Some authors attribute the rocks in this vicinity to the São José do Rio Preto Formation (Méndez, Novas and Iori, 2012; Fernandes and Coimbra, 2017; Delcourt and Iori, 2018).

Anatomical nomenclature and measurements

We followed Wilson et al. (2011) for vertebral fossae; Wilson (2012) for laminae; Wedel et al. (2000) and Wedel (2003, 2007) for pneumatic structures. Histological terms are accordance with standard literature (Francillon-Viellot *et al.*, 1990; Padian and Lamm, 2013). Pneumosteum description following Lambertz et al. (2018) and Aureliano et al. (2020). The terms anterior and posterior were used instead of cranial and caudal.

Anatomical Abbreviations: **cr**, centrum; **po**, postzygaphophysis; **pr**, prezygapophysis; **s**, neural spine.

Laminae: **cpol**, postzygapophyseal centropostzygapophyseal lamina.

Fossae: **pacdf**, parapophyseal centrodiapophyseal fossa; **pocdf**, postzygapophyseal centrodiapophyseal fossa.

Computed tomography

A CT scan of the specimen was obtained before histological sampling using a Philips Diamond Select Brilliance CT 16-slice medical scanner with more than 200 slices and a voxel size of 0.75 mm at the HU-UFSCar. Acceleration voltage varied between 90 and 120 kV in a current of 367 mA. The methodology by Aureliano et al. (2020) was followed to analyze the data and generate the three-dimensional reconstruction with the software *3D Slicer* v4.10 (Fedorov *et al.*, 2012). Figure organization and numbering follow Brum et al. (2018).

Bone histology

Histological samples were conducted to track and describe the 'pneumosteal bone'. Pneumosteum are histological traces in the bone which correlate to the lungs and their diverticula (Lambertz, Bertozzo and Sander, 2018). The transversal section in the pleurocoel were produced following standard procedures (Lamm, 2013). The sample that crossed the entire vertebral center throughout the pleurocoels was obtained from a core drill (Stein and Sander, 2009). See Fig.1 for the planes of section. Thin sections were chipped to a thickness of ~40-50 µm. Thin sections were observed and photographed with a petrographic Leica DM750P microscope with coupled Leica EC3 camera, and imaging software LAS EZ 1.6.0. Pictures were corrected for brightness and contrast in Adobe Photoshop CC 20.0.1 and composite images were prepared in Corel Draw X6.

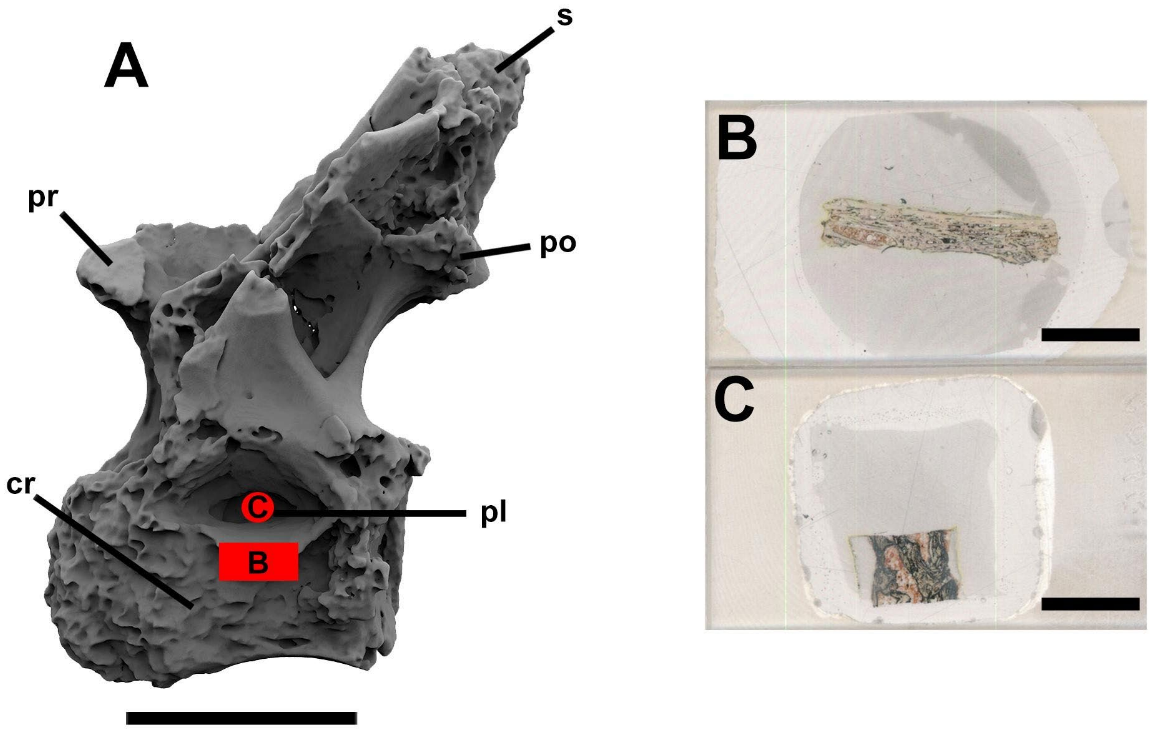

Figure 1. Posterior dorsal vertebra of the Upper Cretaceous Brazilian Saltasauridae titanosaur LPP-PV-0200. Three-dimensional reconstruction from CT scan in left lateral view (A). Red circle and rectangle show sampling planes and the respective thin sections are in B and C. Scale bar in A = 5 cm; in B, C = 1 cm.

RESULTS

CT scan of the Saltasauridae vertebra LPP-PV-0200

The tomography slices allowed a 3D reconstruction of the Saltasauridae specimen LPP-PV-0200 (Fig.1,2). Internal bone architecture survived taphonomical processes and most of the pneumatic structures could be assessed (Fig.2). In the vertebral center, there is an array of elongated parallel cavities extending dorsoventrally in frontal view (Fig.2.1-3), and posteroanteriorly in lateral view (Fig.2.4-5). Camellate architecture presents a general subtrapezoidal 'honeycomb' array (*sensu* Wedel, 2003), especially in the lateral view of the neural arch. Camellae expand radially from the cotyle surface inwards (Fig.2.7-9). Vertebral laminae (cpol, pcdl), pr, po, and the s present slightly thicker bone walls than the remaining structures. Camellae are smaller in the vertebral center (average width = 3.9 mm) but enlarge in the neural arch (average width = 4.8 mm). Pleurocoels are extremely deep in both sides, leaving only a thin bone wall (> 1 cm) of vertebral center and present a ‘bow-tie’ shape in ventral view Fig.2.8).

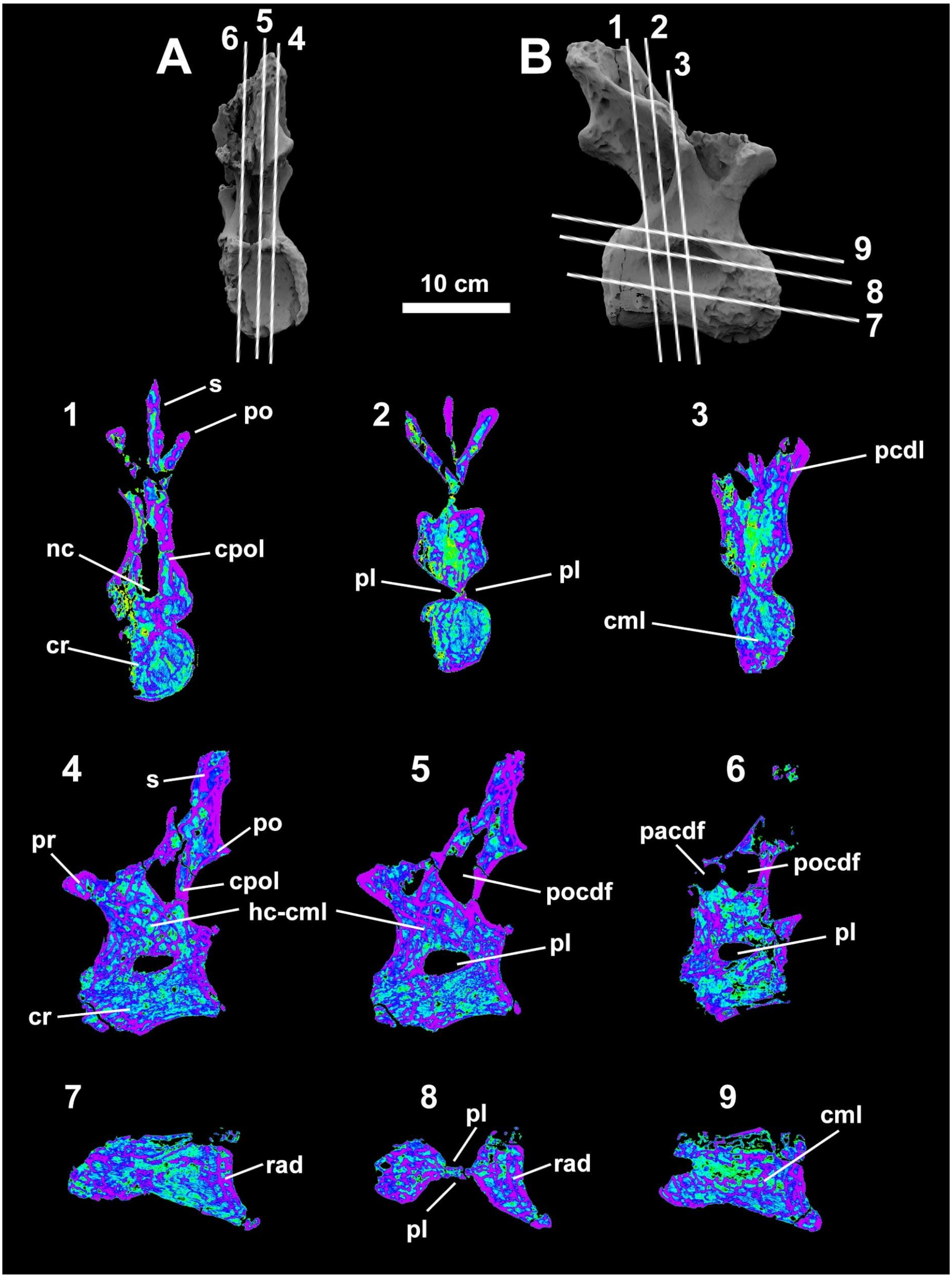

Figure 2. Internal structures of the dorsal vertebra of the Saltasauridae specimen LPP-PV-0200. **R**econstructed tomography model in distal (**A**) and right lateral (**B**) views illustrating

subvertical tangential CT scan slices in false color (**1-9**). Images show that only a few structures had survived diagenesis which restricted the assessment of the internal architecture to limited spaces. Lighter blue and green indicate lower densities (eg. pneumatic cavities). Purple and darker blue demonstrate denser structures (eg. camellate bone). **Abbreviations: cml**, camellae; **hc-cml**, 'honeycomb' camellae; **pl**, pleurocoel; **rad**, radial camellae.

Taphonomy and petrography

The specimen is pretty well preserved and there are no preparation marks on the surface, but the left lateral portion was slightly compromised during early transportation and burial. Sedimentary mineral grains fill trabecular cavities (Fig.3A). Thin oxide layers invade secondary osteons longitudinally in the medial shaft (Fig.3B). These are early diagenetic features (Pfretzschner, 2001). The birefringence of the bone apatite crystallites is well preserved and the microstructure could be assessed.

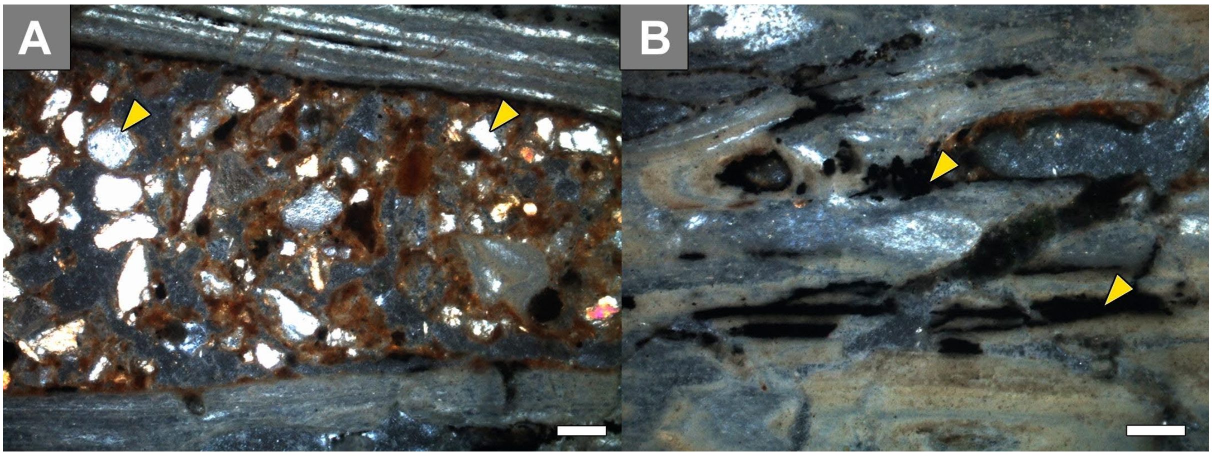

Figure 3. Taphonomical remarks in the microanatomy of LPP-PV-0200. **A**, poorly to moderately sorted subrounded to subangular mineral grains (arrow) and fragments of collapsed bone trabeculae (arrow) amidst the sedimentary matrix. Note the well preserved birefringence of the bone apatite crystallites. **B**, opaque oxide minerals infills the trabecular bone during weathering. Polarized light under crossed nicols. Scale bar = 100 µm.

Histology

The thin sections of the vertebral laminae comprise bone trabeculae with visible camellate architecture (Fig. 4). Pneumosteum is widespread throughout the bone and comprises the secondary bone entirely. Pneumosteum distinguishes from regular trabeculae by comprising an array of tiny asbestiform densely-packed fibers (<60 µm). Pneumosteal bone was found to be present both in vertebral center camellae (Fig.4.D-E) and the pleurocoel floor (Fig.4.A-C).

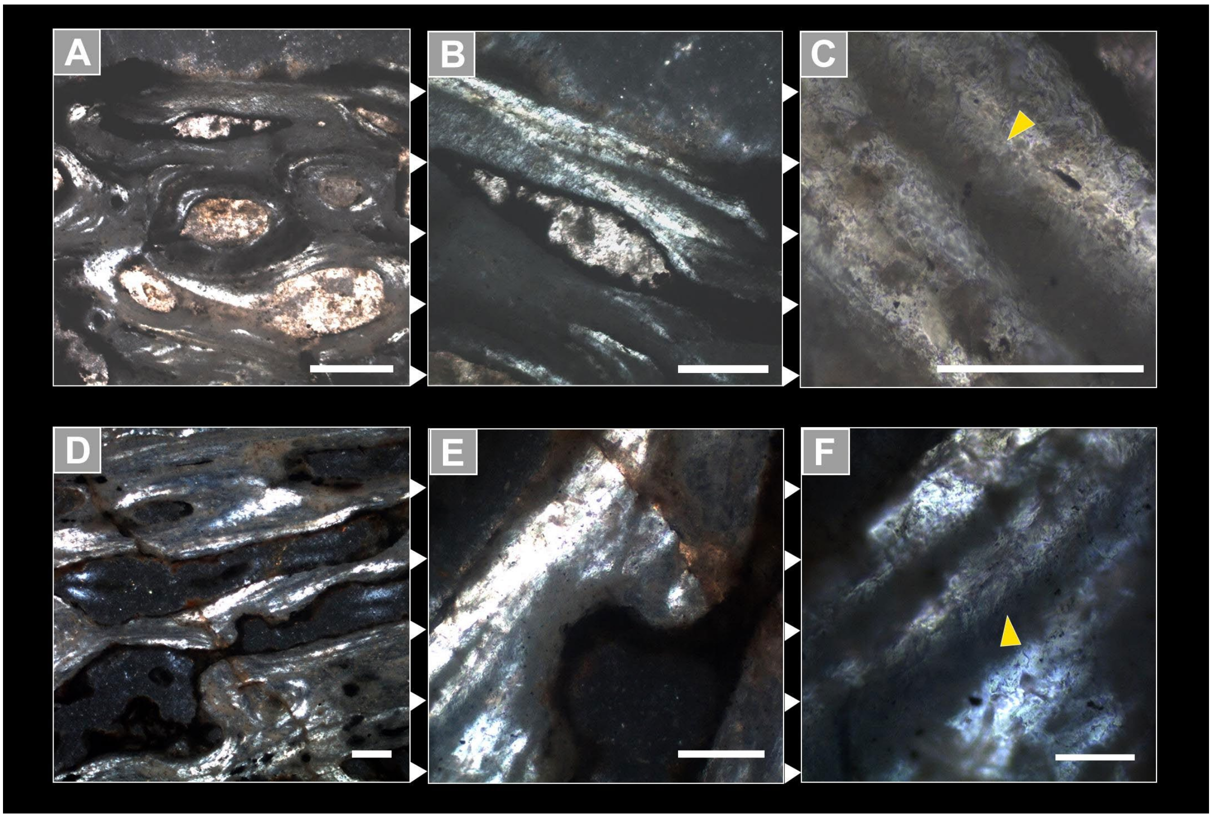

Figure 4. Occurrence of pneumosteum (arrows) in the posterior cervical vertebra of the Saltasauridae titanosaur LPP-PV-0200. **A-C**, secondary bone in the pleurocoel floor comprised entirely by pneumosteum. **D-F**, the trabeculae surrounding the pleurocoel also consist solely of pneumosteum. Pneumosteal bone presents an undulose extinction and tiny asbestiform densely-packed 'hair-like' fibers. Polarized light under crossed nicols. Scale bar in **A** = 200 µm; in **B**, **D** = 100 µm; in **C**, **E** = 50 µm; in **F** = 20 µm.

DISCUSSION

Several pneumatic structures in the titanosaur vertebra LPP-PV-0200 were associated with the organism's respiratory system. The hyperpneumatization in this Saltasauridae specimen is evidenced throughout a complex arrangement of fossae, laminae, and camellate internal architecture. These structures once gave support to pulmonary diverticula, similar to the air sacs system in extant birds. Tomography revealed a camellate architecture throughout most of the vertebral volume. The camellae are elongated in the vertebral center (anteroposteriorly and dorsoventrally), and slightly radial to the cotyle surface. A similar elongated (slightly radial) pattern has been observed in the cervical cotyles of *Austroposeidon magnificus* MCT 1628-R, and *Uberabatitan ribeiroi* CPPLIP-1024 (Bandeira *et al.*, 2016; Aureliano *et al.*, 2020). Therefore, this camellate elongation may correlate to the structural needs of the vertebral articulation surfaces instead of being restricted to any specialized area (either cervical or dorsal). Additionally, Bandeira et al. (2016) indicated that the camellate rings (perpendicular to the cotyle radial walls) may be ontogenetic markers as growth lines. However, the pneumatic architecture in the dorsal vertebral center of LPP-PV-0200 lacks the subtrapezoidal camellate array (in distal midshaft view). This coincides with the pattern observed in *Saltasaurus loricatus* dorsal PVL 4017-17. Coincidently, the subtrapezoidal pattern observed in *S. loricatus* PVL 4017-214 and in the non-Saltasauridae *U. ribeiroi* cervicals might indeed be correlated to the cervical air sacs system. In a counterpart, the chaotic pattern observed in LPP-PV-0200 and PVL 4017-214 might correlate with the lung air sacs system. Data supporting this correlation hypothesis is present in Table 1. Still, further sampling is necessary to test this hypothesis.

Table 1. Camellate architecture in the vertebral centra of titanosaurs and their possibly correlated air sacs system.

Taxon	**Specimen**	**Bibliography**	**Vertebra**	**Vertebral center camellate pattern in cross section**	**Possible related air sacs system**
Saltasaurus loricatus	PVL 4017-214	Cerda et al. (2012)	Posterior cervical	subtrapezoidal	cervical
Saltasaurus loricatus	PVL 4017-47	Cerda et al. (2012)	Middle dorsal	chaotic	lung
Uberabatitan ribeiroi	CPPLIP-1024	Aureliano et al. (2020)	Posterior cervical	subtrapezoidal	cervical
Ibirá Site Saltasauridae	LPP-PV-0200	This article	Posterior dorsal	chaotic	lung

The extreme PSP in Argentinian Saltasauridae was previously reported by Cerda et al. (2012). This study in a small bodied Saltasauridae from Brazil not only corroborates with their study with histological data, but also reinforces their observation that PSP in sauropodomorphs does not always correlate with their giant sizes as previously assumed (Wedel, 2003; Sander *et al.*, 2011).

CONCLUSIONS

This study contributes with some insights for the understanding of the evolution of the respiratory system in dinosaurs. Our highlighted results are listed below.

6) We expanded the occurrence of pneumosteum tissue to the Saltasauridae titanosaur LPP-PV-0200 from the Upper Cretaceous of Southeast Brazil. This also corroborates with the previous hypothesis that the pneumosteal bone tissue is a good signature for indicating the insertion of lung diverticula in the fossil record. This is the fourth non-avian dinosaur taxon in which histological traces of air sacs have been found.
7) We provided detailed description of PSP structures from the CT scan of a dorsal vertebra of the titanosaur LPP-PV-0200. Hopefully, this will be a parameter for comparison with other taxa. The camellate pattern found in the vertebral center of the LPP-PV-0200 and other titanosaurs show distinct architectures. Subtrapezoidal array might be related to the cervical air sacs system. A chaotic arrangement may me related to the lung air sacs system. Further sampling in more taxa is necessary to test this hypothesis.
8) The extreme pneumaticity observed in the Saltasauridae LPP-PV-0200 contrasts with previous assumptions that PSP correlates with giant sizes in dinosaurs. This study reinforces that even small-bodied sauropod clades could be hyperpneumatized.

Five neosauropod taxa have been sampled for pneumosteum description in the literature. Those include the basal *Diplodocus*, *Europasaurus*, the lithostrotian titanosaurs *Uberabatitan* and *'Aeolosaurus' maximus*, and the Saltasauridae LPP-PV-0200. For future approaches, it would be relevant to expand sampling to basal sauropodomorphs.

ACKNOWLEDGEMENTS

We would like to acknowledge Oswaldo Jorge and the rest of the HU-UFSCar team for conducting fossil tomography. To the Departamento de Pós-Graduação do Instituto de Geociências, Unicamp, and to *Colecionadores de Ossos*^{TM}, for funding transportation and thin sections. Authors research grants, scholarships, and financial aid were provided by the Brazilian National Council for Scientific and Technological Development (CNPq 131777/2018-1) (T.A.), the Brazilian Coordination for the Improvement of Higher Education Personnel (CAPES - Finance Code 001) (A.M.G), and FAPESP 2016/20927-0 'Modern accumulation studies and fossil bioclast studies in continental and coastal environments' (F.R.B.).

Bibliography

Aureliano, T. *et al.* (2020) 'Influence Of Taphonomy On Histological Evidence For Vertebral Pneumaticity In An Upper Cretaceous Titanosaur From South America', *Cretaceous Research*, p. 104337. doi: 10.1016/j.cretres.2019.104337.

Bandeira, K. L. N. *et al.* (2016) 'A New Giant Titanosauria (Dinosauria: Sauropoda) from the Late Cretaceous Bauru Group, Brazil', *PloS one*, 11(10), p. e0163373. doi: 10.1371/journal.pone.0163373.

Brum, A. S. *et al.* (2018) 'Description of uncommon pneumatic structures of a noasaurid (Theropoda, Dinosauria) cervical vertebra from the Bauru Group (Upper Cretaceous), Brazil', *Cretaceous Research*, 85, pp. 193–206. doi: 10.1016/j.cretres.2017.10.012.

Castro, M. C. *et al.* (2018) 'A Late Cretaceous mammal from Brazil and the first radioisotopic age for the Bauru Group', *Royal Society open science*, 5(5), p. 180482. doi: 10.1098/rsos.180482.

Cerda, I. A., Salgado, L. and Powell, J. E. (2012) 'Extreme postcranial pneumaticity in sauropod dinosaurs from South America', *Paläontologische Zeitschrift*. Springer, 86(4), pp. 441–449. doi: 10.1007/s12542-012-0140-6.

Curry Rogers, K. and Kulik, Z. (2018) 'Osteohistology of Rapetosaurus krausei (Sauropoda: Titanosauria) from the Upper Cretaceous of Madagascar', *Journal of Vertebrate Paleontology*. Taylor & Francis, pp. 1–24. doi: 10.1080/02724634.2018.1493689.

Delcourt, R. (2018) 'Ceratosaur palaeobiology: new insights on evolution and ecology of the southern rulers', *Scientific reports*. nature.com, 8(1), p. 9730. doi: 10.1038/s41598-018-28154-x.

Delcourt, R. and Iori, F. V. (2018) 'A new Abelisauridae (Dinosauria: Theropoda) from São José do Rio Preto Formation, Upper Cretaceous of Brazil and comments on the Bauru Group fauna', *Historical biology*. Taylor & Francis, pp. 1–8. doi: 10.1080/08912963.2018.1546700.

Fedorov, A. *et al.* (2012) '3D Slicer as an image computing platform for the Quantitative

Imaging Network', *Magnetic resonance imaging*, 30(9), pp. 1323–1341. doi: 10.1016/j.mri.2012.05.001.

Fernandes, L. A. and Coimbra, A. M. (2017) 'Revisão estratigráfica da parte oriental da Bacia Bauru (Neocretáceo)', *Revista brasileira de Geociências*. ppegeo.igc.usp.br, 30(4), pp. 717–728. Available at: http://www.ppegeo.igc.usp.br/index.php/rbg/article/download/10990/10444.

Francillon-Viellot, H. *et al.* (1990) 'Microstructure and mineralization of vertebrate skeletal tissues. In (J. Carter, Ed.) Skeletal Biomineralization: Patterns, Processes and Evolutionary Trends, vol. 1'. New York: Van Nostrand Reinhold.

Ibrahim, N. *et al.* (2014) 'Semiaquatic adaptations in a giant predatory dinosaur', *Science*, 345(6204), pp. 1613–1616. doi: 10.1126/science.1258750.

Lambertz, M., Bertozzo, F. and Sander, P. M. (2018) 'Bone histological correlates for air sacs and their implications for understanding the origin of the dinosaurian respiratory system', *Biology letters*. rsbl.royalsocietypublishing.org, 14(1). doi: 10.1098/rsbl.2017.0514.

Lamm, E.-T. (2013) 'Preparation and Sectioning of Specimens', in *Bone Histology of Fossil Tetrapods*. University of California Press. doi: 10.1525/california/9780520273528.003.0004.

Li, Q. *et al.* (2012) 'Reconstruction of Microraptor and the evolution of iridescent plumage', *Science*. science.sciencemag.org, 335(6073), pp. 1215–1219. doi: 10.1126/science.1213780.

Mateus, O., Maidment, S. C. R. and Christiansen, N. A. (2009) 'A new long-necked "sauropod-mimic" stegosaur and the evolution of the plated dinosaurs', *Proceedings. Biological sciences / The Royal Society*, 276(1663), pp. 1815–1821. doi: 10.1098/rspb.2008.1909.

Méndez, A. H., Novas, F. E. and Iori, F. V. (2012) 'First record of Megaraptora (Theropoda, Neovenatoridae) from Brazil', *Comptes rendus. Palevol*. Elsevier, 11(4), pp. 251–256. doi: 10.1016/j.crpv.2011.12.007.

Mitchell, J. and Sander, P. M. (2014) ‘The three-front model: a developmental explanation of long bone diaphyseal histology of Sauropoda’, *Biological journal of the Linnean Society. Linnean Society of London*. Oxford University Press, 112(4), pp. 765–781. doi: 10.1111/bij.12324.

Müller, R. T., Langer, M. C. and Dias-da-Silva, S. (2018) ‘An exceptionally preserved association of complete dinosaur skeletons reveals the oldest long-necked sauropodomorphs’, *Biology letters*. royalsocietypublishing.org, 14(11). doi: 10.1098/rsbl.2018.0633.

Norman, D. B. *et al.* (2011) ‘The Lower Jurassic ornithischian dinosaur Heterodontosaurus tucki Crompton & Charig, 1962: cranial anatomy, functional morphology, taxonomy, and relationships’, *Zoological journal of the Linnean Society*. Oxford Academic, 163(1), pp. 182–276. doi: 10.1111/j.1096-3642.2011.00697.x.

O’Connor, P. M. (2006) ‘Postcranial pneumaticity: an evaluation of soft-tissue influences on the postcranial skeleton and the reconstruction of pulmonary anatomy in archosaurs’, *Journal of morphology*. Wiley Online Library, 267(10), pp. 1199–1226. Available at: https://onlinelibrary.wiley.com/doi/abs/10.1002/jmor.10470.

Pacheco, C. *et al.* (2019) ‘Gnathovorax cabreirai: a new early dinosaur and the origin and initial radiation of predatory dinosaurs’, *PeerJ*, 7, p. e7963. doi: 10.7717/peerj.7963.

Padian, K. and Lamm, E.-T. (2013) *Bone Histology of Fossil Tetrapods: Advancing Methods, Analysis, and Interpretation*. University of California Press. Available at: https://market.android.com/details?id=book-EBVNmk1nm6MC.

Pfretzschner, H.-U. (2001) ‘Pyrite in fossil bone’, *Neues Jahrbuch für Geologie und Paläontologie - Abhandlungen*, 220(1), pp. 1–23. doi: 10.1127/njgpa/220/2001/1.

Sander, P. M. *et al.* (2011) ‘Biology of the sauropod dinosaurs: the evolution of gigantism’, *Biological reviews of the Cambridge Philosophical Society*. Wiley Online Library, 86(1), pp. 117–155. doi: 10.1111/j.1469-185X.2010.00137.x.

Sander, P. M. (2013) ‘An evolutionary cascade model for sauropod dinosaur gigantism--overview, update and tests’, *PloS one*. journals.plos.org, 8(10), p. e78573. doi:

10.1371/journal.pone.0078573.

Stein, K. *et al.* (2010) ‘Small body size and extreme cortical bone remodeling indicate phyletic dwarfism in Magyarosaurus dacus (Sauropoda: Titanosauria)’, *Proceedings of the National Academy of Sciences of the United States of America*, 107(20), pp. 9258–9263. doi: 10.1073/pnas.1000781107.

Methods in fossil preparation: proceedings of the first annual Fossil Preparation and Collections Symposium. ebook]: Petrified Forest National Park, pp. 69–80. Available at: http://www.academia.edu/download/44573693/Histological_core_drilling_a_less_destru20160409-9077-3nz6af.pdf.Stein, K. and Sander, P. M. (2009) ‘Histological core drilling: a less destructive method for studying bone histology’, in

Wedel, M. J. (2003) ‘Vertebral pneumaticity, air sacs, and the physiology of sauropod dinosaurs’, *Paleobiology*. Cambridge University Press, 29(2), pp. 243–255. doi: 10.1017/S0094837300018091.

Wedel, M. J. (2006) ‘Origin of postcranial skeletal pneumaticity in dinosaurs’, *Integrative zoology*, 1(2), pp. 80–85. doi: 10.1111/j.1749-4877.2006.00019.x.

Wedel, M. J. (2007) ‘What pneumaticity tells us about “prosauropods”, and vice versa’, *Special Papers in Palaeontology*. researchgate.net, 77, pp. 207–222. Available at: https://www.researchgate.net/profile/Mathew_Wedel/publication/272152712_What_pneumaticity_tells_us_about_prosauropods’_and_vice_versa/links/57d2e0e108ae5f03b48cd10c/What-pneumaticity-tells-us-about-prosauropods-and-vice-versa.pdf.

Wedel, M. J. (2009) ‘Evidence for bird-like air sacs in saurischian dinosaurs’, *Journal of experimental zoology. Part A, Ecological genetics and physiology*. Wiley Online Library, 311(8), pp. 611–628. Available at: https://onlinelibrary.wiley.com/doi/abs/10.1002/jez.513.

Wedel, M. J., Cifelli, R. L. and Sanders, R. K. (2000) ‘Osteology, paleobiology, and relationships of the sauropod dinosaur Sauroposeidon’, *Acta palaeontologica Polonica*. -, 45(4). Available at: http://yadda.icm.edu.pl/yadda/element/bwmeta1.element.agro-article-46c7b594-4a8b-476d-aa1c-4c117ed1f8fa/c/app45-343.pdf.

Wilson, J. A. *et al.* (2011) ‘A nomenclature for vertebral fossae in sauropods and other saurischian dinosaurs’, *PloS one*. journals.plos.org, 6(2), p. e17114. doi: 10.1371/journal.pone.0017114.

Wilson, J. A. (2012) ‘New vertebral laminae and patterns of serial variation in vertebral laminae of sauropod dinosaurs’. Museum of Paleontology, The University of Michigan. Available at: https://deepblue.lib.umich.edu/bitstream/handle/2027.42/92460/Contributions32no7-HR-c08-15-2012.pdf?sequence=2.

Yates, A. M., Wedel, M. J. and Bonnan, M. F. (2012) ‘The Early Evolution of Postcranial Skeletal Pneumaticity in Sauropodomorph Dinosaurs’, *Acta palaeontologica Polonica*. BioOne, 57(1), pp. 85–100. doi: 10.4202/app.2010.0075.

6 Conclusões

Os resultados obtidos contribuem para a compreensão da evolução do sistema respiratório dos arcossauros, por meio de amostragem em três *taxa* de titanossauros derivados brasileiros. Contribuem, também, para uma melhor compreensão, de como distintos sistemas deposicionais afetaram a qualidade de preservação da microanatomia dos fósseis, sobretudo a impressão de tecidos moles, como osso pneumosteal e fibras de Sharpey (cicatrizes de músculos e tendões). Adicionalmente, também foram estabelecidos parâmetros descritivos, como protocolo para distinguir estes dois tipos de tecidos, o que pode contribuir para estudos em outros *taxa*.

Pouco é conhecido sobre a relação entre paleoparasitologia e paleopatologia. Um dos resultados deste mestrado fornece a primeira evidência de um hospedeiro dinossauro em uma doença vetorial. Isto inclui a presença de dezenas de indivíduos de um novo táxon de parasita, preservados dentro dos canais vasculares e da medula óssea de um saurópode senil. Este registro histológico confirma que saurópodes eram parasitados por tripanossomatídeos. Ademais, este estudo abriu uma nova possibilidade para pesquisas paleontológicas ao unir os campos da histologia, patologia e parasitologia. O titanossauro amostrado apresenta osteomielite crônica, associada à leishmaniose, com ulcerações elípticas semelhante ao kala-azar moderno. Por conseguinte, antecipou-se a primeira ocorrência da leishmaniose patogênica no Novo Mundo do Oligoceno-Mioceno da República Dominicana para o Cretáceo Superior do Brasil.

Portanto, este estudo forneceu resultados que contribuem substancialmente para a compreensão da histologia da impressão de tecidos moles do sistema respiratório de dinossauros, do desenvolvimento da osteomielite, e da macroevolução e ecologia dos parasitas relacionados a doenças tropicais. Outrossim, também contribuiu-se para o conhecimento da tafonomia em relação à paleohistologia, através da apresentação de tecidos de dinossauros preservados em diferentes contextos deposicionais e de microorganismos parasíticos preservados em condições nunca antes registradas na literatura (*in situ*, no hospedeiro, ao invés de em âmbar ou coprólitos).

REFERÊNCIAS BIBLIOGRÁFICAS

ANDRADE, R. C. L. P. DE. Descrição paleohistológica, inferências adaptativas, fisiológicas e evolutivas de Notosuchia do Cretáceo do Brasil (Archosauria, Crocodyliformes). 2018.

AURELIANO, T.; GHILARDI, A. M.; BUCK, P. V.; FABBRI, M.; SAMATHI, A.; DELCOURT, R.; FERNANDES, M. A.; SANDER, M. Semi-aquatic adaptations in a spinosaur from the Lower Cretaceous of Brazil. **Cretaceous Research**, v. 90, p. 283–295, 1 out. 2018.

BARBOSA, F. H. DE S.; MARINHO, T. DA S.; IORI, F. V.; PASCHOA, L. DA S. A case of infection in an Aeolosaurini (Sauropoda) dinosaur from the Upper Cretaceous of São Paulo, southeastern Brazil, and the impact on its life. **Cretaceous Research**, 7 dez. 2018.

BARBOSA, F. H. DE S.; PEREIRA, P. V. L. G. DA C.; BERGQVIST, L. P.; ROTHSCHILD, B. M. Multiple neoplasms in a single sauropod dinosaur from the Upper Cretaceous of Brazil. **Cretaceous Research**, v. 62, p. 13–17, 1 jul. 2016.

BATEZELLI, A. 2003. Análise da sedimentação cretácea no Triângulo Mineiro esua correlação com áreas adjacentes. Rio Claro, 2003. Tese (Doutorado em Geociências) – Instituto de Geociências e Ciências Exatas, Universidade Estadual Paulista, Rio Claro, SP. 183 p.

CERDA, I. A.; CHINSAMY, A.; POL, D.; APALDETTI, C.; OTERO, A.; POWELL, J. E.; MARTÍNEZ, R. N. Novel insight into the origin of the growth dynamics of sauropod dinosaurs. **PloS one**, v. 12, n. 6, p. e0179707, 27 jun. 2017.

CHINSAMY-TURAN, A. The microstructure of dinosaur bone: deciphering biology with fine-scale techniques. 2005.

DENTZIEN-DIAS, P. C.; POINAR, G., Jr; FIGUEIREDO, A. E. Q. DE; PACHECO, A. C. L.; HORN, B. L. D.; SCHULTZ, C. L. Tapeworm eggs in a 270 million-year-old shark coprolite. **PloS one**, v. 8, n. 1, p. e55007, 30 jan. 2013.

DIAS-BRITO, D.; MUSACCHIO,E.A.; CASTRO, J. D.; MARANHAO, M. S.; SUÁREZ, J. M. Grupo Bauru: uma unidade continental do Cretáceo no Brasil-concepções baseadas em dados micropaleontológicos, isotópicos e estratigráficos. *Revue de Paléobiologie*, *20*(1), 245-304, 2001.

DYKE, G.; KAT, R. DE; PALMER, C.; KINDERE, J. VAN DER; NAISH, D.;

GANAPATHISUBRAMANI, B. Aerodynamic performance of the feathered dinosaur Microraptor and the evolution of feathered flight. **Nature communications**, v. 4, p. 2489, 2013.

FERNANDES, L. A.; COIMBRA, A. M. (1996). Bacia Bauru (Cretáceo Superior, Brasil). *Anais da Academia Brasileira de Ciências*, *68*(2), 195-205, 1996.

FRANCILLON-VIELLOT, H.; BUFFRÉNIL, V. DE; CASTANET, J.; GÉRAUDIE, J.; MEUNIER, F. J.; SIRE, J. Y.; ZYLBERBERG, L.; RICQLÈS, A. DE. **Microstructure and mineralization of vertebrate skeletal tissues. In (J. Carter, Ed.) Skeletal Biomineralization: Patterns, Processes and Evolutionary Trends, vol. 1**New York: Van Nostrand Reinhold, , 1990.

HUDGINS, M. N.; UHEN, M. D.; HINNOV, L. A. The evolution of respiratory systems in Theropoda and Paracrocodylomorpha, the end-Triassic extinction, and the role of Late Triassic atmospheric O2 and CO2. **Palaeogeography, palaeoclimatology, palaeoecology**, p. 109638, 10 fev. 2020.

IBRAHIM, N.; DAL SASSO, C.; MAGANUCO, S.; FABBRI, M.; MARTILL, D. M.; GORSCAK, E.; LAMANNA, M. C. Evidence of a derived titanosaurian (Dinosauria, Sauropoda) in the “Kem Kem beds” of Morocco, with comments on sauropod paleoecology in the Cretaceous of Africa. **Cretaceous Period: Biotic Diversity and Biogeography. New Mexico Museum of Natural History and Science Bulletin**, v. 71, p. 149–159, 2016.

LAMBERTZ, M.; BERTOZZO, F.; SANDER, P. M. Bone histological correlates for air sacs and their implications for understanding the origin of the dinosaurian respiratory system. **Biology letters**, v. 14, n. 1, jan. 2018.

MARCHETTI, I.; RICARDI-BRANCO, F.; CALLEFO, F.; DELCOURT, R.; GALANTE, D.; JURIGAN, I.; CARVALHO, I. S.; TAVARES, S. A. S. Fossildiagenesis and ontogenetic insights of crocodyliform bones from the Adamantina Formation, Bauru Basin, Brazil. **Journal of South American Earth Sciences**, v. 96, p. 102327, 1 dez. 2019.

MENEGAZZO, M. C.; CATUNEANU, O.; CHANG, H. K.. The South American retroarc foreland system: The development of the Bauru Basin in the back-bulge province. *Marine and Petroleum Geology*, *73*, 131-156, 2016.

MITCHELL, J.; SANDER, P. M. The three-front model: a developmental explanation of long bone diaphyseal histology of Sauropoda. **Biological journal of the Linnean Society. Linnean Society of London**, v. 112, n. 4, p. 765–781, 1 ago. 2014.

O'CONNOR, P. M. Postcranial pneumaticity: an evaluation of soft-tissue influences on the postcranial skeleton and the reconstruction of pulmonary anatomy in archosaurs. **Journal of morphology**, v. 267, n. 10, p. 1199–1226, 2006.

PADIAN, K.; LAMM, E.-T. **Bone Histology of Fossil Tetrapods: Advancing Methods, Analysis, and Interpretation**. [s.l.] University of California Press, 2013.

PERRY, S. F.; CHRISTIAN, A.; BREUER, T.; PAJOR, N.; CODD, J. R. Implications of an avian-style respiratory system for gigantism in sauropod dinosaurs. **Journal of experimental zoology. Part A, Ecological genetics and physiology**, v. 311, n. 8, p. 600–610, 2009.

POINAR, G. A primitive triatomine bug, Paleotriatoma metaxytaxa gen. et sp. nov. (Hemiptera: Reduviidae: Triatominae), in mid-Cretaceous amber from northern Myanmar. **Cretaceous Research**, v. 93, p. 90–97, 1 jan. 2019.

POINAR, G., Jr. Leptoconops nosopheris sp. n.(Diptera: Ceratopogonidae) and Paleotrypanosoma burmanicus gen. n., sp. n.(Kinetoplastida: Trypanosomatidae), a biting midge-trypanosome vector association from the Early Cretaceous. **Memorias do Instituto Oswaldo Cruz**, v. 103, n. 5, p. 468–471, 2008.

POINAR, G., Jr; POINAR, R. Paleoleishmania proterus n. gen., n. sp., (Trypanosomatidae: Kinetoplastida) from Cretaceous Burmese amber. **Protist**, v. 155, n. 3, p. 305–310, set. 2004.

POINAR, G.; POINAR, R. Evidence of Vector-Borne Disease of Early Cretaceous Reptiles. **Vector-Borne and Zoonotic Diseases**, v. 4, n. 4, p. 281–284, 1 dez. 2004.

ROTHSCHILD, B. M.; MARTIN, L. D. **Skeletal Impact of Disease**. [s.l.] New Mexico Museum of Natural History and Science, 2006. v. Bulletin 33

SALGADO, L.; CARVALHO, I. S. UBERABATITAN RIBEIROI, A NEW TITANOSAUR FROM THE MARÍLIA FORMATION (BAURU GROUP, UPPER CRETACEOUS), MINAS GERAIS, BRAZIL. **Palaeontology**, 2008.

SANDER, P. M. *et al.* Biology of the sauropod dinosaurs: the evolution of gigantism. **Biological reviews of the Cambridge Philosophical Society**, v. 86, n. 1, p. 117–155, fev. 2011.

SANTUCCI, R. M.; ARRUDA-CAMPOS, A. C. DE. A new sauropod (Macronaria, Titanosauria) from the Adamantina Formation, Bauru Group, Upper Cretaceous of Brazil and the phylogenetic relationships of Aeolosaurini. **Zootaxa**, v. 3085, p. 1–33, 2011.

SILVA JUNIOR, J. C. G.; MARINHO, T. S.; MARTINELLI, A. G.; LANGER, M. C. Osteology and systematics of Uberabatitan ribeiroi (Dinosauria; Sauropoda): a Late Cretaceous titanosaur from Minas Gerais, Brazil. **Zootaxa**, v. 4577, n. 3, p. 401–438, 2019.

SURMIK, D.; SZCZYGIELSKI, T.; JANISZEWSKA, K.; ROTHSCHILD, B. M. Tuberculosis-like respiratory infection in 245-million-year-old marine reptile suggested by bone pathologies. **Royal Society open science**, v. 5, n. 6, p. 180225, jun. 2018.

WEDEL, M. J. The evolution of vertebral pneumaticity in sauropod dinosaurs. **Journal of Vertebrate Paleontology**, v. 23, n. 2, p. 344–357, 17 jun. 2003.

WEDEL, M. J. What pneumaticity tells us about “prosauropods”, and vice versa. Special Papers in Palaeontology, v. 77, p. 207–222, 2007.

WEDEL, M. J. Evidence for bird-like air sacs in saurischian dinosaurs. **Journal of experimental zoology. Part A, Ecological genetics and physiology**, v. 311, n. 8, p. 611–628, 2009.

WILSON, J. A.; D’EMIC, M. D.; IKEJIRI, T.; MOACDIEH, E. M.; WHITLOCK, J. A. A nomenclature for vertebral fossae in sauropods and other saurischian dinosaurs. **PloS one**, v. 6, n. 2, p. e17114, 28 fev. 2011.

XING, L.; ROTHSCHILD, B. M.; RANDOLPH-QUINNEY, P. S.; WANG, Y.; PARKINSON, A. H.; RAN, H. Possible bite-induced abscess and osteomyelitis in Lufengosaurus (Dinosauria: sauropodomorph) from the Lower Jurassic of the Yimen Basin, China. **Scientific reports**, v. 8, n. 1, p. 5045, 22 mar. 2018.

XU, X.; ZHENG, X.; SULLIVAN, C.; WANG, X.; XING, L.; WANG, Y.; ZHANG, X.; O’CONNOR, J. K.; ZHANG, F.; PAN, Y. A bizarre Jurassic maniraptoran theropod with preserved evidence of membranous wings. **Nature**, v. 521, n. 7550, p. 70–73, 7 maio 2015.